Summer 6-15-2010

Bead Modeling of Transport Properties of Macromolecules in Free Solution and in a Gel

Hongxia Pei
Georgia State University

BEAD MODELING OF TRANSPORT PROPERTIES OF MACROMOLECULES IN FREE SOLUTION AND IN A GEL

by

HONGXIA PEI

Under the Direction of Dr. Stuart Allison

ABSTRACT

On the bead modeling methodology, or BMM, a macromolecule is modeled as a rigid, non-overlapping bead array with arbitrary radii. The BMM approach was pioneered by Kirkwood and coworkers (Kirkwood, J.G., Macromolecules, E.P. Auer (Ed.), Gordon and Breach, New York, 1967; Kirkwood, J.G., Riseman, J., J. Chem. Phys., 1948, 16, 565) and applied to such transport properties as diffusion, sedimentation, and viscosity. With the availability of computers, a number of investigators extended the work to account for the detailed shape of biomolecules in the 1970s.

A principle objective of my research has been to apply the BMM approach to more complex transport phenomena such as transport in a gel, electrophoresis (free solution and in a gel), and also transport in more complex media (such as the viscosity of alkanes and benzene). Variables considered by the BMM include the number of beads (N), the radii of the beads, net charge and charge distribution, conformations, salt type, and salt concentration. The BMM has been extended to: (1) account for the existence of a gel; (2) characterize the charge and secondary structure of macromolecules; (3) account more accurately for hydrodynamic interaction (remove the orientationnal preaveraging approximation of hydrodynamic interaction); (4) study the effect

of ion relaxation for particles in arbitrary size, shape, and charge; (5) consider the salt dependence of electrokinetic properties; (6) account for the formation of possible complex between guest ions and BGE ions. We also did diffusion constant measurement by NMR for amino acids and short peptides in 10%D_2O-90% H_2O at room temperature and applied to our modeling study by BMM.

INDEX WORDS: Agarose gel, Bead model, Complex formation, DNA, Effective medium, Hydrodynamic interaction, NMR, Peptide, Relaxation, Salt dependence.

BEAD MODELING OF TRANSPORT PROPERTIES OF MACROMOLECULES IN FREE SOLUTION AND IN A GEL

by

HONGXIA PEI

A Dissertation Submitted in Partial Fulfillment of the Requirements for the Degree of

Doctor of Philosophy

in the College of Arts and Sciences

Georgia State University

2010

BEAD MODELING OF TRANSPORT PROPERTIES OF MACROMOLECULES IN FREE SOLUTION AND IN A GEL

by

HONGXIA PEI

Committee Chair: Stuart Allison

Committee: Markus Germann

Donald Hamelberg

Jenny Yang

Electronic Version Approved:

Office of Graduate Studies

College of Arts and Sciences

Georgia State University

August 2010

To my parents, my brother and my sister-in-law

ACKNOWLEDGMENTS

This dissertation has been accomplished with the assistance and support of many people. First and foremost, I would like to express my sincere appreciation and gratitude to my advisor, Dr. Stuart Allison. He taught me how to start academic pursuits from the very beginning. From him I have learned a lot and have improved in the area of computational chemistry. Without his encouragement and help I could not have completed my PhD work. I would like to thank Dr. Germann for giving me the chance to do NMR experiments in his Lab.

I would also thank my committee members: Dr. Markus Germann, Dr. Donald Hamelberg, and Dr. Jenny Yang for their great advice on my dissertation. I would like to thank the Department of Chemistry at Georgia State University for offering me this great opportunity to pursue my Ph.D. degree, for offering great classes and the opportunity to teach undergraduate tutorials. All of these provided me good training in academic progress. Thanks Dr. Stuart Allison, Dr. Markus Germann, Dr. David Wilson, Dr. Jerry Smith, Dr. Dabney Dixon, Dr. Kathryn Grant, Dr. Thomas Netzel, Dr. Jenny Yang, and Dr. Donald Hamelberg for their impressive classes.

I would also like to thank Yao Xin, Hengfu Wu, Umar Twahir, other group members, and my friends for discussions and help.

Last but not least, I would like to express my gratitude to my family. I would like to thank for their love and support. Having them proud of me is one of my motivations to work hard.

TABLE OF CONTENTS

LIST OF TABLES

LIST OF FIGURES

Chapter 1

Introduction

1.1 Introduction of Electrophoresis

The technique of electrophoresis is of considerable value in chemistry, molecular biology, and colloid science because it is both simple to implement (application of a voltage across a gel or capillary) and powerful in its ability to separate a mixture of molecules or colloidal particles (1). This separation occurs because of differences in charge, charge distribution, size, and/or shape of the constituents that are present. When a charged particle is placed in a constant external electric field, $\underline{e}$, its electrophoretic mobility, μ (average drift velocity/$|\underline{e}|$), will depend on the balance of electrical and hydrodynamic forces that act on it. The central problem of electrophoresis theory is to determine these forces for particular model systems. This theory as applied to a single particle is made difficult because of the "electrophoretic effect" (hydrodynamic backflow on the particle produced by the motion of its ion atmosphere) and the "relaxation effect" (distortion of the ion atmosphere of the particle from equilibrium due to the presence of a (non-equilibrium) external electric and flow field] (2). To illustrate this, it is helpful to review the one system that has been thoroughly investigated, the electrophoretic mobility of a uniformly charged sphere.

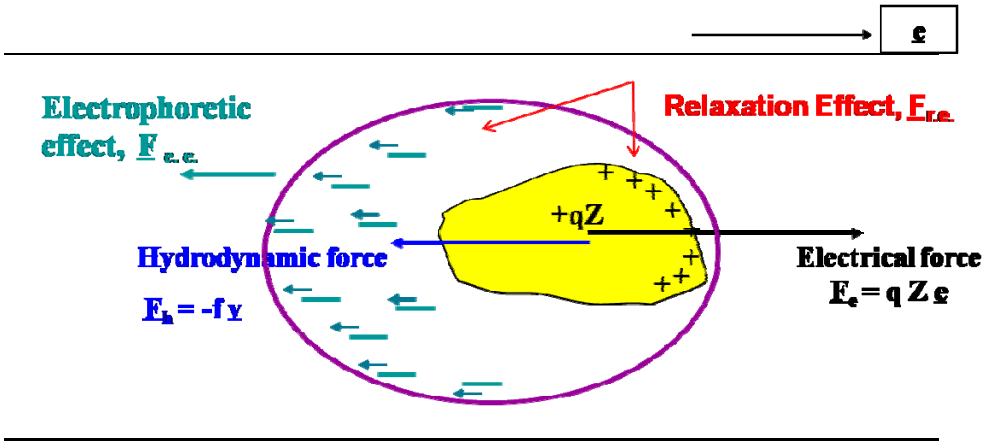

Figure 1-1) A charged particle of arbitrary shape moving in an electric field in salt containing mobile ions.

1.2 Other Modeling Methodologies of Free Solution Electrophoresis

For free solution electrophoresis (no gel support medium present), Henry developed the theory for a sphere of arbitrary size that accounted for the electrophoretic effect, but not the relaxation effect (3). Neglecting the relaxation effect is valid for weakly charged particles where the absolute surface, or "ζ potential", does not exceed 25 mV (4), or the absolute electrophoretic mobility does not exceed approximately 0.20 cm^2/kV sec (5). Overbeek (6) and Booth (7) derived analytical expressions for the free solution electrophoretic mobility of spheres that accounted, to lowest order, for the relaxation effect. A complete treatment of the "free solution" problem was not achieved until numerical algorithms were developed first by Wiersema and coworkers (2) and later by O'Brien and White (8). A third complication involves accounting for the influence of a gel (if present) on mobility. The extension of the theory of electrophoresis to spheres of arbitrary charge *in a gel* was carried out recently by our group (9).

Other simple model geometries have also been considered. The free solution electrophoresis of long cylinders (10-11), weakly (12-13) and highly (14) charged ellipsoids, and spheres containing a "hairy" layer on their outer surface (15-17) have also been treated. However, more realistic models are needed in biochemistry and molecular biology since biomolecules are typically complex in shape and have complex distributions of charge on their surface or interior. In the late 1970's, detailed modeling of diffusion and sedimentation of biomolecules in solution was carried out (18-23). The solvent is modeled as an incompressible Newtonian fluid continuum and the solvent-particle velocities are set equal at their interface ("stick" hydrodynamic boundary conditions). A short time later, a number of groups investigating ionic distributions around high molecular weight DNA showed that continuum electrostatic theory (in this case, solutions of the nonlinear Poisson-Boltzmann equation) gives reasonable electrostatic potentials and mobile ion distributions around DNA provided the mobile ions are univalent and small compared to the diameter of DNA (about 2 nm) (24-26). This success has stimulated the use of continuum electrostatic modeling around biomolecules in general (27-31). *Detailed* modeling of electrophoresis and related electrokinetic transport phenomena based on the same continuum representation of solvent and mobile ions requires simultaneous numerical solution of the hydrodynamic (18-23) and electrostatic (27-31) problems. When the relaxation effect is also included, an ion transport equation must also be solved for each mobile ion species present (6-11,14). Based on the Boundary Element, BE, approach for both hydrodynamics (23) and electrostatics (28), a numerical algorithm has been developed (32) and applied to the free solution electrophoresis of a number of systems including proteins (5,33,34), nucleic acids (35), and irregular silica sols containing a "hairy" layer on their outer

surface (36). In this approach, a closed molecular surface, or more precisely the surface of hydrodynamic shear, is represented as a series of flat, interconnected triangular plates. Arbitrary fixed charge distributions can be placed within this closed surface. The BE approach discussed above yields mobilities in quantitative agreement with experiment when realistic models are used that account for the detailed size, shape, and charge distribution of the actual biopolymer. These include a number of proteins (5, 33, 34) and short duplex DNA in alkali halide salt solutions (35). The BE method as applied to electrokinetic transport has been reviewed previously (37).

A disadvantage of the BE approach is that it is time consuming from a computational standpoint (35). This has made it impractical to apply this approach to duplex DNA longer than about 100 bp or to flexible structures that require sampling of multiple conformations. In order to deal with this problem, a faster and more efficient method has been developed where the basic structural unit is a spherical bead of arbitrary radius and charge (38-40). The model structure consists of an arbitrary, non-overlapping array of beads. In this approach, the electrophoretic effect is accounted for explicitly, but not the relaxation effect. For globular biomolecules, however, it is possible to correct for the relaxation effect using the corresponding correction for spheres (40). A second approximation involves "orientational preaveraging" of hydrodynamic interaction. The consequences of this approximation were discussed previously (38) and it was concluded that it results in an overestimation of μ by at most several percent.

1.3 Objectives of My PhD Study

The objectives of my PhD study are threefold. First, further develop the bead method applied to free solution electrophoresis discussed above. This will represent a generalization of

previous work (38-42) where (1) account is made of the possible presence of a gel; (2) characterize the charge and secondary structure of macromolecules; (3) account more accurately for hydrodynamic interaction; (4) study the effect of ion relaxation for particles of arbitrary size, shape, and charge; (5) consider the salt dependence of electrokinetic properties; (6) account for the formation of possible complex between guest ions and BGE ions. The technical details of the bead modeling methodology, BMM, of free solution electrophoresis are placed in the next section of this chapter. The improvements of the BMM carried out by our group are discussed in detail in subsequent chapters. The particles in interest are peptides, DNA fragments, nanoparticles, alkanes, *etc*. Second, apply the BMM to the diffusion constant of a set of amino acid, peptides, and DNA fragments (43-45) in free solution and in a gel. We believe that this serves as a convincing demonstration of the accuracy and efficacy of the method. Third, it shall be applied to simulate the free solution viscosity for macromolecules (46-47).

1.4 Bead Modeling Methodology, BMM

Bead modeling methodology, BMM, is a numerical method further developed by our group to model the electrophoresis of irregularly shaped model particles with an arbitrary charge distribution inside. In the bead modeling methodology, BMM, the solute is represented as a rigid, possibly irregularly shaped particle, or rigid bead array, immersed in a continuum incompressible Newtonian fluid (the solvent) of viscosity η_0. Solute-solvent interactions are assumed to arise strictly from short range excluded volume repulsions present at the solute-solvent interface. It is also assumed that the solvent obeys the low Reynolds Number Navier-Stokes equation (49,50). In most applications of the BMM, solute and solvent velocities are assumed to match at their

interface ("stick" hydrodynamic boundary conditions). In the case of "slip" boundary conditions, only the velocity components normal to the interface match and the hydrodynamic stress forces at the interface are also assumed to be normal (51). The applications of the BMM model discussed in the present work employ "stick" boundary conditions.

4A) Micromolecules Modeled by BMM

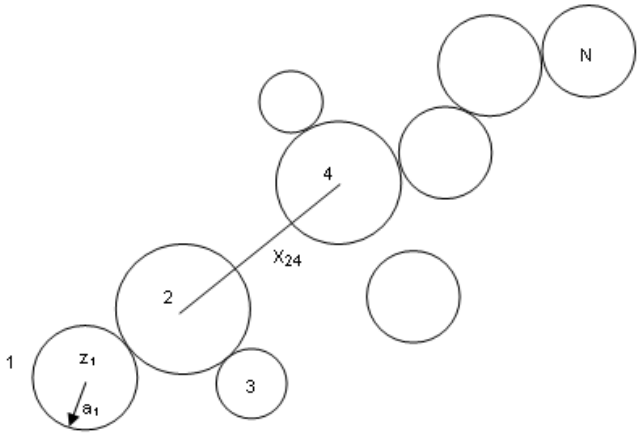

Figure 1-2) Schematic of the general bead model. The model is represented as N beads of variable radius, a_j, with variable charge, z_j, (in protonic units) place at their center. The backbone beads may have side beads. The beads may touch, but cannot overlap.

The solute is represented as an N bead array and is depicted in Figure 1-2. Bead J ($1 \leq J \leq N$) consists of an inner solid core of radius a_J and an outer fluid surface of radius b_J. In general, these radii can vary from bead to bead. The outer bead radii do not overlap. Stick hydrodynamic boundary conditions are assumed to prevail on the inner core bead surfaces, but an external force/volume, $\underline{s}(\underline{x})$, may be present in the fluid domain exterior to a_J, but interior to b_J, V_{eJ}. In the present work, it is useful to view $\underline{s}(\underline{x})$ as arising from the short range solute-solvent interactions that may represent "solvent breaking" or "solvent stabilizing" influences that arise

when the solute is placed in the solvent. In the present work, it shall be assumed that the solute is present in dilute concentration and that solute-solute interactions (interactions between different bead arrays) can be neglected. Outside of the V_{eJ}'s, it is assumed that $\underline{s}(\underline{x})$ can be set zero. The bead array is immersed in a simple shear field with shear gradient γ (in sec^{-1}) and it is assumed that $1/\gamma$ is long on the timescale of the array's Brownian translational and rotational motions. It is also assumed that γ is sufficiently small so that deformation of the bead array can be ignored and that its average orientation remains isotropic. Let the bead array translate with instantaneous overall velocity, $\underline{u}_0$, relative to a center of rotation, $\underline{d}$. Also let the instantaneous angular velocity of the entire bead array about $\underline{d}$ be denoted by $\underline{\omega}$, and let $\underline{x}_K$ denote the instantaneous position of the center of bead K. By "instantaneous", we mean a timescale short compared to average translational and rotational displacements of the beads, but long compared to the impulsive collision time between beads and solvent. If point $\underline{y}$ lies on the fluid/inner core surface of bead K and stick boundary conditions hold, then the rigid body particle velocity and fluid velocities match at $\underline{y}$.

$$\underline{v}_{RBM}(\underline{y}) = \underline{u}_0 + \underline{\omega} x (\underline{x}_K - \underline{d}) + \underline{\omega} x (\underline{y} - \underline{x}_K) \qquad (1-1)$$

In Eq. (1-1) above, "x" denotes the vector cross product.

4B) Continuum Modeling

Generally, it is assumed the model peptide is immersed in an incompressible Newtonian fluid of viscosity η_0 and that this fluid obeys the low Reynolds Number Navier-Stokes and solvent incompressibility equations defined by (49,50)

$$\eta_0 \nabla^2 \underline{v}(\underline{x}) - \underline{\nabla}\, p(\underline{x}) = -\underline{s_e}(\underline{x}) \qquad (1-2)$$

$$\underline{\nabla} \cdot \underline{v}(\underline{x}) = 0 \qquad (1-3)$$

Above, η_0 is the solvent viscosity, $\underline{v}(\underline{x})$ is the local fluid velocity at point $\underline{x}$ in the fluid, p is the local pressure, and $\underline{s}_e(\underline{x})$ is the electrical force/volume on the fluid. It is also assumed that fluid and particle velocities match at the fluid-bead interface ("stick" hydrodynamic boundary conditions) and that the peptides were present in the limit of high dilution (inter-peptide interactions were ignored). The hydrodynamic stress tensor at any point in the fluid is given by (49,50)

$$\underline{\underline{\sigma}}(\underline{x}) = -p(\underline{x})\,\underline{\underline{I}} + \eta_0 \left(\underline{\underline{\nabla v}}(\underline{x}) + \underline{\underline{\nabla v}}(\underline{x})^T\right) \qquad (1-4)$$

where $\underline{\underline{I}}$ is the 3 by 3 identity tensor and the "T" superscript denotes transpose. Before proceeding with the model development, it will be helpful to review the viscosity theory of a Newtonian fluid containing dilute solute particles represented as irregularly shaped (rigid) objects.

The solution, which contains background electrolyte, BGE, in addition to (dilute) peptides, is subjected to a constant electric field strength, $\underline{e}$. For a weakly charged array of beads, the external force/volume can be approximated (52)

$$\underline{s}_e(\underline{x}) = -q\kappa^2 \underline{e} \sum_{J=1}^{N_c} h_J\, F(\kappa, r_J') \qquad (1-5)$$

where q is the protonic charge, $r_J' = |\underline{x}-\underline{x}_J|$ where $\underline{x}_J$ is the position of the center of bead J, N_c is the number of charged beads in the model peptide, $\underline{F}(\kappa, r) = e^{-\kappa r}/(4\pi r)$, h_J is given by Eq. (A28) of reference 52, and

$$\kappa^2 = \frac{C q^2}{\varepsilon_w k_B T} \sum_j c_{j0} z_j'^2 \qquad (1-6)$$

In Eq. (1-6), κ is the Debye-Huckel screening parameter, $C = 4\pi$ (in CGS units) or $1/\varepsilon_0$ where ε_0 is the permittivity of free space (in MKSA units), ε_w is the relative permittivity of the solvent, k_B is Boltzmann's constant, T is absolute temperature, the sum over j extends over all ionic species of concentration c_{j0} and valence z_j' that make up the BGE. In the limit of small beads ($\kappa a_J \to 0$ where a_J is the radius of bead J), h_J appearing in Eq. (3) can be approximated with z_J where z_J is the charge (in protonic units) of bead J. For a weakly charged bead array, the equilibrium electrostatic potential of bead j, ζ_j, in the absence of an external electric field is given by (52)

$$\zeta_j = \frac{\kappa q X}{4\pi\varepsilon_w} \sum_{k,m} A_{jk}^{-1} B_{km} z_m \qquad (1-7)$$

where

$$A_{jk} = \begin{pmatrix} 1 - k_0(\kappa a_k) s(\kappa a_k)/2 & j = k \\ -i_0(\kappa a_j) k_0(\kappa r_{jk}) s(\kappa a_k)/2 & j \neq k \end{pmatrix} \qquad 1-(8)$$

$$B_{jk} = \begin{pmatrix} i_0(\kappa a_k) k_0(\kappa a_k) & j = k \\ i_0(\kappa a_j) i_0(\kappa a_k) k_0(\kappa r_{jk}) & j \neq k \end{pmatrix} \qquad (1-9)$$

$$s(\kappa a_k) = e^{\kappa a_k}(\kappa a_k - 1) + e^{-\kappa a_k}(\kappa a_k + 1) \qquad (1-10)$$

r_{jk} is the distance between the centers of beads j and k, $k_0(x) = e^{-x}/x$, and $i_o(x) = \sinh(x)/x$. Also, A_{jk} in Eq. (1-8) represents a single component of an N by N matrix, **A**. In Eq. (1-7), A_{jk}^{-1} represents the jk-th component of the inverse matrix of **A**, $\mathbf{A}^{-1}$. Eq. (1-7) is the solution of the linear Poisson-Boltzmann equation and for that reason is strictly valid only at low $|\zeta_j|$. However, finite ion effects are included and Eq. (1-7) can be viewed as a first order approximation of the potential for more highly charged systems.

The charge of a peptide results from the protonation of basic and deprotonation of acidic residues and these, in turn, depend on the pK_a's of these groups. As discussed in the Peptide Model section of this chapter, the pK_a of a particular bead (bead j), pK_{aj} is divided into an intrinsic (high salt) term, pK_{aj}^0, and a term that depends on charge-charge interactions between neighboring charge groups in the peptide. At the level of the linear Poisson-Boltzmann equation, the electrical free energy, G^{el}, of a charge system can be written (29, 31, 53, 54)

$$G^{el} = \frac{q}{2}\sum_j z_j \zeta_j = \sum_{j,k} z_j z_k C_{jk} \qquad (1-11)$$

$$C_{jk} = \frac{\kappa q^2 X}{8\pi\varepsilon_w}\sum_m A_{jm}^{-1} B_{mk} \qquad (1-12)$$

Suppose bead j is an acidic group. (A very similar analysis follows for deprotonation of a basic group, but is omitted here for the sake of brevity.) The single molecule free energy change, $\Delta G(HX_j \rightarrow X_j^-)$, is related to pK_{aj} by (29, 31, 53, 54)

$$pK_{aj} = \frac{1}{2.303 k_B T}\Delta G(HX_j \rightarrow X_j^-) \qquad (1-13)$$

Let the corresponding quantities in the absence of net charge-net charge interactions between neighboring groups be written $\Delta G^0(HX_j \rightarrow X_j^-)$ and pK_{aj}^0. Using thermodynamic cycle arguments (55), it is straightforward to show

$$pK_{aj} = pK_{aj}^0 - \frac{1}{2.303 k_B T} \sum_{j \neq k} z_k (C_{jk} + C_{kj}) \qquad (1-14)$$

In Eq. (1-14), equate z_k to the average charge state of site k at a particular pH. From Eqs. (1-8) to (1-11), we can compute C_{jk} once a conformation is specified.

Initially, we do not know what the z_k's are since the pK_{aj}'s are unknown. As an initial estimate, approximate pK_{ak} with pK_{ak}^0 and then use either Eqs. (1-15) or (1-16) to obtain a first order estimate, $z_k^{(1)}$. If the charge group associated with bead j is acidic, its average charge state is taken to be

$$z_j = -\frac{10^{pH-pK_{aj}}}{1+10^{pH-pK_{aj}}} \qquad (1-15)$$

If the charge group is basic,

$$z_j = +\frac{1}{1+10^{pH-pK_{aj}}} \qquad (1-16)$$

These are then used on the right hand side of Eq. (1-14) to obtain revised estimates, $pK_{aj}^{(1)}$, for all sites that could potentially bear a net charge. New charges, $z_k^{(2)}$, are then estimated using the $pK_{ak}^{(1)}$'s and the procedure is repeated until the charges and pK_{aj}'s converge.

The following relation was previously derived (52) for the electrophoretic mobility of a single (peptide) conformation, μ,

$$\mu = \frac{q\kappa}{6\pi\eta}\left(\sum_{j=1}^{N} P_1^{(j)} g_j - \frac{1}{2}P_2\right) \Big/ \left(\chi - \frac{1}{2}P_3\right) \qquad (1-17)$$

Expressions for $P_1^{(j)}$, P_2, P_3, χ, and other related quantities are given in Appendix B of reference 52 and shall not be reproduced here. Suffice it to say that they involve terms similar to A_{jk} and B_{jk} defined by Eqs. (1-7, 1-8) and are straightforward to compute once a conformation is known. What the unknowns in Eq. (1-17) are the dimensionless hydrodynamic forces, g_j. From Eq. (B48) of reference 52 (see the same reference for D_{jk}^{-1} and ξ_k),

$$g_j = \sum_{k=1}^{N} D_{jk}^{-1} \xi_k \qquad (1-18)$$

Once a conformation is generated and its charge state estimated, Eqs. (1-17, 1-18) are used to compute μ for a single conformation. The translational diffusion constant, D_t, is also computed using well established methods (22, 56).

1.5 Outline of the Dissertation

In Chapter 2, we are discussing the application of BMM of free solution electrophoresis of peptides to characterize the charge and secondary structure. Next, in Chapter 3, we extended the BMM to model the free solution electrophoretic mobility of peptides to account for the effect of orientationally preaveraged hydrodynamic interaction, OPHI. In Chapter 4, we first developed the bead array-effective medium, BAEM, model for the electrophoresis of macromolecules and

nanoparticle arrays. Chapter 5 is the brownian dynamics application to DNA diffusion in an agarose gel. The DNA fragments are modeled as rods and wormlike chains, and the gel fluid is modeled as a cubic lattice. In Chapter 6, we are studying the measurement of translational diffusion constants of short peptides by pulse field NMR and their use in structure study of peptides. In the last chapter, Chapter 7, we extended the BMM to simulate the viscosity of dilute model bead arrays at low shear.

Chapter 2

Bead Modeling Mehodology of Electrophoresis of Peptides to Characterize the Charge and Secondary Structure

2.1 Introduction of Electrophoresis in Free Solution

In this chapter, we are focused on applying the bead modeling method discussed in previous chapter to simulate the free solution electrophoretic mobility of peptides. Capillary electrophoresis, CE, has been a powerful and widely used tool in the separation and characterization of biomolecules in general (57) and peptides in particular (58-72) over the last 20 years. The method is sensitive (requires little sample) and is also powerful in its ability to separate biomolecules on the basis of size and conformation. Most of the peptide studies cited previously (58-72) involved free solution capillary electrophoresis, FSCE, under dilute conditions. Under the conditions of FSCE, theoretical modeling at a fundamental level (2,3,6-8,12) is possible, and that has enabled the investigator to relate experimental electrophoretic mobility, μ, to chemico-physical properties such as charge, overall size, and conformation. Realistic modeling of peptides pose a particular challenge since the structures are irregular in shape and charge distribution whereas much of the fundamental theory is restricted to spherical particles with a centrosymmetric charge distribution (2,3,6-8).

Modeling has been approached differently by different investigators. Perhaps the most widely used are semi-empirical in nature and based on the Offord model (73), and have their basis in the mobility relation of spheres (3). The mobility is usually written in the form $\mu = A\ Z/M^{\alpha}$ or $A\ \log(Z+B)/M^{\alpha}$, where A, B, and α are constants, Z is the total peptide charge, and M is

the molecular weight (58-65,67-69). Related but more complex and sophisticated semi-empirical models have been developed which account in more detail for the charge distribution, peptide composition, and number of amino acids in the peptide being modeled (67, 69,72). For small peptides, modeling in terms of an "effective sphere" can be very useful in elucidating the variation in charge/conformation with pH (66). The "effective sphere" approach, coupled with attention to the detailed charge state of the model particle, has also been applied to globular proteins (74). Without much additional difficulty, this can be generalized to an "effective ellipsoid" approach (12) and applied to globular proteins (5,13). In order to deal in a more realistic way with the irregular topography and charge distribution of a peptide or protein at the atomic or at least primary structure level, boundary element, BE, (5, 35) and "bead model" (52, 75,76) approaches are available. The latter "bead model" approach is particularly useful when multiple conformations need to be sampled as is the case of particular peptides under a variety of solvent-buffer-pH conditions.

In this chapter, we apply the "bead model" method (52, 75,76) in modeling the free solution electrophoresis of a number of specific peptides (66,68) in order to illustrate how this approach can be used to estimate the pK_a's of specific side groups and also what the influence of conformation has on mobility. This structure based methodology is grounded on fundamental electrohydrodynamic theory. It has previously been applied to 73 peptides ranging in size from 2 to 42 amino acids and, on average, yields model mobilities in good agreement with experiment (52,76). In these studies, however, few restrictions were placed on the dihedral angles that determine the overall conformation of model peptides. As discussed in the next section, detailed accounting of the peptide conformation is taken at the level of both its primary and secondary

structure. In the present work, more attention is given to possible secondary structural characteristics of the model peptides. In principle, the pK_a's of specific charge groups in peptides depend on a variety of factors including their local environments within the peptide (29-31,53,77,78). In this chapter, we follow a straightforward extension of the approach of Lee et al. (78) of separating the environmental effects of charge-charge interactions from other interactions in estimating the pK_a's of charge groups. The electrostatics is solved at the level of the linear Poisson-Boltzmann equation in which the finite size of the subunits is accounted for. In addition, the effect of ion relaxation (distortion of the charge distribution from equilibrium) on mobility is accounted for to lowest order (52).

2.2 Peptide Modeling

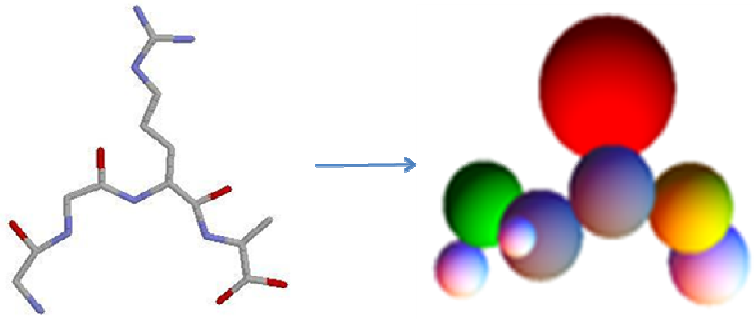

Figure 2-1) Peptide Bead Model. Shown in this example is the 4 amino acid peptide, Gly-Gly-Arg-Ala. Each amino acid is represented by 2 beads, a backbone and a side bead. The coloring scheme of the beads is: N-terminal, green; C-terminal, yellow; interior backbone, dark grey; uncharged side, light grey, basic side, red; acidic side, blue. The commercial program, Mathematica 6.0, is used to construct this Figure. (Particular use is made of the graphics command, "Sphere".)

As shown in Figure 2-1, a peptide made up of N' amino acids is modeled as N = 2N' beads with each amino acid represented by two touching beads. One of these is a "backbone"

bead of radius 0.19 nm and the other bead, representing the "side" bead, is of variable radius. This gives a distance between neighboring touching backbone beads of 3.8 nm that reproduces the C_α to C_α distance in peptides (79). The initial radius of a side bead depends on the amino acid being represented and whether it is interior or at one of the ends of the chain. The hydrodynamic radius, R_h, of a free amino acid is defined in terms of its translational diffusion constant, D_t

$$R_h = \frac{k_B T}{6 \pi \eta D_t} \qquad (2-1)$$

where k_B is Boltzmann's constant, T is absolute temperature, and η is the solvent viscosity. These have been measured for all amino acids and have been reviewed previously (80). When free amino acids condense to form peptides, a single water molecule is released for each amino acid that is added to the peptide chain, and a van der Waals volume, $\delta v = 0.0186$ nm^3, is lost (76,81). If a small molecule with hydrodynamic radius R_h loses volume δv, the resultant hydrodynamic radius, R_s, can be approximated (76)

$$R_s = R_h \left(1 - \frac{3 \delta v}{4 \pi R_h^3} \right)^{1/3} \qquad (2-2)$$

For an "interior" amino acid, we set $\delta v = 0.0186$ nm^3 and for an end amino acid, half this amount. Resulting R_h and R_s's for all amino acids are given in Table 2-1. Since each amino acid is modeled as a dimer of two touching beads with one (the backbone bead) having a radius of 0.19 nm, it is also necessary to know what the radius of the side bead, a_s, has to be to give a

hydrodynamic radius of R_s. These radii are given in Table 2-1 and are computed using well established methodologies in bead hydrodynamics (22,56).

Table 2-1. Radii (in nm) for the Amino Acids

Amino acid (end)	Rh as (int)	Rs as (int)	(int) as (end)	Rs (end)
Ala(A)	0.266	0.243	0.255	0.174	0.192
Arg(R)	0.360	0.348	0.354	0.312	0.319
Asn(N)	0.298	0.280	0.289	0.228	0.239
Asp(D)	0.302	0.285	0.294	0.234	0.246
Cys(C)	0.286	0.267	0.277	0.210	0.224
Gln(Q)	0.323	0.308	0.316	0.264	0.273
Glu(E)	0.314	0.298	0.306	0.251	0.261
Gly(G)	0.232	0.200	0.217	0.0818	0.127
His(H)	0.349	0.336	0.343	0.298	0.306
Ile(I)	0.324	0.309	0.317	0.265	0.275
Leu(L)	0.339	0.326	0.332	0.285	0.294
Lys(K)	0.369	0.358	0.363	0.323	0.329
Met(M)	0.308	0.292	0.300	0.243	0.254
Phe(F)	0.335	0.321	0.328	0.280	0.288
Pro(P)	0.268	0.246	0.257	0.178	0.196
Ser(S)	0.276	0.255	0.265	0.192	0.207
Thr(T)	0.304	0.287	0.296	0.237	0.248
Trp(W)	0.350	0.337	0.344	0.299	0.306
Tyr(Y)	0.357	0.345	0.351	0.308	0.316
Val(V)	0.332	0.318	0.325	0.276	0.284

2.3 Determine the φ, ψ Angels and Conformations

Due to the rigidity of the peptide bond unit, the conformation of a peptide chain can be accurately defined by a succession of dihedral angles, $\{\phi_k, \psi_k\}$ (82-84). For a given amino acid in a peptide that is in a particular secondary structural motif, which shall be referred to as the SSM, specific (ϕ, ψ)'s, or ranges thereof, can be identified. In a right handed α helix, for example, $(\phi, \psi) = (-57°, -47°)$ or (-1.00, -0.82) where the latter set is in radians. (In the present

work, we follow the post 1969 convention of defining the "all trans" conformation of (ϕ, ψ) = (-180°, -180°). In much of the pre 1969 literature, one needs to add 180° to all ϕ, ψ angles. For more general cases, Ramachandran and coworkers (85) constructed diagrams to represent the permitted ranges of (ϕ, ψ) over which there is little steric overlap. Similar diagrams that accounted more accurately for the actual conformational energies of peptides were constructed by Flory and coworkers (86). For polyalanine in a disordered, or "random" conformation, two rather broad regions of (ϕ, ψ)-space can be identified that represent stable conformationals states (see Fig. 3 (p. 253) and Fig. 6 (p. 262) of reference 86). To a good approximation, one region (region 1) consisting of 18.7 % of the allowed (ϕ, ψ)-space has ϕ and ψ falling in the range -2.62 to -1.05 and -1.05 to -0.70, respectively. The remaining region (region 2) has ϕ and ψ falling in the range -2.62 to -1.05 and 1.57 to 3.14, respectively. To mimic this distribution in the generation of a specific peptide conformation, a random number, u, uniformly distributed on the interval (0, 1) is generated. If $u < w_1$ where w_1 is the weighting probability of region 1 (0.187 in the above example), then region 1 is selected for subsequent generation of (ϕ, ψ). Otherwise region 2 is selected. Then, two new independent random numbers, v_1, v_2, are generated and we set

$$\phi = \phi_n + v_1 \Delta\phi_n \qquad (2-3)$$

$$\psi = \psi_n + v_2 \Delta\psi_n \qquad (2-4)$$

where n denotes the region (1 or 2), (ϕ_n, ψ_n) denote the lower bounds on (ϕ, ψ) for this region, and ($\Delta\phi_n$, $\Delta\psi_n$) the corresponding ranges. These quantities are summarized in Table 2-2 for a

variety of different secondary structural motifs, SSMs. These are discussed in a number of texts. We would like to mention Schulz and Schirmer (82) of the I-turn and Flory (86) for the others. For most of these, a single region is sufficient. It would be straightforward to elaborate on this procedure in future study.

Table 2-2. Secondary Structural Motif (SSM) Parameters

Type	SSM	w_1	ϕ_1	$\Delta\phi_1$	ψ_1	$\Delta\psi_1$	ϕ_2	$\Delta\phi_2$	ψ_2	$\Delta\psi_2$
random	R	0.187	-2.62	1.57	-1.05	0.35	-2.62	1.57	1.57	1.57
glycine	G	1.00	-3.14	6.28	-3.14	6.28				
α-helix	H	1.00	-1.00	0.00	-0.82	0.00				
β-sheet	B	1.00	-2.08	0.00	1.97	0.00				
proline-II	J	1.00	-3.14	2.44	1.75	0.69				
I-turn	T	1.00	-1.13	0.31	-1.01	0.76				
I-turn	U	1.00	-1.44	0.31	-0.25	0.88				
trans	X	1.00	-3.14	0.00	-3.14	0.00				

Once the (ϕ, ψ) angles are specified, a unique conformation can be generated using the rotation matrix approach of Flory (86) and employed in previous work (52,76). Consider the generation of a particular conformation and suppose 2k beads (representing k amino acids) have been generated. To add the next amino acid, tentative (ϕ_{k+1}, ψ_{k+1}) are generated following the procedure described in the previous paragraph. Rotation matrices are then used to tentatively place beads 2k+1 (backbone) and 2k+2 (side) at possible positions in the growing chain. If the new backbone bead overlaps any other backbone bead, (ϕ_{k+1}, ψ_{k+1}) is rejected and a new set of dihedral angles is generated. In our work, this strict approach was applied to all beads. To account for the possibility that side groups are frequently flexible and can possibly adopt a more compact conformation in a peptide relative to a single amino acid free in solution, some degree

of "shrinkage" of the side beads is allowed in the present work. In the event of side bead overlap, the side bead (or beads) is (are) tentatively shrunk to the point overlap is eliminated keeping it (them) just touching its (their) associated backbone bead(s). If a tentative side bead radius exceeds the lesser of the current bead radius or a*, the conformation and bead radius is accepted. Otherwise the (ϕ_{k+1}, ψ_{k+1}) set is rejected and a new set of dihedral angles is generated. Setting a* to a large value leads to our earlier approach of not allowing any shrinkage. In the present work, a* is usually set to 0.1 nm. This procedure is continued until the entire peptide is generated. It should be emphasized that not shrinking the backbone beads leads to preservation of the overall conformation of the model peptide.

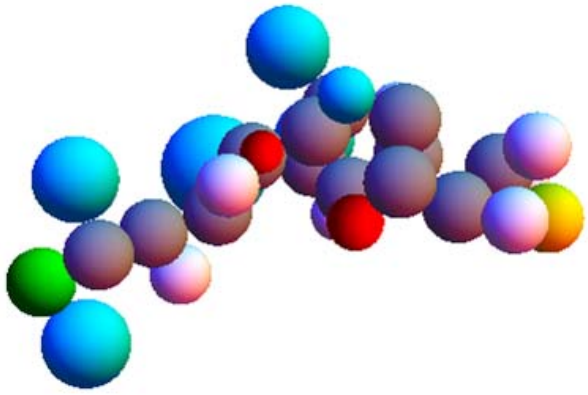

Figure 2-2) Peptide bead model for the 15 amino acid peptide, DDALYDDKNWDRAPQ. The 6th through 12th amino acids are in a α-helical conformation and the end groups are in random conformations. Each amino acid is represented by 2 beads, a backbone and a side bead. The coloring scheme of the beads can be seen in Figure 2-1.

Shown in Figure 2-2 is a sample conformation of the 15 subunit peptide, DDALYDDKNWDRAPQ which shall be called #4 following the convention of reference 68. In generating this particular conformation, the SSM parameters were set to RRRRRHHHHHHHJRR, or $R_5H_7JR_2$ for short. As discussed elsewhere (68), the central 7

residues, DDKNWDR, are likely to be in a helical conformation and the helix breaking proline forces the (ϕ, ψ) angles of the preceding amino acid into the SSM we call J (86). It is not being asserted that the solution conformation of #4 is that shown in Figure 2-2, but only that this represents a plausible structure. One of the objectives of the present study is to combine modeling with electrophoretic mobilities to identify possible solution structures.

2.4 Characterizing the Charge and Secondary Structure of Peptides

We applied the "bead model" method (52,75,76) in modeling the free solution electrophoresis of a number of specific peptides (66, 68) in order to illustrate how this approach can be used to estimate the pK_a's of specific side groups and also what the influence of conformation has on mobility. This structure based methodology is grounded on fundamental electrohydrodynamic theory. Once a conformation is generated, it is necessary to determine the charge state of the peptide at a particular pH under specific solvent/buffer conditions. Let pK_{aj} correspond to the proton disassociation constant of bead j in the peptide. This includes the N- and C- terminals which are backbone beads, as well as the side beads of acidic or basic amino acids. Its average charge state z_j can be calculated by Eqs. (1-15) if the charge group associated with bead j is acidic (Y, C, D, E, C-terminal) or Eqs. (1-16) if the charge group is basic (H, K, R, N-terminal).

A number of factors determine pK_{aj} (29-31, 53, 77). In the present work, net charge-net charge interactions between the group/amino acid of interest and neighboring groups are separated from other factors where the contribution to pK_{aj} from these "other factors" are lumped in the term pK_{aj}^0. Since net charge-net charge interactions are effectively eliminated by solvent screening in the limit of high salt, it is useful to view the pK_{aj}^0's as corresponding to the "high

salt" acid disassociation constants. It should be emphasized that they are not the pK_a's of the free amino acids. In principle, pK_{aj}^0 depends not only on the amino acid, solvent, and buffer; but on the details of the primary and secondary structure in the vicinity of the group/amino acid of interest (29-31,53,77). Following Nozaki et al. (87), and Antosciewicz et al. (30), they shall be approximated with average values of charged amino groups in peptides: 3.8 (C-terminal), 7.5 (N-terminal), 12.0 (R), 10.4 (K), 9.6 (Y), 8.3 (C), 6.3 (H), 4.4 (E), and 4.0 (D). These values represent averages and may lead to inaccurate pK_{aj}'s in particular cases. Eq. (1-14) summarizes how charge-charge interactions contribute to alter pK_{aj}.

Since the majority of the peptides reported in this work are semi-flexible, many conformations are generated (typically 300 to 1000) and the average mobility, μ, is computed. In addition, the correlation of μ with D_t and net charge, Z, with D_t is also examined.

2.5 Test the Accuracy of Bead Modeling Methodology

The BMM discussed in chapter 1 has firstly been applied to characterize the charge and secondary structure of peptides. In order to test the accuracy of the methodology, 73 peptides ranging in size from 2 to 42 amino acids are studied by BMM in the first step. On average, it yields model mobilities in good agreement with experiment (52,76). The result is shown in Table 2-3 and Figure 2-3. In these studies, however, few restrictions were placed on the dihedral angles that determine the overall conformation of model peptides. In discussion below, detailed accounting of the peptide conformation is taken at the level of both its primary and secondary structure. More attention is given to possible secondary structural characteristics of the model peptides. In principle, the pK_a's of specific charge groups in peptides depend on a variety of

factors including their local environments within the peptide (29-31,53,77). In this section, we follow a straightforward extension of the approach of Lee et al. (78) of separating the environmental effects of charge-charge interactions from other interactions in estimating the pK_a's of charge groups. The electrostatics is solved at the level of the linear Poisson-Boltzmann equation in which the finite size of the subunits is accounted for. In addition, the effect of ion relaxation (distortion of the charge distribution from equilibrium) on mobility is accounted for to lowest order (52).

Table 2-3. Mobilities of 73 Peptides

# aa	Sequence	z_T	μ_{exp}	μ_{nr}	μ_r
2	DD	0.694	.103	.122	0.120
2	FD	0.773	.130	.121	0.119
2	EE	0.769	.125	.120	0.118
2	GG	0.818	.217	.205	0.197
2	AA	0.818	.193	.174	0.168
2	PG	0.818	.184	.182	0.176
2	VV	0.817	.154	.124	0.122
2	FG	0.818	.152	.145	0.142
2	FA	0.817	.149	.138	0.135
2	FV	0.817	.139	.120	0.118
2	FF	0.817	.128	.115	0.113
2	FL	0.817	.133	.123	0.120
2	LL	0.817	.146	.131	0.128
2	WW	0.817	.110	.114	0.112
2	YY	0.817	.121	.111	0.109
2	MM	0.817	.139	.142	0.139
3	AAA	0.888	.154	.154	0.150
3	SSS	0.884	.132	.148	0.144
3	FFF	0.886	.104	.0998	0.0982
4	AAAA	0.913	.139	.135	0.132
4	KKKK	4.380	.330	.439	0.341
5	AAAAA	0.921	.123	.122	0.120

5	KKKKK	5.315	.330	.472	0.346
5	YGGFL	0.918	.0975	.0934	0.0921
5	YGGFM	0.921	.095	.096	0.095
5	RPPGF	1.888	.184	.203	0.193
9	AAGIGILTV	0.936	.065	.076	0.075
9	YMDGTMSQV	0.882	.060	.064	0.063
9	VLQELNVTV	0.918	.066	.063	0.063
9	RPPGFSPFR	2.777	.197	.213	0.200
9	AFLPWHRLF	2.831	.166	.196	0.184
9	ACHGRDRRT	4.467	.265	.336	0.285
9	VVRRYPHHE	4.628	.274	.315	0.265
9	ACHGRDRRT	4.467	.99	.336	0.285
10	VISNDVCAQV	0.895	.058	.061	0.061
10	KLVVVGADGV	1.882	.131	.132	0.128
10	KLVVVGAAGV	1.923	.141	.137	0.133
11	NSFCMGGMNRR	2.718	.183	.184	0.178
11	RPKPQQFFGLM	2.904	.170	.189	0.178
11	ACLGRDRRTEE	3.602	.210	.235	0.213
11	CRHRRRHRRGC	8.480	.297	.546	0.317
12	DAEKSDICTDEY	1.644	.099	.101	0.100
12	TTIHYNYICNSS	1.926	.106	.118	0.115
12	PHRERCSDSDGL-ace	2.739	.195	.176	0.167
13	ACPGTDRRTGGGN	2.796	.151	.186	0.175
13	ACPGKDRRTGGGN	3.717	.191	.243	0.219
13	HMTEVRRYPHHER	6.290	.264	.351	0.282
13	HMTEVRHCPHHER	6.287	.264	.363	0.290
14	MGGMNWRPILTIIT	1.926	.102	.112	0.110
14	SPALNKMFCELAKT	2.838	.157	.166	0.159
14	HMTEVVRHCPHHER	6.323	.264	.344	0.279
15	HRSCRRRKRRSCRHR	11.20	.303	.579	0.310
15	RTHCQSHYRRRHCSR	8.423	.290	.440	0.306
15	YAEDGVHATSKPARR	4.441	.214	.247	0.224
16	LAKTCPVRLWVDSTPP	2.857	.151	.150	0.144
16	VVRRCPHQRCSDSGL	4.734	.208	.241	0.212
17	LGRNSFEVCVCACPGRD	2.81	.137	.148	0.143
17	KLVVVGAGDVGKSALTI	2.855	.137	.144	0.139
17	TPPPGTRVQQSQHMTEV	2.878	.142	.143	0.137

17	YKLVVVGAAGVGKSALT	2.903	.142	.147	0.141
17	YKLVVVGACGVGKSALT	2.907	.143	.146	0.140
17	YNYMCNSSGMGGMNRRP	2.824	.143	.148	0.143
17	YKLVVVGAVGVGKSALT	2.903	.151	.144	0.138
17	YKLVVVGARGVGKSALT	3.883	.178	.191	0.178
17	PPPGTRVRVMAIYKQSQ	3.887	.182	.191	0.177
17	DGLAPPQHRIRVEGNLR	4.496	.195	.227	0.205
17	DGLAPPQHRIRVFGNLR	4.532	.190	.228	0.206
17	NHQLLSPAKTGWRIFHP	4.772	.194	.239	0.216
20	VPYEPPEVGSVYHHPLQLHV	3.753	.153	.161	0.152
25	RTHGQSHYRRRHCSRRRLHRIH RRQ	15.29	.290	.543	0.262
30	FLTPKKLQCVDLHVISNDVCAQ VHPQKVTK	6.478	.187	.209	0.189
39	HQIINMWQEVGKAMYAPPISGQI RRIHIGPGRAFYTTKN	7.762	.175	.213	0.189
39	KQIINMWQEVGKAMYAPPISGQI RRIHIGPGRAFYTTKN	7.775	.178	.209	0.186
42	DRVIEVVQGAYRAIRHIPRRIRG QLERRIHIGPGRAFYTTKN	12.17	.208	.292	0.218

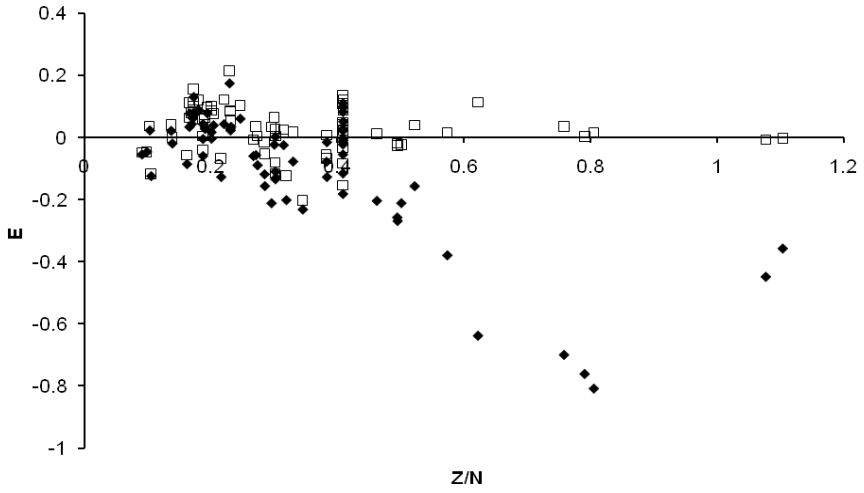

Figure 2-3) E versus Z/N for model mobilities. E is a reduced mobility defined by $(\mu_{exp}-\mu_m)/\mu_{exp}$ where μ_{exp} and μ_{mod} are the experimental and model mobilities, respectively. Results of 73 peptides are included. Unfilled square and filled diamonds correspond to model mobilities with and without the ion relaxation correction, respectively.

2.6 Results

Initially, we shall consider the free solution mobility of the simple peptides GGQA, GGNA, GGRA, and RPPGF studied by Messana and coworkers (66) over the pH range 2 to 4. Given this pH range, the only variable with respect to charge is the pK_a of the C-terminal, pK_a(C-term), since the N-terminal and arginine side chain (in the cases of GGRA and RPPGF) are expected to be fully protonated. By fitting the mobility data versus pH using an effective sphere model, Messana et al. (66) were able to estimate pK_a(C-term) as well as an effective hydrodynamic radius, R_h, of a given peptide. For some peptides (GGQA and GGNA, for example) they found a single R_h was able to fit the data over the entire pH range studied. For others (GGRA and RPPGF, for example), this was not the case. The latter two cases demonstrate that conformation does influence the mobility of these peptides. With the bead model methodology, we are able to investigate the role of conformation in a more specific manner than was previously possible.

The experiments were carried out at 25 °C in 80 mM $Na^+H_2PO_4^-$ (η = 0.0089 poise and ε_w = 78.3). Shown in Figure 2-4 to Figure 2-7 are experimental mobilities (diamonds) of GGNA along with the results of three different bead models. In modeling, the "standard" pKa^0's were used (pK_a(C-term) = 3.80) and 300 different conformations were sampled for the random (solid line, SSM = R_4) and I-turn (dashed line, SSM = GTUR) secondary structure models. Due to the very narrow allowed (ϕ,ψ) of the α-helix, only 10 conformations were carried out for this case (dotted line, SSM = H_4). Due to different average charge-charge interactions in these models, the effective pK_a(C-term) are expected to be different for these three models and that is the case. The pK_a(C-term)'s equal 3.64 (random), 3.37 (I-turn), and 3.40 (helix).

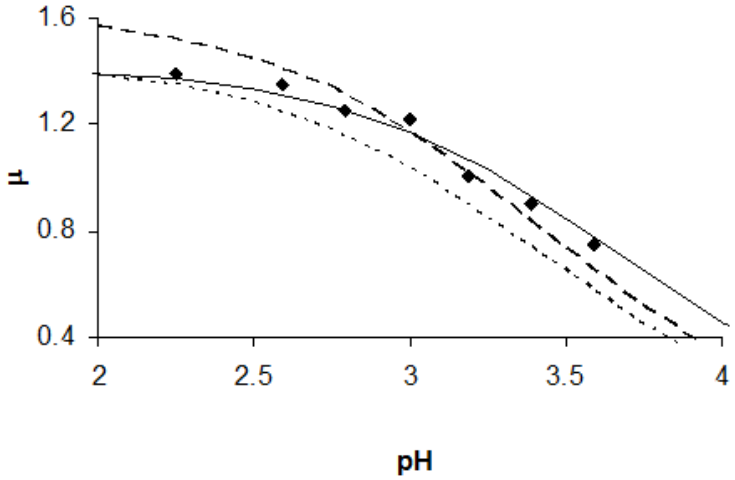

Figure 2-4) Mobility versus pH for GGNA. Experiments (filled diamonds) were carried out in 80 mM aqueous $Na^{+}H_2PO_4^{-}$ buffer at 25 °C (66). Model results are: random (solid line), helix (dotted line), I-turn (dashed line). In these cases, pKa^{0}(C-term) = 3.80.

From Figure 2-4, the "random" bead model is in good agreement with experiment and the pKa(C-term) of 3.64 agrees very well with the value of 3.60 cited by Messana et al. (10). If, however, we examine the α-helix model setting pKa0(C-term) = 4.0 (pKa(C-term) = 3.60), the dotted line in Figure 2-4 is shifted to the right and coincides closely with the "random" model (pKa0(C-term) = 3.8) in the figure. Thus, by minor adjustment of the input parameters, it is straightforward to identify different models that are consistent with the experimental data in this case. For GGQA, the conclusions are similar. In order to say anything more specific about the solution conformation, additional independent experimental data and modeling would be necessary. If, for example, translational diffusion constants, Dt, of the peptides were measured and compared to experiment, it might be possible to further distinguish the solution structure. For the above three bead models, for example, we find Dt = 5.31, 5.54, and 6.08 x 10-6 cm2/sec for the random, α-helix, and I-turn models, respectively.

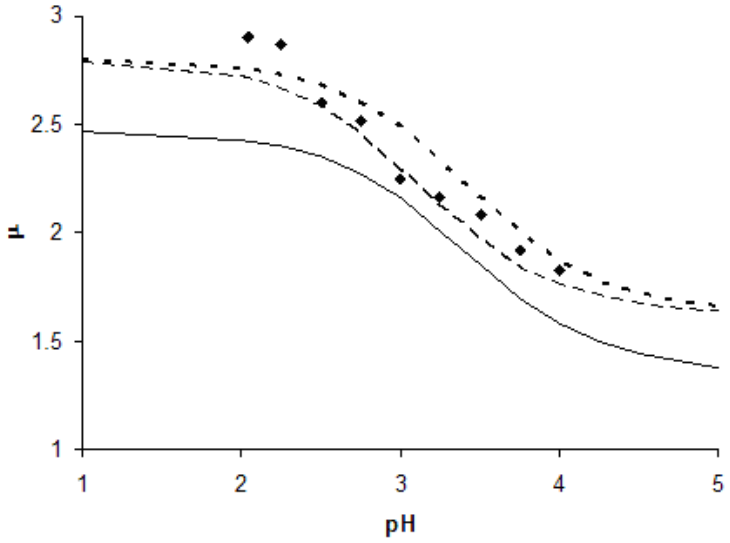

Figure 2-5) Mobility versus pH for GGRA. Experiments (filled diamonds) were carried out in 80 mM aqueous $Na^+H_2PO_4^-$ buffer at 25 °C (66). Model results are: random, pKa^0(C-term) = 3.80 (solid line); I-turn, pKa^0(C-term) = 3.80 (dashed line); I-turn, pKa^0(C-term) = 4.10 (dotted line).

For GGRA, the "random" as well as many other SSM models (H_4 for example) yield mobilities that lie well below experimental values. Compact conformations (which have large D_t's) tend to have high $|\mu|$'s. Thus, models that yield large D_t's appear to be most consistent with experiment in this case. One such model is the I-turn (SSM = GTUR). Shown in Figure 2-5 are experimental mobilities (diamonds) along with random (solid line, SSM = R_4, pKa^0(C-term) = 3.80, pK_a(C-term) = 3.34) and two I-turn models with different pKa^0(C-term). The dashed line corresponds to pKa^0(C-term) = 3.80 (pK_a(C-term) = 3.00) and the dotted line to pKa^0(C-term) = 4.10 (pK_a(C-term) = 3.29). In this example, a compact model (containing an I-turn, for example) with pK_a(C-term) ≅ 3.10 appears to be most consistent with experiment. Shown in Figure 2-6 are typical I-turn (left) and random (right) model conformations. Compared to the typical random conformation, a typical I-turn conformation is more compact. Since steric clashes are

more common in the latter case, there is a greater probability of a side bead such as that of arginine, R, being shrunk to eliminate overlap. Physically, this might correspond to a folding of the R side group in towards the backbone of the peptide (perhaps to form an internal hydrogen bond) relative to a single amino acid in solution. We are not asserting that the solution structure of GGRA necessarily contains an I-turn. However, in order to obtain model mobilities that match experimental ones, the solution conformation must be quite compact and the I-turn model discussed above represents a possible structure.

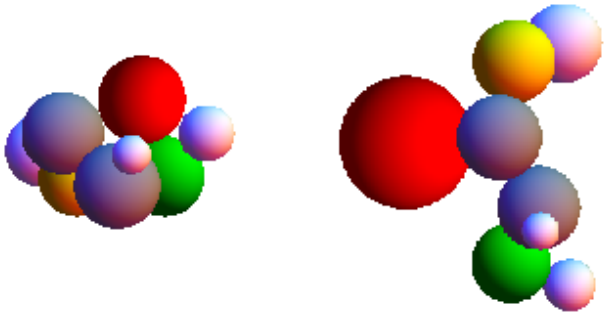

Figure 2-6) Representative conformations for GGRA. Shown at left is an I-turn and at right a "random" model conformation. Note the shrinkage of the arginine, R, side group of the I-turn model. See the caption of Figure 2-1 for an explanation of the color scheme.

To investigate further the relationship between conformation and mobility, the bradykinin fragment 1-5, RPPGF, shall be considered (66). This fragment results from the cleavage of the potent vasodilator bradykinin, RPPGFSPFR, that adopts a compact conformation in solution stabilized by head-to-tail ionic interactions and intramolecular hydrogen bonds (88). Less is known about the solution structure of RPPGF, but there is evidence that a compact conformation adopted in organic solvents gives way to a more unfolded structure in the presence of water (89). Shown in Figure 2-7 is the μ versus pH behavior for RPPGF under the same conditions as the

peptides considered earlier in this section. The filled squares represent experimental mobilities (66), the open diamonds a random model (SSM = R_4), and the x's an I-turn model (SSM = J_2RTU). For the I-turn model, an amino acid preceding a proline is forced into the J secondary structure motif (86) and the "TU" at the end forces the chain into a more compact conformation (82). As in the case of the peptides considered previously, the only adjustable parameter related to charge is pKa^0(C-term). In order to obtain the best agreement between model and experiment, pKa^0(C-term) = 3.30 for this peptide. This, in turn, gives pK_a(C-term) = 3.11 for the random and 3.12 for the I-turn model. The I-turn model is clearly in better agreement with experiment and supports a compact average comformation of this peptide in solution. The corresponding average model D_t's for the random and I-turn models are 4.16 and 4.56 x 10^{-6} cm^2/sec, respectively.

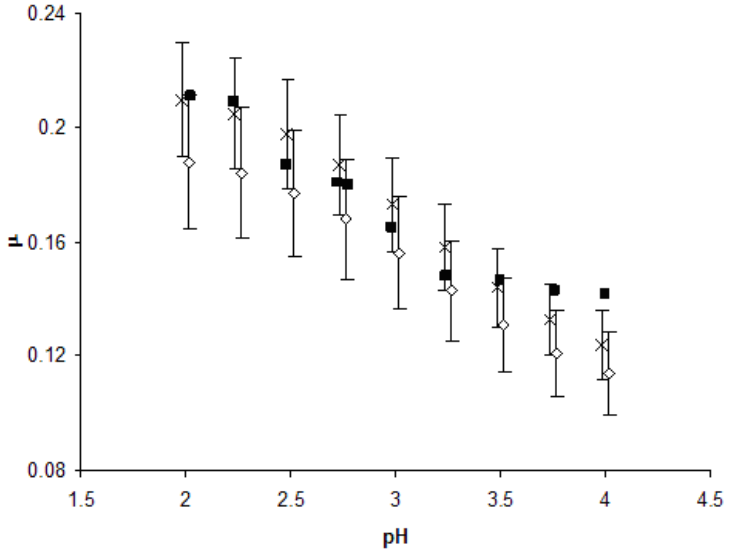

Figure 2-7) Mobility versus pH for RPPGF. Experiments (filled squares) were carried out in 80 mM aqueous $Na^+H_2PO_4^-$ buffer at 25 °C (66). Model results are: random (open diamonds); I-turn (x's). Vertical bars on the model studies represent ranges in μ seen over a large number of different conformations. The parameter, pKa^0(C-term), is set to 3.30 for this peptide.

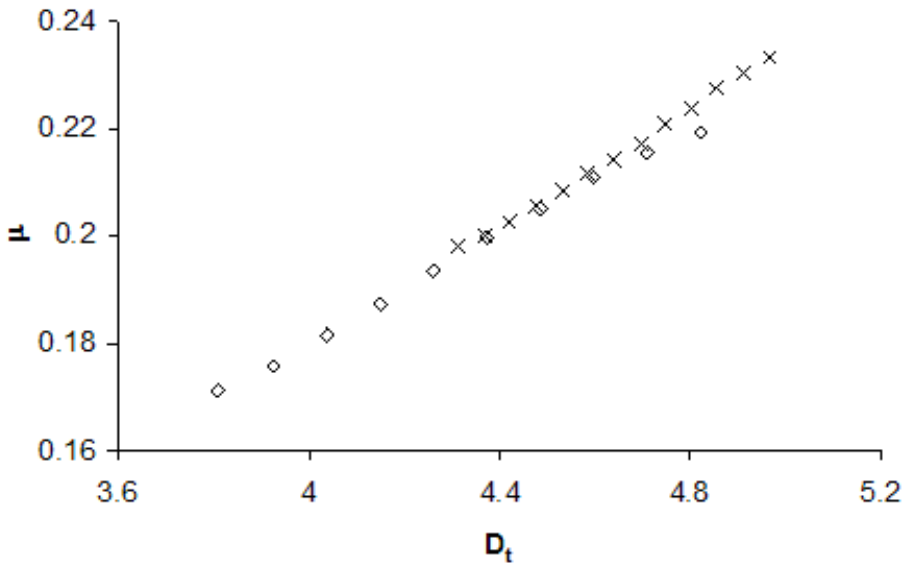

Figure 2-8) Mobility versus D_t for random (diamonds) and I-turn (x's) models. The peptide is RPPGF in 80 mM aqueous $Na^+H_2PO_4^-$ buffer, T = 25 °C, pH = 2.

It should be emphasized that the model mobilities denoted by the diamonds and x's in Figure 2-7 represent the average over many independent conformations (2000 for both random and I-turn models at each pH in the case of this particular peptide), and that there can be considerable variation in μ from one conformation to the next. The vertical bars in Figure 2-7 denote the range of μ seen for each model at each pH. To demonstrate that compact (high D_t) conformations tend to have large |μ|'s and vice versa, it is straightforward to construct a correlation diagram between μ and D_t for a large number of different conformations. The results are plotted in Figure 2-8 for the random (diamonds) and I-turn (x's) models at pH = 2.0. Although, on average, the random model has a lower |μ| and D_t than the I-turn model, this is not true for specific cases. Figure 2-8 clearly shows a direct correlation between μ and compactness

(D_t), and that specific conformations with the same D_t are expected to have nearly identical μ's regardless of their SSM.

As a final illustrative example of how our modeling methodology can be applied to electrophoretic mobility data in an attempt to extract information about group pK_a's and conformation, several peptides studied by Sitaram an coworkers (68) shall be examined. The set of peptides in this study were chosen on the basis of their propensity to adopt specific secondary structures in solution. The mobility measurements were carried out in aqueous media at 25 °C, pH = 3.0, 50 mM $Na^+H_2PO_4^-$. Using the numbering scheme of reference 68, we shall consider,

#4 DDALYDDKNWDRAPQ

#14 DDALYDDKNWDRAPQRCYYQ

and #15 which is identical to #14 except that the C-terminal is amidated (and can bear no charge). The experimental mobility ies of these three peptides is 0.72, 1.17, and 1.52 x 10-8 m2/(V sec) for #4, #14, and #15, respectively. Making the reasonable assumption that #14 and #15 have similar average conformations, the difference in μ between them is most likely due to the protonation state of the C-terminal in #14. In order to account for the difference in μ between #14 and #15, it is necessary to set pKa0(C-term) quite low. By setting pKa0(C-term) = 2.8, modeling is able to account for the mobility difference between the two peptides and that holds for a variety of SSM models. Also note that the three peptides each contain three aspartic acid groups, D, and model mobilities are expected to be sensitive to pKa^0(D). If pKa^0 (D) is set to 4.10 (which is very close to the "average" value of 4.0 mentioned previously), we obtain the

average model μ's summarized in Table 2-4. For #4, the second entry (SSM = $R_5H_7JR_2$) was chosen since it represents what is probably the most plausible conformation for this peptide (68) with the central residues in a helical form and the proline forcing the preceding amino acid into a J secondary motif. The other two entries (SSM = R_{15} (all random), and H_{15} (all helix)) are included for comparison. The limited secondary structure present in $R_5H_7JR_2$ yields a mobility that is not much different from the "all random" model. The "all helix" model, which is an unlikely solution structure and is simply included for the sake of comparison, gives a μ that is substantially larger than the other two. Models R_{15} and $R_5H_7JR_2$ give μ's in good agreement with experiment. A similar strategy is used for #14 and results for three models are shown in Table 2-4. In addition to an "all random" (SSM = R_{20}) and a "partial helix" model with random ends (SSM = $R_5H_7JR_7$), a third "partial helix plus turn" model (SSM = $R_5H_7JTUR_5$) is included as well. In the case of this peptide as observed previously for GGRA and RPPGF, it appears necessary to introduce a turn into the secondary structure in order to account for the large |μ| observed experimentally. The mobility of this last model for #15 is also included in the table. Model mobilities for #14 and #15 in the "partial helix plus turn" model are in fairly good agreement with experiment. We are not claiming that this SSM corresponds to the actual solution secondary structure of these peptides. However, we do assert that in order to account for the large |μ|'s seen experimentally for #14 and #15, a fairly "compact" average conformation is required. The "partial helix plus turn" model is an entirely plausible one that can account for the experimental mobilities.

Table 2-4 . Model Results for Three Peptides from Reference 68.

Peptide	SSM	μ
#4	R_{15}	0.70
"	$R_5H_7JR_2$	0.72
"	H_{15}	0.93
#14	R_{20}	0.88
"	$R_5H_7JR_7$	0.88
"	$R_5H_7JTUR_5$	1.12
#15	"	1.42

2.7 Summary

The principal objective of this study has been to determine, using a fairly detailed modeling procedure, what free solution electrophoretic mobilities of peptides can tell us about: (a) the pK_a's of specific side groups, and (b) possible secondary structure. This structure based modeling procedure is firmly grounded in electrohydrodynamic theory. A peptide consisting of N' amino acids is represented by N = 2N' beads of variable radii and charge state. For flexible peptides, multiple conformations are generated. Conformations are obtained by randomly generating appropriate sets of (ϕ,ψ) angles and then using rotation matrices to place the beads following the long established approach of Flory (46). Secondary structure is incorporated into modeling by specifying secondary structural motifs, SSMs, associated with each amino acid. An SSM, in turn, limits the allowed range of (ϕ,ψ) associated with a particular amino acid (82-86). In order to estimate the pK_a's of specific charge groups, the approach is taken of separating effects of charge-charge interactions from other factors, which are contained in an intrinsic pKa^0 that is left as input parameters for specific charge groups (30, 87). The mobility of a flexible

peptide is estimated by determining the average mobility of a large number (100-5000) of independent conformations.

Modeling is first applied to mobility versus pH data of several small peptides (66) where the only adjustable parameter associated with the charge state of the peptide is the pK_a of the C-terminal. In addition to examining this parameter, the question of possible secondary structure is addressed. For two of the peptides considered, GGNA and GGQA, it is possible to account for the observed mobilities using "random" models. For GGRA and RPPGF, "compact" models (possibly involving an I-turn) must be used to match modeling mobilities with experiment. Finally, three more complicated peptides ranging in size from 15 to 20 amino acids are also examined and characterized (68). Here also, we find evidence of I-turns or some other "compact" structure in 2 of the 3 peptides examined.

Hopefully, the examples examined in this work will stimulate renewed interest in extracting physico-chemical data from mobility experiments. Measurements of electrophoretic mobility coupled with measurement of other transport properties such as translational diffusion constants would be of particular value. Our FORTRAN modeling program is still in the developmental stage and could be generalized in a number of ways. Several possibilities could include a more refined approach of shrinking overlapping side beads or estimating the pK_a's of side groups. The program, upon request to the authors, will be made available free of charge. The program is "stand alone" and does not require access to particular subroutine libraries, but a FORTRAN compiler is necessary. Computing time varies roughly as (# conformations)*N^2. For 5000 conformations of the 5 amino acid peptide RPPGF, overall computation time on a single processor of a Silicon Graphics 4D-380-SX computer was approximately 1 minute.

Chapter 3

Modeling the Free Solution Electrophoretic Mobility of Peptides: Effect of Orientationally Preaveraged Hydrodynamic Interaction

3.1 Introduction

Over the past few years, a principal research effort of our lab has been the development of a modeling methodology that, on the one hand, is firmly grounded in continuum electro hydrodynamic theory at a fundamental level, and on the other hand, can handle models that are complex enough to account for the actual charge distribution and conformation of the actual peptide (38-50, 42,52,75,76). This methodology continues to evolve and a principle objective of the present work is to remove the approximation of orientationally preaveraged hydrodynamic interaction, OPHI, (42, 75) in modeling peptide mobilities. The effect of the OPHI approximation on peptides is studied by examining 73 peptides ranging in size from 2 to 42 amino acids. Experimental (67-69) and model mobilities were compared subject to the OPHI approximation (52,76). In the cases studied here, the OPHI approximation tends to underestimate mobilities by about 2 %. A secondary objective shall be modeling the free solution electrophoretic mobility of several insect oostatic, IO, peptides, in different buffer systems ranging in pH from 2.25 to 8.1 reported by Solinova and coworkers (90). This study illustrates just how well our modeling methodology can reproduce experimental mobilities with little if any adjustment of input parameters.

The outline of this chapter is as follows. In Section 2, the details of the improvements of the methodology are reviewed first in addition to continuum modeling and then the model peptide.

In Section 3, we first examine the effect of the OPHI approximation on the mobility of 73 peptides, and then model and experimental mobilities of IO peptides in several buffer systems are compared. In Section 4, the principal conclusions are stated.

3.2 Theory of BMM to Remove the Approximation of Orientationally Preaveraging Hydrodynamic Interaction, OPHI

The fluid and the peptides studied in this work are also modeled in the BMM discussed in chapter 1 and 2. Starting from the Lorentz reciprocal theorem (49,50) and the singular solution of a point charge in a BGE (91), the fluid velocity, $\underline{v}(\underline{y})$ at position **y** in the vicinity of a N bead array translating with velocity $\underline{u}$ can be written

$$\underline{v}(\underline{y})\Phi(\underline{y},V) = \sum_{J=1}^{N}\int_{S_J} dS_x \underline{\underline{U}}(\underline{r})\cdot\underline{f}(\underline{x}) + \int_V dV_x[\kappa^2 F(\kappa,r)\underline{v}(\underline{x}) + \underline{\underline{U}}(\underline{r})\cdot\underline{s}_e(\underline{x})] + \underline{u}\sum_{J=1}^{N}[\Phi(\underline{y},V_{eJ}) - \kappa^2\int_{V_{eJ}} dV_x F(\kappa,r)] \qquad (3-1)$$

In Eq. (3-1), $\Phi(\underline{y}, V)$ equals 0 if $\underline{y}$ lies outside of the fluid domain, V, equals 1 if **y** lies inside V, and ½ if **y** lies on the surface(s) that just enclose(s) V, $\underline{r} = \underline{x} - \underline{y}$, $r = |\underline{r}|$, S_J denotes the surface enclosing bead J, V_{eJ} denotes the volume exterior to bead J, and κ is the Debye Huckel screening parameter defined by Eq. (1-6). $\underline{F}$ is given by

$$F(\alpha,r) = \frac{e^{-\alpha r}}{4\pi r} \qquad (3-2)$$

$\underline{\underline{U}}$ appearing in Eq. (3-1) is the singular solution (91). It is convenient to break $\underline{\underline{U}}$ up into "isotropic", U_0, and "anisotropic", $\underline{\underline{Z}}$, terms since this decomposition makes the preaveraging

approximation easier to understand. In the preaveraging approximation, all terms involving $\underline{\underline{Z}}$ are simply set to zero. These terms can be written (91)

$$\underline{\underline{U}}(\underline{r}) = U_0(r)\underline{\underline{I}} - \underline{\underline{Z}}(\underline{r}) \qquad (3-3)$$

$$U_0(r) = \frac{2}{3\eta}F(\kappa, r) \qquad (3-4)$$

$$\underline{\underline{Z}}(\underline{r}) = \frac{1}{4\pi\eta\kappa^2}\left(\underline{\underline{nn}} - \frac{1}{3}\underline{\underline{I}}\right)\upsilon(r) \qquad (3-5)$$

$$\upsilon(r) = (3w_3 + 3\kappa w_2 + \kappa^2 w_1) - 3v_3 \qquad (3-6)$$

$$\underline{\underline{nn}} = \frac{1}{r^2}\underline{\underline{rr}} \qquad (3-7)$$

$$w_n = \frac{e^{-\kappa r}}{r^n} \qquad (3-8)$$

$$v_n = \frac{1}{r^n} \qquad (3-9)$$

The quantity, $\underline{I}$, that appears in Eqs. (3-3) and (3-5) is the 3 by 3 identity tensor, and κ is the Debye-Huckel screening parameter. Finally, $\underline{f}(\underline{x})$ represents the hydrodynamic force/area exerted by a particular bead on the fluid, and $\underline{s}_e(\underline{x})$ represents the electrical force/volume on the fluid and is given by Eq. (1-5).

In the present work as in most, but not all (92, 45) theoretical transport studies of bead arrays in an incompressible fluid, it shall be assumed that $\underline{f}(\underline{x})$ is constant over the surface of any given bead, J,

$$\underline{f}(\underline{x}) = \frac{\underline{F}_J}{S_J} \qquad (3-10)$$

where $\underline{F}_J$ is the average hydrodynamic force exerted by bead J on the fluid and S_J is the surface area of bead J. The fluid velocities appearing on the right hand side of Eq. (3-1) are approximated with a sum of singular terms (42),

$$\underline{v}(\underline{x}) = q\sum_{J=1}^{N} \underline{\underline{U}}(\underline{r}_J') \cdot \underline{\underline{c}}_J \cdot \underline{e} \qquad (3-11)$$

where $\underline{r}_J' = \underline{x} - \underline{x}_J$, q is the protonic charge, and the $\underline{\underline{c}}_J$'s are constant tensors to be determined from the boundary conditions as discussed later.

In Eq. (3-1), we are free to choose $\underline{y}$. Choose $\underline{y} = \underline{x}_K$ (center of bead K). It was shown previously (52),

$$\sum_{J=1}^{N}[\Phi(\underline{x}_K, V_{eJ}) - \kappa^2 \int_{V_{eJ}} dV_x F(\kappa, r_K')] = -e^{-\kappa a_K}(\kappa a_K + 1) + \sum_{J\neq K=1}^{N} G_{JK} \qquad (3-12)$$

$$G_{JK} = \frac{1}{2} k_0(\kappa x_{JK})[e^{\kappa a_J}(\kappa a_J - 1) + e^{-\kappa a_J}(\kappa a_J + 1)] \qquad (3-13)$$

$\underline{x}_{JK} = \underline{x}_J - \underline{x}_K$, $\underline{\mathbf{x}}_{JK} = |\underline{x}_{JK}|$, and $k_0(z) = e^{-z}/z$. Also define the following dimensionless integrals

$$\underline{\underline{W}}^{(1)}_{JK} = \frac{6\pi\eta}{\kappa S_J}\int_{S_J} dS_x \underline{\underline{U}}(\underline{r}'_K) \qquad (3-14)$$

$$\underline{\underline{W}}^{(2)}_{JK} = 12\pi\eta\kappa\int_V dV_x F(\kappa, r'_J)\underline{\underline{U}}(\underline{r}'_K) \qquad (3-15)$$

A convenient expansion for $\underline{F}(\kappa,r)$ appearing in Eqs. (3-1)and (3-4) is (52)

$$F(\alpha,r) = \alpha\sum_{n=0}^{\infty}\sum_{m=-n}^{n} i_n(\alpha r_<)k_n(\alpha r_>)Y^*_{n,m}(\Omega_x)Y_{n,m}(\Omega_y) \qquad (3-16)$$

where $Y_{n,m}$ is a spherical harmonic, * denotes complex conjugation, and $r_<$ ($r_>$) is the lesser (greater) of x and y, Ω_x and Ω_y denote the angular coordinates of $\underline{x}$ and $\underline{y}$ in some convenient frame of reference, and i_n and k_n are modified spherical Bessel functions (93). The lowest order terms are: $i_0(z) = \sinh(z)/z$, $i_1(z) = \cosh(z)/z-\sinh(z)/z^2$, $i_2(z) = \sinh(z)/z-3\cosh(z)/z^2+3\sinh(z)/z^3$, $k_0(z)= e^{-z}/z$, $k_1(z) = e^{-z}(1/z+1/z^2)$, $k_2(z) = e^{-z}(1/z+3/z^2+3/z^3)$. Eq. (3-16) makes it possible to perform the necessary averages over the "isotropic" portion of $\underline{\underline{U}}$ exactly.

In evaluating Eq. (3-14), consider the J = K terms first where it is straightforward to show

$$\underline{\underline{W}}^{(1)}_{KK} = k_0(\kappa a_K)\underline{\underline{I}} \qquad (3-17)$$

For J ≠ K, Eq. (3-16) is used in the isotropic term and the averages can be evaluated exactly. For the anisotropic term, consider a Taylor expansion of $\underline{\underline{Z}}$ about $\underline{x}_{JK} = \underline{x}_J - \underline{x}_K$. Choosing the origin to be the center of bead J, then $\underline{x}$ denotes a position relative to $\underline{x}_J$. Below, let lower case j, k, m, and n denote Cartesian components

$$Z_{jk}(\underline{x}_{JK}+\underline{x}) = Z_{jk}(\underline{x}_{JK})+\sum_{m=1}^{3} x_m \nabla_m Z_{jk}(\underline{x}_{JK}) + \frac{1}{2}\sum_{m,n=1}^{3} x_m x_n \nabla_m \nabla_n Z_{jk}(\underline{x}_{JK}) + O(x^3) \qquad (3-18)$$

In what follows, $\underline{\underline{Z}}$ shall be approximated with the first three terms on the right hand side of Eq. (3-18). It can be shown (J ≠ K)

$$\underline{\underline{W}}^{(1)}_{JK} = i_0(\kappa a_J) k_0(\kappa x_{JK}) \underline{\underline{I}} - \frac{3}{2}\left[\underline{\underline{T}}^{(1)}_{JK} + \frac{\kappa^2 a_J^2}{6}\underline{\underline{T}}^{(2)}_{JK}\right] \qquad (3-19)$$

where $\underline{n}_{JK} = \underline{x}_{JK}/x_{JK}$, and

$$\underline{\underline{T}}^{(1)}_{JK} = \frac{1}{\kappa^3}[(3w_3 + 3\kappa w_2 + \kappa^2 w_1) - 3v_3]\left(\underline{\underline{n_{JK} n_{JK}}} - \frac{1}{3}\underline{\underline{I}}\right) \qquad (3-20)$$

$$\underline{\underline{T}}^{(2)}_{JK} = \frac{1}{\kappa^3}(3w_3 + 3\kappa w_2 + \kappa^2 w_1)\left(\underline{\underline{n_{JK} n_{JK}}} - \frac{1}{3}\underline{\underline{I}}\right) \qquad (3-21)$$

In Eqs. (3-20,3--21) above, the argument of w_n and v_n (given by Eqs. (3-8,3--9)) is x_{JK}. For the volume average defined by Eq. (3-15), separate the "isotropic" and "anisotropic" terms,

$$\underline{\underline{W}}^{(2)}_{JK} = I_{JK}\underline{\underline{I}} - 12\pi\eta\kappa\int_V dV_x F(\kappa, r_J')\underline{\underline{Z}}(\underline{r}_K') \qquad (3-22)$$

where

$$I_{JK} = 8\pi\kappa\int_V F(\kappa, r_J') F(\kappa, r_K') dV_x \qquad (3-23)$$

Analytical expressions for I_{JK} are given by Eqs. (B16) through (B22) of reference (52) and shall not be repeated here. These terms can be solved to high order in $(\kappa a_J)^n$. For the second term on the right hand side of Eq. (3-22), we shall only consider solutions to order $(\kappa a_J)^2$ which limits our results to models with κa_J less than about 0.2. Define

$$\underline{\underline{Z}}_{JK} = 12\pi\eta\kappa\int_V dV_x F(\kappa, r_J')\underline{\underline{Z}}(\underline{r}_K') = \underline{\underline{Z}}_{JK}^{as} - \sum_{P=1}^{N}\underline{\underline{Z}}_{JK}^{P} \qquad (3-24)$$

For the final terms on the right hand side of Eq. (3-24), the domain of integration, V, is replaced with "all space" for $\underline{\underline{Z}}_{JK}^{as}$ and V_P (volume of bead P) for $\underline{\underline{Z}}_{JK}^{P}$. It is straightforward to show that $\underline{\underline{Z}}_{KK}^{as} = \underline{\underline{Z}}_{KK}^{K} = 0$. For the remaining terms, $\underline{\underline{Z}}(\underline{r}_K')$ is expanded following Eq. (3-18) and the integrals solved. However, if only terms to order $(\kappa a_J)^2$ are retained, the only remaining terms are $\underline{\underline{Z}}_{JK}^{as}$ and $\underline{\underline{Z}}_{JK}^{K}$. Eq. (3-22) can be written

$$\underline{\underline{W}}_{JK}^{(2)} = I_{JK}\underline{\underline{I}} + 3[k_2(\kappa x_{JK})[\gamma_1(\kappa a_K) - \gamma_1(\kappa x_{JK})] - i_2(\kappa x_{JK})\gamma_2(\kappa x_{JK})]\underline{\underline{N}}_{JK} \qquad (3-25)$$

where

$$\underline{\underline{N}}_{JK} = \underline{\underline{n_{JK}n_{JK}}} - \frac{1}{3}\underline{\underline{I}} \qquad (3-26)$$

$$\gamma_1(z) = -\frac{3}{2z^3}(1-e^{-2z}) + \frac{3}{z^2}e^{-2z} + \frac{3}{2z}(1+e^{-2z}) - \frac{1}{4}(1-e^{-2z}) + \frac{z}{2} + \frac{3}{z^3}\sinh(z) - \frac{3}{z^2}\cosh(z) \qquad (3-27)$$

$$\gamma_2(z) = \left(\frac{3}{z^3} + \frac{6}{z^2} + \frac{3}{z} + \frac{1}{2}\right)e^{-2z} - \left(\frac{3}{z^3} + \frac{3}{z^2}\right)e^{-z} \qquad (3-28)$$

This completes the evaluation of $\underline{\underline{W}}_{JK}^{(1)}$ and $\underline{\underline{W}}_{JK}^{(2)}$ defined by Eqs. (3-14,3-A15).

To determine the $\underline{c}_J$ appearing in Eq. (3-11), average Eq. (3-11) over S_K and set $\langle \underline{v}(\underline{x}) \rangle_K = \underline{\underline{\mu}} \cdot \underline{e}$ where $\underline{\underline{\mu}}$ is the electrophoretic mobility tensor. Since this is true for arbitrary $\underline{e}$,

$$\underline{\underline{\mu}} = \frac{q\kappa}{6\pi\eta} \sum_{J=1}^{N} \underline{\underline{W}}_{KJ}^{(1)} \cdot \underline{\underline{c}}_J \qquad (3-29)$$

We can view the 9 components of $\underline{\underline{W}}_{KJ}^{(1)}$ to be, in turn, particular components of a 3N by 3N supermatrix, $\underline{\underline{W}}^{(1)}$. Once a structure is defined $\underline{\underline{W}}^{(1)}$ is readily determined. Furthermore, $\underline{\underline{W}}^{(1)}$ is invertible and let $\underline{\underline{Y}}^{-1}$ denote the inverse of $\underline{\underline{W}}^{(1)}$. Multiplying Eq. (3-29) by $\underline{\underline{Y}}_{LK}^{-1}$ (a 3 by 3 matrix made up of elements: (row, column) (3L+1,3K+1) to (3L+3,3K+3) of $\underline{\underline{Y}}^{-1}$) and summing over K,

$$\underline{\underline{c}}_J = \frac{6\pi\eta}{q\kappa} \underline{\underline{d}}_J \cdot \underline{\underline{\mu}} \qquad (3-30)$$

$$\underline{\underline{d}}_J = \sum_{K=1}^{N} \underline{\underline{Y}}_{JK}^{-1} \qquad (3-31)$$

Now let

$$\underline{\underline{\chi}}_K = [e^{-\kappa a_K}(\kappa a_K + 1) - \sum_{J \neq K=1}^{N} G_{JK}]\underline{\underline{I}} \qquad (3-32)$$

$$q\underline{\underline{g}}_J \cdot \underline{e} = \underline{F}_J \qquad (3-33)$$

Setting $\underline{y} = \underline{x}_K$ and using Eqs. (3-10) to Eqs. (3-15), Eqs. (3-29) to Eqs. (3-32), Eq. (3-1) becomes

$$(\underline{\underline{\chi}}_K - \frac{1}{2}\sum_{J=1}^{N}\underline{\underline{W}}_{KJ}^{(2)} \cdot \underline{\underline{d}}_J) \cdot \underline{\underline{\mu}} = \frac{q\kappa}{6\pi\eta}\sum_{J=1}^{N}[\underline{\underline{W}}_{JK}^{(1)} \cdot \underline{\underline{g}}_J - \frac{1}{2}h_J\underline{\underline{W}}_{JK}^{(2)}] \qquad (3-34)$$

Next, define

$$S_T = \sum_{J=1}^{N} S_J \qquad (3-35)$$

$$m_K = \frac{S_K}{S_T} \qquad (3-36)$$

$$\underline{\underline{P}}_1^{(K)} = \sum_{J=1}^{N} m_J \underline{\underline{W}}_{KJ}^{(1)} \qquad (3-37)$$

$$\underline{\underline{P}}_2^{(K)} = \sum_{J=1}^{N} h_J \underline{\underline{W}}_{JK}^{(2)} \qquad (3-38)$$

$$\underline{\underline{P}}_3^{(K)} = \sum_{J=1}^{N} \underline{\underline{W}}_{KJ}^{(2)} \cdot \underline{\underline{d}}_J \qquad (3-39)$$

$$\underline{\underline{\chi}} = \sum_{K=1}^{N} m_K \underline{\underline{\chi}}_K \qquad (3-40)$$

$$\underline{\underline{P}}_s = \sum_{K=1}^{N} m_K \underline{\underline{P}}_s^{(K)} \qquad (s=1 \text{ to } 3) \qquad (3-41)$$

Multiplying Eq. (3-34) by m_K, summing over K, and solving for $\underline{\underline{\mu}}$,

$$\underline{\underline{\mu}} = \frac{q\kappa}{6\pi\eta}(\underline{\underline{\chi}} - \frac{1}{2}\underline{\underline{P}}_3)^{-1} \cdot (\sum_{J=1}^{N}\underline{\underline{P}}_1^{(J)} \cdot \underline{\underline{g}}_J - \frac{1}{2}\underline{\underline{P}}_2) \qquad (3-42)$$

Using Eq. (3-42) in (3-34) to eliminate $\underline{\mu}$, the reduced forces, $\underline{g}_J$, must satisfy the series of equations

$$\sum_{J=1}^{N} \underline{\underline{D}}'_{KJ} \cdot \underline{g}_J = \underline{\xi}'_K \qquad (3-43)$$

$$\underline{\underline{D}}'_{KJ} = (\underline{\chi}_K - \frac{1}{2}\underline{\underline{P}}_3^{(K)}) \cdot (\underline{\chi} - \frac{1}{2}\underline{\underline{P}}_3)^{-1} \cdot \underline{\underline{P}}_1^{(J)} - \underline{\underline{W}}_{JK}^{(1)} \qquad (3-44)$$

$$\underline{\xi}'_K = \frac{1}{2}(\underline{\chi}_K - \frac{1}{2}\underline{\underline{P}}_3^{(K)}) \cdot (\underline{\chi} - \frac{1}{2}\underline{\underline{P}}_3)^{-1} \cdot \underline{\underline{P}}_2 - \frac{1}{2}\underline{\underline{P}}_2^{(K)} \qquad (3-45)$$

The 3N by 3N matrix, $\underline{\underline{D}}$', formed from the 3 by 3 $\underline{\underline{D}}_{KJ}$' matrices, is not invertible. We have, however, an additional relation resulting from overall force balance on the bead array (75).

$$\sum_{J=1}^{N} \underline{g}_J = z_T \underline{\underline{I}} \qquad (3-46)$$

where z_T is the total charge of the bead array,

$$z_T = \sum_{J=1}^{N} z_J \qquad (3-47)$$

Multiply both sides of Eq. (3-46) by D_{KK}' = Tr($\underline{\underline{D}}_{KK}$')/3, and then subtract right and left hand sides from the right and left hand sides of Eq. (3-43), and defining

$$\underline{\underline{D}}_{KJ} = \underline{\underline{D}}_{KJ}' - D_{KK}' \underline{\underline{I}} \qquad (3-48)$$

$$\underline{\xi}_K = \underline{\xi}_K' - D_{KK}' z_T \underline{\underline{I}} \qquad (3-49)$$

The resulting set of equations can be written in the form of a 3N by 3N matrix, $\underline{\underline{D}}$, and 3N by 3 matrices, $\underline{\underline{\xi}}$ and $\underline{\underline{g}}$,

$$\underline{\underline{D}} \cdot \underline{\underline{g}} = \underline{\underline{\xi}} \qquad (3-50)$$

The matrix, $\underline{\underline{D}}$, is invertible and let $\underline{\underline{D}}^{-1}$ denote its inverse. Inverting Eq. (3-50),

$$\underline{\underline{g}} = \underline{\underline{D}}^{-1} \cdot \underline{\underline{\xi}} \qquad (3-51)$$

yields the reduced hydrodynamic force tensors, $\underline{\underline{g}}_J$.

We shall conclude by summarizing our approach for the determination of $\underline{\underline{\mu}}$. Once a structure and solution conditions are defined, all terms appearing in Eqs. (3-48) and (3-49) are computed using equations given in this section or in previous work (38,52). $\underline{\underline{D}}$ (from Eqs. (3-44) and (3-48)) and its inverse are then determined. Eq. (3-51) is then used to determine the $\underline{\underline{g}}_J$'s. Finally, these and other known quantities are used in Eq. (3-42) to determine $\underline{\underline{\mu}}$.

In this chapter, four background electrolytes, BGEs, shall be considered. In the peptide studies of Janini and coworkers (67, 69) the experiments were carried out at 22 °C in 50 mM phosphoric acid, H_3PO_4, that was adjusted to pH = 2.5 (relative permittivity of the solvent and solvent viscosity are taken to be 80.00 and 0.955 cp (= 0.00095 kg/(m s)), respectively). Using a pK_a of 2.12 for the first acid dissociation constant of phosphoric acid, the ionic strength, I, is estimated to be 35.3 mM. (The ionic species present are: 3.2 mM H^+, 32.1 mM Na^+, and 35.3 mM $H_2PO_4^-$.) In the IO peptide study of Solinova and coworkers (90), three BGEs covering a range of different pHs are modeled at 25 °C (relative permittivity of solvent and solvent viscosity

are taken to be 78.30 and 0.89 cp, respectively). What shall be called BGE 1 (to use the terminology of reference 90) consists of 50 mM Tris plus 100 mM H_3PO_4 at pH = 2.25. This is modeled as 55.6 mM $H_2PO_4^-$, 5.6 mM H^+, and 50 mM Tris-H^+ (NH_3^+-$C(CH_2OH)_3$), which has an ionic strength, I, of 55.6 mM. BGE 3 consists of 50 mM iminodiacetic acid (NH_2^+-$(CH_2CO_2H)_2$) at pH = 2.40. This is modeled as 8.08 mM NH_2^+-$(CH_2CO_2H)_2$, 4.00 mM H^+, 11.16 mM NH_2^+-$(CH_2CO_2^-)_2$, plus 0.92 mM Cl^- (I = 12.08 mM). The purpose of the Cl^- is to maintain charge neutrality of the solution at this pH. Finally, BGE 4 consists of 40 mM Tris plus 40 mM Tricine ($C(CH_2OH)_3$-NH_2^+-$CH_2CO_2^-$ = Tricine$^-$ -H^+) at pH = 8.1. This is modeled as 20 mM Tris-H^+ plus 20 mM Tricine$^-$ (I = 20 mM). Solinova and coworkers also study an additional buffer, BGE 2, that shall not be considered here since it is similar to BGE 3. There is a relaxation correction procedure included for these buffer conditions that has been explained in detail previously (52). Due to the low charge of the peptides of interest, however, the relaxation correction is small and amounts to less than a 5 % correction.

3.3 Results

3A) Test of the Preaveraging Approximation as Applied to Peptides

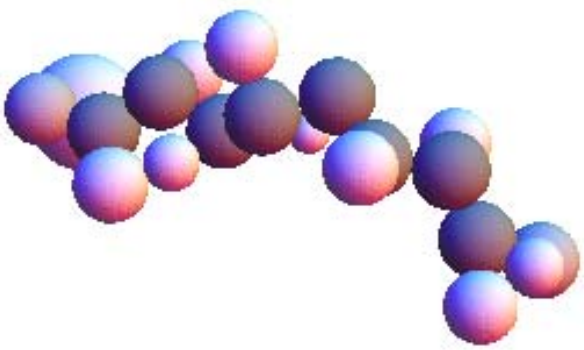

Figure 3-1) Sample Peptide Model. The peptide is $YDPAP_6$ (10 amino acids represented by 20 beads) in a "random" conformation. Interior backbone beads and side beads are denoted by dark grey and white beads, respectively. The terminal backbone beads (at the extreme left and right of the figure) are denoted by an intermediate grey color.

We applied the peptide model and the methodology described in the chapter 1 and 2 to the electrophoretic mobility of 73 peptides (67,69). These have been modeled previously, subject to the approximation of orientationally preaveraged hydrodynamic interaction, OPHI, and model mobilities have been compared with experiment without (76) and with (52) the relaxation correction. A total of 73 peptides are considered ranging in size from 2 to 42 amino acids. Model mobilities without, μ_{model}, and with, μ_{opa}, the OPHI approximation are compared with each other and with experimental mobilities, μ_{exp}, from references 76 and 52. Under the conditions of the experiment (T = 22 °C and 50 mM phosphoric acid at pH = 2.5), the peptides are expected to be largely unfolded. Consequently, peptides are generated using a "random" secondary structural motif (38). Basically, phi-psi angles are chosen at random and possible conformations are accepted or rejected on the basis of steric overlap conditions described previously (38). Typically, mobilities are computed for 100 randomly generated conformations and these are then averaged. Shown in Table 3-1 are the sequences, net charges, z_T, experimental and model mobilities (in $cm^2/kV\ s$). (Note that 1 $cm^2/kV\ s = 10^{-7}\ m^2/kV\ s$). Details regarding the estimation of z_T that includes the "charge regulation" effect can be found elsewhere (38, 52). To see more clearly the accuracy of modeling, consider the reduced mobility, E, defined by

$$E = \frac{\mu_{\exp} - \mu_m}{\mu_{\exp}} \qquad (3-52)$$

where μ_m equals μ_{model} (model without preaveraging) or μ_{opa} (model with orientational preaveraging of hydrodynamic interaction, OPHI). This is plotted in Figure 3-2 versus the net charge to number of amino acids, n, ratio, z_T/n. From Table 3-1 and Figure3-2, the

approximation of orientationally preaveraged hydrodynamic interaction has only a minor effect on model mobilities for the peptides studied. The average E for all 73 peptides equals 0.025 (no preaveraging) and -.002 (with preaveraging). Absolute values of model mobilities without preaveraging are, on average about 2 percent smaller than those with preaveraging. Given the scatter in the data of Figure 3-2, we do not believe that the 2 percent discrepancy between μ_{exp} and μ_{model} is significant. As discussed previously, we believe the main source of discrepancy between modeling and experiment lies in inaccurate estimation of z_T (52), or the assumed form of the peptide conformation (38).

Table 3-1. Mobilities of 73 Peptides

n	Sequence	z_T	μ_{exp}	μ_{model}	μ_{opa}
2	DD	0.690	.103	.124	0.127
2	FD	0.766	.130	.129	0.132
2	EE	0.765	.125	.132	0.135
2	GG	0.818	.217	.198	0.203
2	AA	0.818	.193	.169	0.172
2	PG	0.818	.184	.179	0.184
2	VV	0.817	.154	.133	0.136
2	FG	0.817	.152	.150	0.156
2	FA	0.817	.149	.145	0.148
2	FV	0.817	.139	.133	0.135
2	FF	0.817	.128	.132	0.134
2	FL	0.817	.133	.131	0.134
2	LL	0.817	.146	.130	0.133
2	WW	0.817	.110	.127	0.129
2	YY	0.817	.121	.124	0.126
2	MM	0.817	.139	.144	0.146
3	AAA	0.905	.154	.149	0.155
3	SSS	0.905	.132	.143	0.149
3	FFF	0.905	.104	.116	0.122
4	AAAA	0.926	.139	.131	0.136
4	KKKK	4.416	.330	.329	0.356
5	AAAAA	0.936	.123	.116	0.121
5	KKKKK	5.386	.330	.331	0.355

5	YGGFL	0.936	.098	.097	0.102
5	YGGFM	0.936	.095	.099	0.104
5	RPPGF	1.916	.184	.195	0.205
9	AAGIGILTV	0.947	.065	.073	0.078
9	YMDGTMSQV	0.887	.060	.063	0.069
9	VLQELNVTV	0.928	.066	.064	0.070
9	RPPGFSPFR	2.832	.197	.191	0.207
9	AFLPWHRLF	2.871	.166	.185	0.200
9	ACHGRDRRT	4.508	.265	.270	0.290
9	VVRRYPHHE	4.697	.274	.262	0.288
10	VISNDVCAQV	0.906	.058	.061	0.065
10	KLVVVGADGV	1.902	.131	.123	0.133
10	KLVVVGAAGV	1.940	.141	.126	0.137
11	NSFCMGGMNRR	2.709	.183	.164	0.179
11	RPKPQQFFGLM	2.935	.170	.170	0.185
11	ACLGRDRRTEE	3.626	.210	.205	0.220
11	CRHRRRHRRGC	8.697	.297	.295	0.321
12	DAEKSDICTDEY	1.642	.099	.095	0.103
12	TTIHYNYICNSS	1.942	.106	.112	0.121
12	PHRERCSDSDGL-ace	2.750	.195	.152	0.164
13	ACPGTDRRTGGGN	2.806	.151	.161	0.172
13	ACPGKDRRTGGGN	3.704	.191	.201	0.214
13	HMTEVRRYPHHER	6.427	.264	.268	0.294
13	HMTEVRHCPHHER	6.433	.264	.270	0.297
14	MGGMNWRPILTIIT	1.942	.102	.102	0.110
14	SPALNKMFCELAKT	2.853	.157	.146	0.162
14	HMTEVVRHCPHHER	6.469	.264	.261	0.287
15	HRSCRRRKRRSCRHR	11.37	.303	.292	0.320
15	RTHCQSHYRRRHCSR	8.604	.290	.284	0.312
15	YAEGDVHATSKPARR	4.499	.214	.200	0.218
16	LAKTCPVRLWVDSTPP	2.891	.151	.132	0.144
16	VVRRCPHQRCSDSGL	4.840	.208	.198	0.215
17	LGRNSFEVCVCACPGRD	2.816	.137	.127	0.138
17	KLVVVGAGDVGKSALTI	2.881	.137	.126	0.136
17	TPPPGTRVQQSQHMTEV	2.909	.142	.128	0.139
17	YKLVVVGAAGVGKSALT	2.933	.142	.127	0.139
17	YKLVVVGACGVGKSALT	2.933	.143	.127	0.139
17	YNYMCNSSGMGGMNRRP	2.828	.143	.127	0.138
17	YKLVVVGAVGVGKSALT	2.932	.151	.127	0.138
17	YKLVVVGARGVGKSALT	3.923	.178	.162	0.178
17	PPPGTRVRVMAIYKQSQ	3.916	.182	.165	0.183
17	DGLAPPQHRIRVEGNLR	4.604	.195	.188	0.205

17	DGLAPPQHRIRVFGNLR	4.648	.190	.188	0.206
17	NHQLLSPAKTGWRIFHP	4.836	.194	.197	0.214
20	VPYEPPEVGSVYHHPLQLHV	3.808	.153	.141	0.154
25	RTHGQSHYRRRHCSRRRLHRIHRRQ	15.55	.290	.257	0.283
30	FLTPKKLQCVDLHVISNDVCAQVHPQKVTK	6.615	.187	.166	0.184
39	HQIINMWQEVGKAMYAPPISGQIRRIHIGPG RAFYTTKN	7.820	.175	.162	0.181
39	KQIINMWQEVGKAMYAPPISGQIRRIHIGPG RAFYTTKN	7.820	.178	.162	0.180
42	DRVIEVVQGAYRAIRHIPRRIRGQLERRIHIG PGRAFYTTKN	12.41	.208	.204	0.228

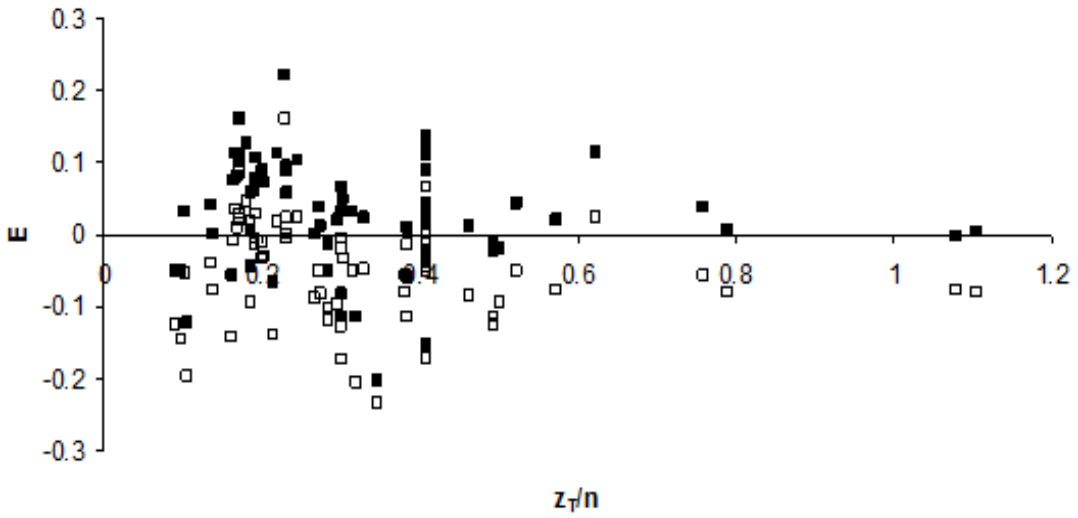

Figure 3-2) E versus z_T/n. E is a reduced mobility defined by $(\mu_{exp}-\mu_m)/\mu_{exp}$ where μ_{exp} and μ_m are the experimental and model mobilities, respectively. All 73 peptides described in Table 3-1 are included in this figure. Filled squares compare experiment with model mobilities without preaveraging, μ_{model}. Unfilled squares compare experiment with model mobilities with preaveraging, μ_{opa}.

3B) Application to Insect Oostatic, IO, Peptides

The sequence of IO peptides: YD, YDP, YDPA, YDPAP, $YDPAP_2$, $YDPAP_3$, $YDPAP_4$, $YDPAP_5$, and $YDPAP_6$ serves as a convenient set to study models and modeling trends as a function of peptide length holding net charge approximately constant. Experimental mobilities

were reported in reference 90. As an initial modeling set, we shall consider "all random" models and use the standard input pK_a^0s given in the previous section. The resulting experimental (asterisks) and model (squares) mobilities in BGE 1, 3, and 4 buffers are summarized in Figures 3-3, 3-4 respectively. Except for the high pH BGE 4 buffer system, agreement between modeling and experiment is quite good. In BGE 4, modeling underestimates the absolute mobility seen experimentally and that could be due to an underestimation of the net absolute charge of the model peptides. At a pH of 8.1, the charge of this particular set of model peptides is particularly sensitive to the pK_a of the N-terminal group, and the pK_a^0(N-term) is set to 7.50 for the squares in Figure 3-4. If this value is reduced from 7.50 to 7.20 (denoted by the triangles in Figure 3-4, much better agreement is obtained.

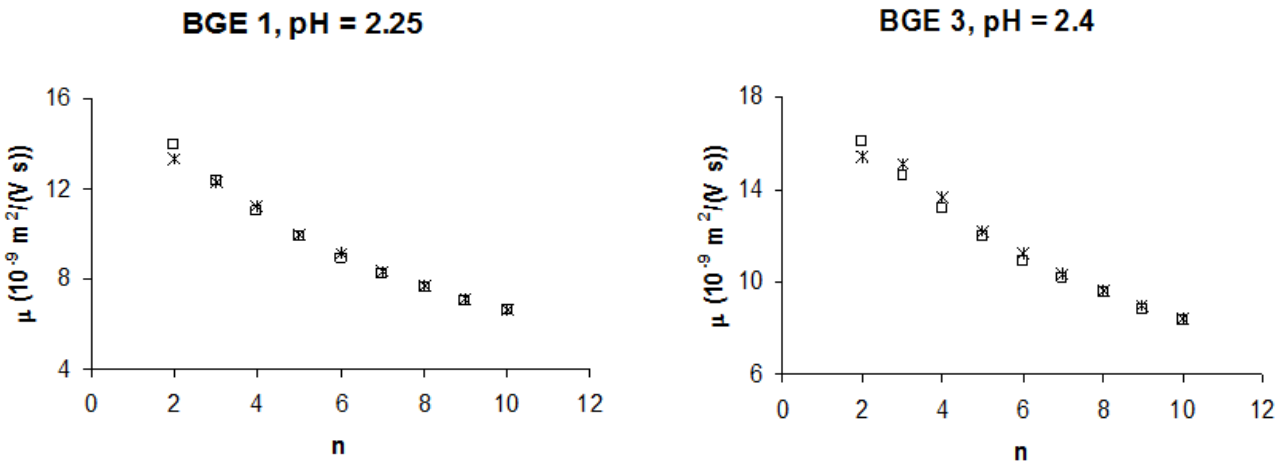

Figure 3-3) Mobilities of IO Peptides in BGE 1 & 3 Buffer, pH = 2.25 & 2.40. Peptides are: YD, YDP, YDPA, YDPAP, $YDPAP_2$, $YDPAP_3$, $YDPAP_4$, $YDPAP_5$, and $YDPAP_6$ for the number of amino acids, n, equal 2 through 10, respectively. Asterisks are experimental mobilities from reference 90 and squares are model mobilities (all random configurations).

Charge regulation can influence the pK_as of individual groups. In BGE 1 or 3 buffer, the net charge of the peptide is sensitive to the pK_a of the C-terminal and also the CO_2H group of

aspartic acid. The pK_as of these two groups are sensitive to the charge state of each other and also the proximity of the N-terminal which is in the protonated (+1) charge state under these buffer conditions. Summarized in the first part of Table 3-2 is pK_a(C-term) as well as net peptide charge, z_T, in protonic units. All pK_a^0 values are set to their standard values. Note that the C-terminal is most acidic for the shortest peptide, YD. This is due to the strong charge-charge interation between C and N-terminals that stabilizes the deprotonated state of the C-terminal. The larger the peptide, the greater the average distance between C and N-terminals and the closer pK_a(C-term) approaches pK_a^0(C-term). In the BGE 4 buffer at pH = 8.1, the C-terminal and aspartic acid side groups are in the deprotonated state. In this case, the peptide charge is particularly sensitive to pK_a(N-term). The pK_a(N-term) as well as z_T for the peptides in BGE 4 are summarized at the end of Table 3-2. In this case, pK_a^0(N-term) is set equal to 7.20. As before, charge regulation is greatest for the shortest peptide where charge-charge interation between C and N-terminals is strongest.

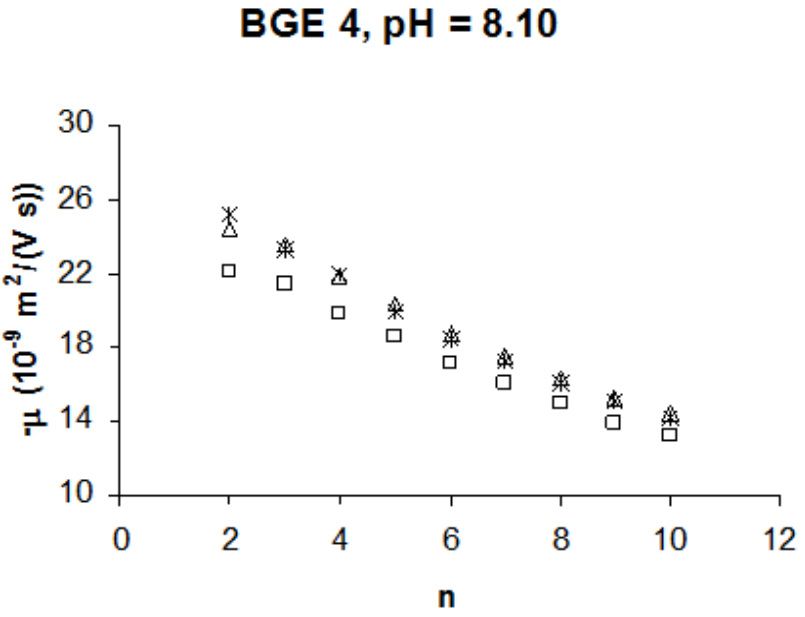

Figure 3-4) Mobilities of IO Peptides in BGE 4 Buffer, pH = 8.10. Peptides are same as in Figure 3-3. Asterisks are experimental mobilities from reference 90, squares are model mobilities with pK_a^0(N-term) = 7.50 (all random configuration), and triangles are model mobilities with pK_a^0(N-term) = 7.20 (all random configurations).

Table 3-2. Charge State and pK_as of Important Groups

Peptide	Buffer	pK_a(C-term)	pK_a(D)	pK_a(N-term)	z_T
YD	BGE 1	3.20	3.66	---	.859
YDP	BGE 1	3.52	3.63	---	.907
YDPA	BGE 1	3.63	3.61	---	.915
YDPAP	BGE 1	3.69	3.64	---	.924
$YDPAP_2$	BGE 1	3.72	3.62	---	.924
$YDPAP_3$	BGE 1	3.74	3.62	---	.925
$YDPAP_4$	BGE 1	3.75	3.61	---	.925
$YDPAP_5$	BGE 1	3.76	3.59	---	.924
$YDPAP_6$	BGE 1	3.76	3.63	---	.928
YD	BGE 4	---	---	8.25	-1.429
YDP	BGE 4	---	---	7.91	-1.621
YDPA	BGE 4	---	---	7.80	-1.676
YDPAP	BGE 4	---	---	7.70	-1.730
$YDPAP_2$	BGE 4	---	---	7.67	-1.742
$YDPAP_3$	BGE 4	---	---	7.65	-1.751
$YDPAP_4$	BGE 4	---	---	7.64	-1.754
$YDPAP_5$	BGE 4	---	---	7.65	-1.753
$YDPAP_6$	BGE 4	---	---	7.61	-1.771

One additional point we would like to address is the sensitivity of μ on the assumed secondary structure of the peptides. In certain cases at least, secondary structure can have a substantial influence on μ (38, 66). The IO peptides considered here, with the exception of YD, tend to have an abundance of prolines. Prolines, in turn, tend to force the dihedral angles of the *preceding* amino acid into a restricted range of values (86). In reference 38, we characterize this restricted range with the secondary structural motif, SSM, called J. Thus, we shall also consider YDP, YDPA, YDPAP, …. $YDPAP_6$ in SSMs RJR, RJRR, RJRJR, …$RJRJ_6R$, respectively. (R

denotes the SSM for "random" secondary structure. In previous cases, the SSM of all the amino acids was R.) In Figure 3-5, we compare experiment (asterisks) with random model (triangles) and "proline restricted" models (diamonds) in BGE 4 buffer. In the model studies pK_a^0(N-term) is set equal to 7.20. In this case, μ is insensitive to the assumed secondary structural model of the peptides.

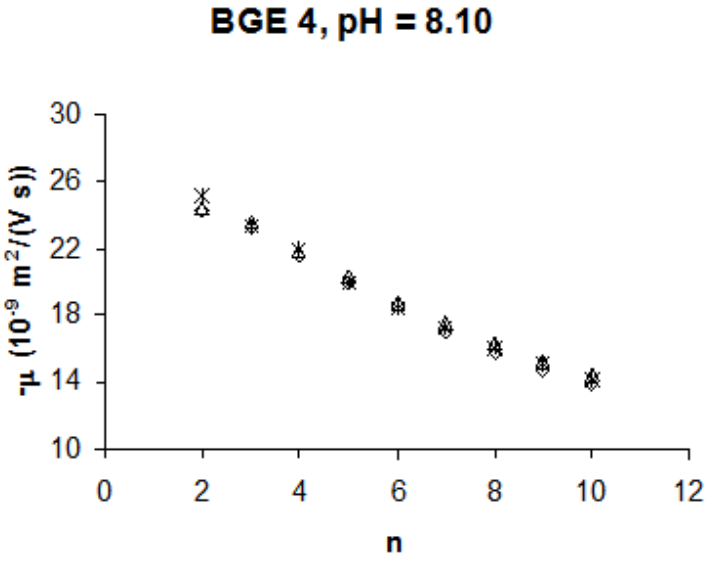

Figure 3-5) Mobilities of IO Peptides in BGE 4 Buffer, pH = 8.10. Peptides are same as in Figure 3-3 and 3-4. Asterisks are experimental mobilities from reference 90, triangles are model mobilities with pK_a^0(N-term) = 7.20 (all random configurations), and diamonds are model mobilities with pK_a^0(N-term) = 7.20 (amino acids preceding prolines in "J configuration").

3.4 Summary

The approximation of orientationally preaveraged hydrodynamic interaction, OPHI, results in an overestimate of mobility by about 2 % for most of the model peptides studied. This value is comparable to the effect seen in the translational diffusion constants of a variety of bead model structures (94). It is likely that other factors such as uncertainties in charge or conformation are responsible for much of the discrepancy between experimental and model mobilities seen in past (52, 76) as well as the present study. We conclude that the OPHI approximation has little effect on the mobilities of model peptides.

Turning next to the study of IO peptides, we have shown that for entirely reasonable model input parameters, it is possible to reproduce quite accurately the free solution electrophoretic mobilities measured previously (90). This is achieved with model peptides in "all random" configurations as well as models in which the prolines force preceding amino acids into more restricted secondary structural motifs. For this set of peptides, we concluded pK_a^0(C-term) ≅ 3.80 and pK_a^0(N-term) ≅ 7.2. The actual pK_as could be quite different from these due to charge regulation.

In further application of this improved bead modeling method, we were able to account for the "internal field" effect. This effect is related to the distortion of an externally applied electric field by the presence of a low dielectric or conducting model structure (75). Preliminary work indicated that this modification altered model mobilities by several percent at most, which is comparable to the OPHI effects seen in the present study. Another area of this study involves carrying out measurements of the translational diffusion constants of peptides by NMR (80) which is discussed in Chapter 6 of this dissertation. It gives the investigator additional information about peptide size and conformation and, coupled with mobility measurements by capillary electrophoresis, a better way of disentangling the influence that both charge and conformation have on mobility.

Chapter 4

The Bead Array-Effective Medium Model for the Electrophoresis of Macromolecules and Nanoparticle Arrays

4.1 Introduction of the Bead Array-Effective Medium Methodology, BAEM

Although several specific areas of application in which electrophoresis is having or has had a profound impact include gel electrophoresis of DNA (95), capillary electrophoresis of peptides (96), and electrophoresis of discrete nanostructure arrays (97), the use of electrophoresis as a tool of *structure elucidation* of biomolecules and nanoparticles has met with more limited success. The reason for this is that the interactions of a particle in solution subjected to a constant external electric field are quite complex and it is a challenge, from a fundamental theoretical standpoint, to account for all of the interactions in sufficient detail to ultimately yield accurate electrophoretic mobilities. A wide variety of different approaches have been used to model variations on the electrophoretic method for different systems. Here, we shall discuss two quite different approaches followed by a discussion of how these two general approaches can be bridged.

Due to the complex shape and charge distribution of many biomolecules and nanoparticle arrays, the simple models discussed in the previous paragraph are approximate at best. Nonetheless, the same fundamental interactions are still present. For complex systems, more approximate approaches have been followed. In the field of peptide separations by free solution capillary electrophoresis, semi-empirical methods based on the Offord model (73) and having their basis in the mobility relation of spheres (3) have been widely used (58, 59, 63, 65, 96).

Related but more complex semi-empirical models have also been developed that account in more detail for charge distribution, peptide composition, and number of amino acids (67, 69, 72). For small peptides and proteins, modeling in terms of an "effective sphere" has proven to be both simple and very useful in structure/charge studies (66, 74, 98). In the field of gel electrophoresis of duplex DNA, the mechanism of DNA migration under constant field conditions depends, to a large extent, on the length of DNA relative to the pore spacing of the gel (95). For long DNAs, reptation theories have been successful in explaining many, but not all of the features of gel electrophoresis (99). For shorter duplex DNAs in a gel, it is possible to make contact with Ogston (100) and related models (101, 102) in which the gel is accounted for as an explicit network of fibers. Brownian dynamics simulation of model DNAs in explicit gels have been carried out (103, 104).

Bead –Array, Effective Medium Methodology, BAEM, is a numerical method further developed by our group to model the electrophoresis of irregularly shaped model particles with an arbitrary charge distribution inside based on the Boundary Element methodology, BEM, which was developed over 10 years ago (32). Like the fundamental approaches considered previously (2, 6-11), the BEM methodology solves the same electro hydrodynamic equations and can be applied to much more realistic model macromolecules such as the free solution electrophoresis of proteins (5, 33, 34), duplex DNA up to 100 base pairs in length (35), and irregular silica sols with a "hairy" outer surface (36). A disadvantage of the BEM approach is that it is time consuming from a computational standpoint (35). This has made it impractical to apply the BEM approach to duplex DNA longer than about 100 bp. It is also impractical to apply it to flexible structures that require sampling of many independent conformations. In order

to deal with this problem, a faster and more efficient method has been developed where the basic structural unit is a spherical bead of arbitrary radius and charge (41, 52, 75, 76). The model structure consists of an arbitrary, non-overlapping array of beads. In this approach, the electrophoretic effect is accounted for explicitly, but not the relaxation effect. For globular biomolecules, however, it is possible to correct for the relaxation effect using the corresponding correction for spheres (52). Recently, this bead method approach was generalized to account for the presence of a gel (41). Long range hydrodynamic interaction is accounted for using the Effective Medium model (105-108). In this chapter, this Bead –Array, Effective Medium, or BAEM methodology is discussed in detail.

The BAEM methodology has several advantages that make it effective and useful in modeling the electrophoresis of biomolecules and nanoparticle arrays both in free solution and in a gel. First, it is grounded firmly in classical electro hydrodynamic theory. Second, it accounts in an approximate way for the irregular shape, charge distribution, and flexibility of a structure of variable size and composition. Third, is capable of yielding accurate electrophoretic mobilities (41, 52, 76). Finally, is sufficiently simple and also computationally fast to be useful to a wide audience. The principle objective of the present work is to generalize the BAEM methodology to remove the approximation of orientational preaveraging of hydrodynamic interaction. This approximation was first introduced by Kirkwood and pervades much of classical polymer theory (109). The error this approximation produces has been studied fairly extensively for the case of the average translational diffusion constant, D_T. For a large thin ring or torus, the preaveraging approximation overestimates D_T by 8.3 % (110). For freely jointed chains of beads, the approximation results in an overestimate of D_T that is usually in the 2 to 3 %

range (111). Although it can be anticipated that the corresponding error the preaveraging approximation produces in the electrophoretic mobility of bead arrays is comparable to those seen in D_T (75), it is a problem that needs to be investigated. In doing so, the BAEM methodology is placed on a firmer foundation. In addition, it now becomes possible to model the individual components of the mobility tensor, $\underline{\mu}$, and explore how mobility depends on the orientation of the model particle relative to an applied electric field.

4.2 Theory/Methodology

In this section, an outline of the derivation of the electrophoretic mobility of a bead array made up of N particles in an Effective Medium, EM, is presented. The fluid is assumed to obey the Brinkman (105) and solvent incompressibility equations defined by

$$\eta \nabla^2 \underline{v}(\underline{x}) - \underline{\nabla}\, p(\underline{x}) = -\underline{s}_e(\underline{x}) + \eta \lambda^2 \underline{v}(\underline{x}) \qquad (4-1)$$

$$\underline{\nabla} \cdot \underline{v}(\underline{x}) = 0 \qquad (4-2)$$

where η is the solvent viscosity, $\underline{v}(\underline{x})$ is the local fluid velocity at point $\underline{x}$ in the fluid, p is the local pressure, $\underline{s}_e(\underline{x})$ is the electrical force/volume on the fluid, and λ (units of 1/length) is a gel screening parameter. In addition to assuming the fluid obeys Eqs. (4-1) and (4-2), the other principal assumptions of the present work are: (a) the perturbation of the electric field in the fluid by the dielectric interior of the bead array (internal field effect) is ignored (75), (b) finite bead size effects are included at least to order $(\lambda a_J)^2$ or $(\kappa a_J)^2$ (where a_J is the radius of bead J and κ (units of 1/length) is the Debye-Huckel screening length of the salt), (c) the hydrodynamic force/area exerted by any bead on the surrounding fluid is approximated with its average value,

(d) electrostatics are treated at the level of the linear Poisson-Boltzmann Equation, (e) the ion relaxation effect is ignored. In past work, detailed derivations of the electrophoretic mobility of bead arrays in free solution (52, 75, 76), and in a EM gel (41) were presented subject to the approximation of preaveraged hydrodynamic interaction (75, 109-111). The principal contribution of the present work is eliminating the approximation of preaveraged hydrodynamic interaction. The interested reader is referred to these earlier works (41, 52, 75, 76) to fill in the gaps in the present treatment.

We begin with the differential form of the Lorentz reciprocal theorem (49, 50),

$$\underline{s}' \cdot \underline{v} + \underline{\nabla} \cdot (\underline{v} \cdot \underline{\underline{\sigma}}_H') \quad = \quad \underline{s} \cdot \underline{v}' + \underline{\nabla} \cdot (\underline{v}' \cdot \underline{\underline{\sigma}}_H) \qquad (4-3)$$

where both primed and unprimed fields satisfy Eqs. (4-1) and (4-2), $\underline{v}$, $\underline{\underline{\sigma}}_H$, and $\underline{s}$ represent the actual fluid velocity, hydrodynamic stress tensor, and external force/volume of our bead model; and $\underline{v}$', $\underline{\underline{\sigma}}_H$', and $\underline{s}$' represent some other field. For the primed field, we choose the singular solution of the Brinkman and solvent incompressibility equations of a point charge located at position $\underline{y}$ of magnitude q z (where q is the protonic charge and z is the valence), in a constant external electric field, $\underline{e}$ (41),

$$\underline{v}'(\underline{x}) \quad = \quad q\, z \underline{\underline{U}}(\underline{r}) \cdot \underline{e} \qquad (4-4)$$

where $\underline{r} = \underline{x} - \underline{y}$,

$$\underline{\underline{U}}(\underline{r}) = \frac{1}{4\pi\eta(\kappa^2-\lambda^2)}\{[w_3+\kappa w_2+\kappa^2 w_1-(w_3'+\lambda w_2'+\lambda^2 w_1')]\underline{\underline{I}}$$

$$-[3w_3+3\kappa w_2+\kappa^2 w_1-(3w_3'+3\lambda w_2'+\lambda^2 w_1')]\underline{\underline{nn}}\} \qquad (4-5)$$

$$\underline{\underline{nn}} = \frac{1}{r^2}\underline{\underline{rr}} \qquad (4-6)$$

$$w_n = \frac{e^{-\kappa r}}{r^n} \qquad (4-7)$$

$$w_n' = \frac{e^{-\lambda r}}{r^n} \qquad (4-8)$$

$$\kappa^2 = \frac{2q^2 CI}{\varepsilon_w k_B T} \qquad (4-9)$$

$$I = \frac{1}{2}\sum_{\alpha} c_{\alpha 0} z_{\alpha}^{\ 2} \qquad (4-10)$$

Above, C = 4π (CGS units), or $1/\varepsilon_0$ where ε_0 is the permittivity of free space (MKS units), ε_w is the solvent dielectric constant, k_B is Boltzmann's constant, T is absolute temperature, $c_{\alpha 0}$ is the ambient concentration of mobile ion species α and z_α is its valence, and the sum in Eq. (4-10) extends over all mobile ion species present. Integration of Eq. (4-3) over the fluid domain, V, exterior to the bead array yields (41)

$$\underline{v}(\underline{y})\Phi(\underline{y},V) = \sum_{J=1}^{N}\int_{S_J} dS_x[\underline{\underline{U}}(\underline{r})\cdot\underline{f}(\underline{x})+\eta\lambda^2(\underline{u}\cdot(\underline{x}-\underline{x}_J))\underline{\underline{U}}(\underline{r})\cdot\underline{n}(\underline{x})]$$

$$+\int_V dV_x[\kappa^2 F(\kappa,r)\underline{v}(\underline{x})+\underline{\underline{U}}(\underline{r})\cdot\underline{s}_e(\underline{x})]+\underline{u}\sum_{J=1}^{N}[\Phi(\underline{y},V_{eJ})-\kappa^2\int_{V_{eJ}} dV_x F(\kappa,r)] \qquad (4-11)$$

In Eq. (4-11), $\underline{u}$ denotes the velocity of the bead array, $\underline{x}_J$ denotes to position of the center of bead J, $\Phi(\underline{y}, V)$ equals 0 if **y** lies outside V, equals 1 if $\underline{y}$ lies inside V, and ½ if $\underline{y}$ lies on the surface(s) that just enclose(s) V, S_J denotes the surface enclosing bead J, and V_{eJ} denotes the volume exterior to bead J. Also, the local unit surface normal, $\underline{n}(\underline{x})$, points outward from a particular bead into the fluid at point $\underline{x}$**,** and $\underline{F}$ is given by

$$F(\alpha, r) = \frac{e^{-\alpha r}}{4\pi r} \qquad (4-12)$$

Finally, $\underline{f}(\underline{x})$ represents the hydrodynamic force/area exerted by a particular bead on the fluid. It is related to the hydrodynamic stress tensor and outward normal by

$$\underline{f}(\underline{x}) = -\underline{\underline{\sigma}}_H(\underline{x}) \cdot \underline{n}(\underline{x}) \qquad (4-13)$$

In the present work as in almost all theoretical transport studies of bead arrays in an incompressible fluid (18-22, 112-114), it shall be assumed that $\underline{f}(\underline{x})$ is constant over the surface of any given bead, J,

$$\underline{f}(\underline{x}) = \frac{\underline{F}_J}{S_J} \qquad (4-14)$$

where $\underline{F}_J$ is the average hydrodynamic force exerted by bead J on the fluid and S_J is the surface area of bead J. The fluid velocities appearing on the right hand side of Eq. (4-11) are approximated with a sum of singular terms (41, 52, 75, 76),

$$\underline{v}(\underline{x}) = q\sum_{J=1}^{N} \underline{\underline{U}}(\underline{r}'_J) \cdot \underline{\underline{c}}_J \cdot \underline{e} \qquad (4-15)$$

where $\underline{r}_J' = \underline{x} - \underline{x}_J$ and the $\underline{c}_J$'s are constant tensors to be determined from the boundary conditions as discussed later. The external electrical forces, $\underline{s}_e(\underline{x})$, are given by (52)

$$\underline{s}_e(\underline{x}) = -q\kappa^2 \underline{e} \sum_{J=1}^{N} h_J F(\kappa, r_J') \qquad (4-16)$$

$r_J' = |\underline{r}_J'|$, and h_J is given by Eq. (A28) of reference (52).

To proceed, choose our field point, $\underline{y}$, to be located at the center of bead K, $\underline{x}_K$. At this stage, it becomes necessary to deal with a number of averages that we turn our attention to. On the basis of previous work (52)

$$\sum_{J=1}^{N} [\Phi(\underline{x}_K, V_{eJ}) - \kappa^2 \int_{V_{eJ}} dV_x F(\kappa, r_K')] = -e^{-\kappa a_K}(\kappa a_K + 1) + \sum_{J \neq K=1}^{N} G_{JK} \qquad (4-17)$$

$$G_{JK} = \frac{1}{2} k_0(\kappa x_{JK})[e^{\kappa a_J}(\kappa a_J - 1) + e^{-\kappa a_J}(\kappa a_J + 1)] \qquad (4-18)$$

$\underline{x}_{JK} = \underline{x}_J - \underline{x}_K$, $\underline{x}_{JK} = |\underline{x}_{JK}|$, and $k_0(z) = e^{-z}/z$. Define the following dimensionless integrals

$$\underline{\underline{W}}_{JK}^{(1)} = \frac{6\pi\eta}{\kappa S_J} \int_{S_J} dS_x \underline{\underline{U}}(\underline{r}_K') \qquad (4-19)$$

$$\underline{\underline{\Theta}}_{JK} = 4\pi\eta\kappa \int_V dV_x F(\kappa, r_J') \underline{\underline{U}}(\underline{r}_K') \qquad (4-20)$$

$$\begin{aligned} \underline{\underline{\Psi}}_{JK} &= \eta\lambda^2 \int_{S_J} dS_x \underline{\underline{U}}(\underline{r}_K') \cdot (\underline{n}(\underline{x})(\underline{x} - \underline{x}_J)) \\ &= \eta\lambda^2 a_J^3 \int d\Omega \underline{\underline{U}}(\underline{x}_{JK} - a_J \underline{n}) \cdot \underline{\underline{nn}} \end{aligned} \qquad (4-21)$$

In the second equality on the right hand side of Eq. (4-21), the integration, $d\Omega$, is over the angular variables of the outward unit normal, $\underline{n}$, to the surface of bead J. (Also, $\underline{\underline{nn}}$ is given by Eq. (4-6).) Shortly, we shall return to the problem of explicitly evaluating Eqs. (4-17) to (4-19). For the moment, we will proceed on the assumption that they are readily determined once a structure has been defined.

To evaluate $\underline{c}_J$, average Eq. (4-15) over S_K and set $\langle \underline{v}(\underline{x}) \rangle_K = \underline{\underline{\mu}} \cdot \underline{e}$ where $\underline{\underline{\mu}}$ is the electrophoretic mobility tensor. Since this is true for arbitrary $\underline{e}$,

$$\underline{\underline{\mu}} = \frac{q\kappa}{6\pi\eta} \sum_{J=1}^{N} \underline{\underline{W}}_{KJ}^{(1)} \cdot \underline{\underline{c}}_J \qquad (4-22)$$

We can view the 9 components of $\underline{\underline{W}}_{KJ}^{(1)}$ to be, in turn, particular components of a 3N by 3N supermatrix, $\underline{\underline{W}}^{(1)}$. Once a structure is defined $\underline{\underline{W}}^{(1)}$ is readily determined. Furthermore, $\underline{\underline{W}}^{(1)}$ is invertible and let $\underline{\underline{Y}}^{-1}$ denote the inverse of $\underline{\underline{W}}^{(1)}$. Multiplying Eq. (4-22) by $\underline{Y}_{LK}^{-1}$ (a 3 by 3 matrix made up of elements: (row, column) (3L+1,3K+1) to (3L+3,3K+3) of $\underline{\underline{Y}}^{-1}$) and summing over K,

$$\underline{\underline{c}}_J = \frac{6\pi\eta}{q\kappa} \underline{\underline{d}}_J \cdot \underline{\underline{\mu}} \qquad (4-23)$$

$$\underline{\underline{d}}_J = \sum_{K=1}^{N} \underline{\underline{Y}}_{JK}^{-1} \qquad (4-24)$$

Now let

$$\underline{\underline{\chi}}_K = [e^{-\kappa a_K}(\kappa a_K + 1) - \sum_{J \neq K=1}^{N} G_{JK}]\underline{\underline{I}} - \sum_{J=1}^{N} \underline{\underline{\Psi}}_{JK} \qquad (4-25)$$

$$\underline{\underline{W}}_{KJ}^{(2)} = 3\underline{\underline{\Theta}}_{JK} \qquad (4-26)$$

$$\underline{\underline{W}}_{KJ}^{(3)} = 3\underline{\underline{\Theta}}_{KJ} \qquad (4-27)$$

$$q\,\underline{\underline{g}}_J \cdot \underline{\underline{e}} = \underline{\underline{F}}_J \qquad (4-28)$$

With the aid of these identities, Eq. (4-25) becomes

$$(\underline{\underline{\chi}}_K - \frac{1}{2}\sum_{J=1}^{N} \underline{\underline{W}}_{KJ}^{(3)} \cdot \underline{\underline{d}}_J) \cdot \underline{\underline{\mu}} = \frac{q\kappa}{6\pi\eta}\sum_{J=1}^{N}[\underline{\underline{W}}_{JK}^{(1)} \cdot \underline{\underline{g}}_J - \frac{1}{2}h_J \underline{\underline{W}}_{KJ}^{(2)}] \qquad (4-29)$$

Next, define

$$S_T = \sum_{J=1}^{N} S_J \qquad (4-30)$$

$$m_K = \frac{S_K}{S_T} \qquad (4-31)$$

$$\underline{\underline{P}}_1^{(K)} = \sum_{J=1}^{N} m_J \underline{\underline{W}}_{KJ}^{(1)} \qquad (4-32)$$

$$\underline{\underline{P}}_2^{(K)} = \sum_{J=1}^{N} h_J \underline{\underline{W}}_{KJ}^{(2)} \qquad (4-33)$$

$$\underline{\underline{P}}_3^{(K)} = \sum_{J=1}^{N} \underline{\underline{W}}_{KJ}^{(3)} \cdot \underline{d}_J \qquad (4-34)$$

$$\underline{\underline{\chi}} = \sum_{K=1}^{N} m_K \underline{\underline{\chi}}_K \qquad (4-35)$$

$$\underline{\underline{P}}_s = \sum_{K=1}^{N} m_K \underline{\underline{P}}_s^{(K)} \qquad (s=1 \; to \; 3) \qquad (4-36)$$

Multiplying Eq. (4-29) by m_K, summing over K, and solving for $\underline{\underline{\mu}}$,

$$\underline{\underline{\mu}} = \frac{q\kappa}{6\pi\eta}(\underline{\underline{\chi}} - \frac{1}{2}\underline{\underline{P}}_3)^{-1} \cdot (\sum_{J=1}^{N} \underline{\underline{P}}_1^{(J)} \cdot \underline{g}_J - \frac{1}{2}\underline{\underline{P}}_2) \qquad (4-37)$$

Using Eq. (4-37) in (4-29) to eliminate $\underline{\underline{\mu}}$, the reduced forces, $\underline{g}_J$, must satisfy the series of equations

$$\sum_{J=1}^{N} \underline{\underline{D}}'_{KJ} \cdot \underline{g}_J = \underline{\xi}'_K \qquad (4-38)$$

$$\underline{\underline{D}}'_{KJ} = (\underline{\underline{\chi}}_K - \frac{1}{2}\underline{\underline{P}}_3^{(K)}) \cdot (\underline{\underline{\chi}} - \frac{1}{2}\underline{\underline{P}}_3)^{-1} \cdot \underline{\underline{P}}_1^{(J)} - \underline{\underline{W}}_{JK}^{(1)} \qquad (4-39)$$

$$\underline{\xi}'_K = \frac{1}{2}(\underline{\underline{\chi}}_K - \frac{1}{2}\underline{\underline{P}}_3^{(K)}) \cdot (\underline{\underline{\chi}} - \frac{1}{2}\underline{\underline{P}}_3)^{-1} \cdot \underline{\underline{P}}_2 - \underline{\underline{P}}_2^{(K)} \qquad (4-40)$$

The 3N by 3N matrix, $\underline{\underline{D}}'$, formed from the 3 by 3 $\underline{\underline{D}}_{KJ}'$ matrices, is not invertible (75). We have, however, an additional relation resulting from overall force balance on the bead array (see Eq. (B18) of reference (41)).

$$\sum_{J=1}^{N} \underline{\underline{g}}_J = z_T \underline{\underline{I}} - \frac{\eta \lambda^2 V_T}{q} \underline{\underline{\mu}} \qquad (4-41)$$

where z_T and V_T are the total charge and volume of the bead array,

$$z_T = \sum_{J=1}^{N} z_J \qquad (4-42)$$

$$V_T = \sum_{J=1}^{N} V_J \qquad (4-43)$$

Using Eq. (4-37) for $\underline{\underline{\mu}}$ in Eq. (4-41)

$$\sum_{J=1}^{N} \left(\underline{\underline{I}} + \frac{\kappa \lambda^2 V_T}{6\pi} \left(\underline{\underline{\chi}} - \frac{1}{2} \underline{\underline{P}}_3 \right)^{-1} \cdot \underline{\underline{P}}_1^{(J)} \right) \cdot \underline{\underline{g}}_J = z_T \underline{\underline{I}} + \frac{\kappa \lambda^2 V_T}{12\pi} \left(\underline{\underline{\chi}} - \frac{1}{2} \underline{\underline{P}}_3 \right)^{-1} \cdot \underline{\underline{P}}_2 \qquad (4-44)$$

Multiplying both sides of Eq. (4-44) by $D_{KK}' = \mathrm{Tr}(\underline{\underline{D}}_{KK}')/3$, subtracting right and left hand sides from the right and left hand sides of Eq. (4-38), and defining

$$\underline{\underline{D}}_{KJ} = \underline{\underline{D}}_{KJ}' - D_{KK}' \left(\underline{\underline{I}} + \frac{\kappa \lambda^2 V_T}{6\pi} \left(\underline{\underline{\chi}} - \frac{1}{2} \underline{\underline{P}}_3 \right)^{-1} \cdot \underline{\underline{P}}_1^{(J)} \right) \qquad (4-45)$$

$$\underline{\underline{\xi}}_K = \underline{\underline{\xi}}_K' - D_{KK}' \left(z_T \underline{\underline{I}} + \frac{\kappa \lambda^2 V_T}{12\pi} \left(\underline{\underline{\chi}} - \frac{1}{2} \underline{\underline{P}}_3 \right)^{-1} \cdot \underline{\underline{P}}_2 \right) \qquad (4-46)$$

The resulting set of equations can be written in the form of a 3N by 3N matrix, $\underline{\underline{D}}$, and 3N by 3 matrices, $\underline{\underline{\xi}}$ and $\underline{\underline{g}}$,

$$\underline{\underline{D}} \cdot \underline{\underline{g}} = \underline{\underline{\xi}} \qquad (4-47)$$

The matrix, $\underline{\underline{D}}$, is invertible and let $\underline{\underline{D}}^{-1}$ denote its inverse. Inverting Eq. (4-47),

$$\underline{\underline{g}} = \underline{\underline{D}}^{-1} \cdot \underline{\underline{\xi}} \qquad (4-48)$$

yields the reduced hydrodynamic force tensors, $\underline{\underline{g}}_J$.

It is worthwhile at this point to summarize our approach to predicting the electrophoretic mobility tensor, $\underline{\underline{\mu}}$, of a model structure. Once a structure and solution conditions are defined, all terms appearing in Eqs. (4-39), (4-40), (4-45), and 4-(46) can be readily determined. Explicit equations for many of the needed terms are given in the Appendix. Then $\underline{\underline{D}}$ (from Eq. (4-45)) and its inverse are determined. Eq. (4-48) is then used to determine the $\underline{\underline{g}}_J$'s. Finally, these and other known quantities are used in Eq. (4-37) to determine $\underline{\underline{\mu}}$.

4.3 Results

3A) Electrophoretic Mobility of Weakly Charged Bead Arrays in an Effective Medium

In this section, we shall first apply the BAEM methodology to rigid rods, rings, and discrete wormlike chain models of various lengths and, in the case of wormlike chains, flexibility. We shall choose bead parameters appropriate for duplex DNA where the hydrodynamic radius, R, equals 1.0 ± 0.1 nm (115, 116) (viewing duplex DNA on a local scale as a right circular cylinder), and the contour length, L (in nm), equals 0.34 n_{bp} where n_{bp} is the number of base pairs. In order

to relate this to a bead model of N identical touching beads of radius a, we use the Hagerman model of a discrete wormlike chain (117, 118). We set L = 2Na and also set the volume of a right circular cylinder, $\pi R^2 L$, equal to that of N identical non-overlapping beads, $4\pi Na^3/3$. This gives $a = (3/2)^{1/2}R = 1.225$ nm and $n_{bp} = 7.2$ N. For the studies reported in this work, the ambient salt is NaCl at a concentration of 0.02 M, the temperature-, T, equals 293.15 K, the solvent viscosity, η, equals 1.002 cp (appropriate for water at 293.15 K), and the solvent dielectric constant, ε_w, equals 80.36. Rather than report directly the effective medium mobility, μ_{EM}, we shall report reduced dimensionless mobilities, E_{EM} and H, defined by

$$H = \frac{E_{EM}}{y} = \frac{3C\eta q}{2\varepsilon_w k_B T}\left(\frac{\mu_{EM}}{y}\right) \qquad (4-49)$$

where $C = 4\pi$ (in CGS units), or $1/\varepsilon_0$ where ε_0 is the permittivity of free space (in MKS units), q is the protonic charge, and $y = q\langle\Lambda_0\rangle/k_B T$ where k_B is Boltzmann's constant and $\langle\Lambda_0\rangle$ is the electrostatic potential averaged over the surface of all beads in the model. Electrostatic potentials for long (119) and finite (120) rods in the framework of the non linear Poisson-Boltzmann equation have been available for some time. Boundary Element procedures are also available to compute $\langle\Lambda_0\rangle$ for arbitrary model particles (28, 32).

The primary objective of the present work is to investigate the effect of orientational preaveraging hydrodynamic interaction on the electrophoretic mobility of nonspherical particles such as rods, rings, and wormlike chains. With that goal in mind, we shall follow the procedure of determining the mobility of a *weakly charged* bead array in an Effective Medium. This simplifies the calculation of $\langle\Lambda_0\rangle$ (47), allows us to ignore the relaxation effect (2, 6-8), as well

as the "steric effect" of a gel (if present) (9, 108). With these simplifications, the procedure outlined in the previous section yields H. This, in turn, is related to the actual reduced mobility, E, by

$$E = H\,y\,X\,S \qquad (4-50)$$

where H is the reduced mobility of a weakly charged bead array given by Eq. (4-49), y is the reduced potential appropriate for the actual particle under the conditions of the experiment, X (which lies between 0 and 1) is the correction for the relaxation effect, and S represents the "steric effect" due to the presence of a gel. We shall return to X in Part B of the Results section. The steric term, S, has been described previously for spherical particles (9, 108), but the form it assumes for nonspherical particles remains largely unexplored. In the present study, it shall not be considered further.

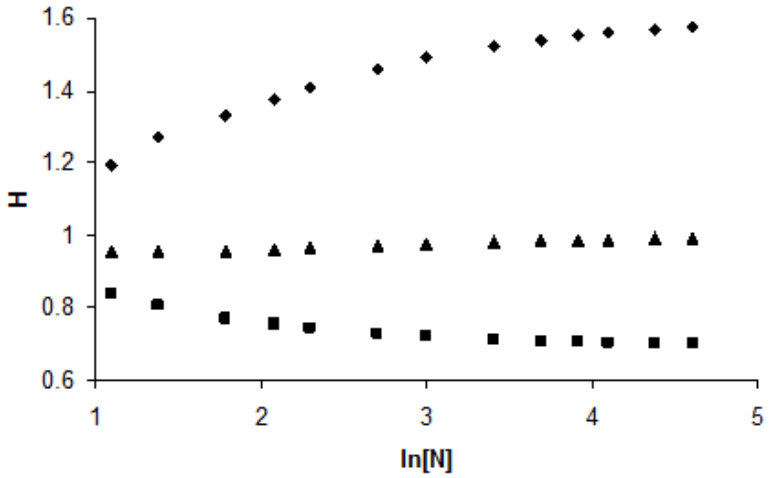

Figure 4-1) Reduced mobility versus bead number for straight rods (no gel). Diamonds and squares correspond to $H_{\|}$ and $H_{\perp}$, respectively. Triangles represent the average over all orientations ($H_{ave} = (H_{\|} + 2H_{\perp})/3$). The rods consist of touching beads of radius a = 1.225 nm in a salt solution of ionic strength 0.02M ($\kappa a = 0.5675$).

Shown in Figure 4-1 is H versus ln(N) for rods (linear strings of N touching beads) oriented parallel, $H_{\|}$ (diamonds), and perpendicular, $H_{\perp}$ (squares), to the applied field direction in the absence of a gel. Triangles represent the average over all orientations, $H_{ave} = (H_{\|} + 2H_{\perp})/3$. A similar plot is shown in Figure 4-2 for plane polygonal rings of touching beads. In this case, diamonds correspond to the axis of symmetry of the ring being parallel to the field direction, $H_{\|}$, and squares to the axis of the ring being perpendicular to the field direction. Triangles correspond to H_{ave} as in the case of rods.

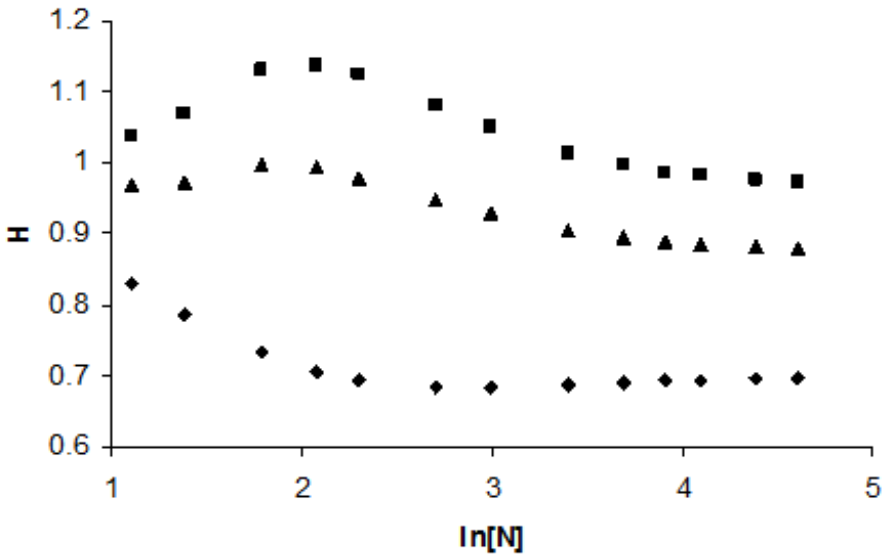

Figure 4-2) Reduced mobility versus bead number for circular rings (no gel). Diamonds correspond to $H_{\|}$ (axis of the ring parallel to the direction of the flow or electric field) and squares to $H_{\perp}$ (axis of the ring perpendicular to direction of electric or flow field). Triangles represent the average over all orientations ($H_{ave} = (H_{\|} + 2H_{\perp})/3$). The rings consist of touching beads of radius a = 1.225 nm in a salt solution of ionic strength 0.02M ($\kappa a = 0.5675$).

In Figure 4-3, $H_{ave}/H_{ave}(opa)$ is plotted versus ln(N) for rods (diamonds) and rings (squares). $H_{ave}(opa)$ is the reduced mobility when inter subunit hydrodynamic interaction is

orientationally preaveraged. What Figure 4-3 tells us is that orientational preaveraging works well for rods, but not so well for large rings. For the largest rings studied (N = 100), orientational preaveraging overestimates H_{ave} by about 12 %. Qualitatively, this is similar to what is seen in the translational diffusion of rods and rings. Orientational preaveraging is very accurate for rods, but less so for large rings (110).

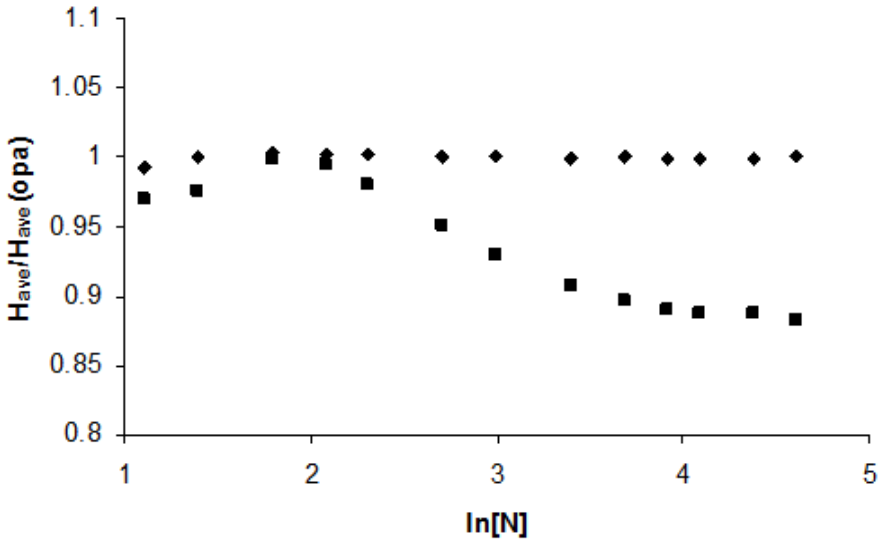

Figure 4-3) Effect of the "orientational preaveraging" approximation on the electrophoretic mobility of rods and rings (no gel). Diamonds and squares correspond to rods and rings, respectively. Conditions are the same as in Figures 4-1 and 4-2.

Although short duplex DNA can be accurately modeled as a rigid rod, a more accurate model for longer DNAs is a wormlike chain with persistence length P. As discussed earlier, we shall next consider the mobility of discrete wormlike chains using the Hagerman model (117, 118). A single chain conformation is generated using random numbers and this procedure is equivalent to selecting a single chain conformation from an equilibrium distribution. The eigenvalues of the electrophoretic mobility tensor as well as an orientationally averaged mobility

are then computed for this particular chain. Mean mobilities are then obtained by simple averaging over an "ensemble" of independent chains. An "ensemble" of 100 chains is usually sufficient to determine the average mobility of wormlike chain to within 1 %. For the persistence length, P, of DNA, a value of about 50 nm is appropriate (121).

At this stage, we would also like to introduce the possible presence of a gel through λ (units of 1/length) starting with Eq. (4-1) and appearing throughout the Methods section of this paper. The gel consists of uniform "segments" of friction coefficient, ζ_s, and number density n_s. These parameters are related to λ by the relation (107)

$$n_s \zeta_s = \eta \lambda^2 \qquad (4-51)$$

Eq. (4-51) makes it possible to relate λ to the characteristics of a particular gel. The gel is typically characterized by its chemical composition (agarose or polyacrylamide, for example), its mass concentration, M, (typically in gm of dry gel material/total volume), dry density of gel material, ρ_g, (which equals 1.64 gm/ml for agarose (122)), the ratio of dry gel volume to hydrated gel volume, ω_s (which equals 0.625 for agarose (123)), and hydrated segment radius, σ, (which might be equated to the fiber radius of 1.9 nm which comes from low angle X-ray scattering (124)). Accounting for the hydrodynamic interaction between the gel segments and making use of the friction coefficient of a bead of radius σ in an EM of screening parameter λ (125)

$$\zeta_s = 6\pi\eta\sigma(1 + \lambda\sigma + \frac{1}{9}\lambda^2\sigma^2) \qquad (4-52)$$

In terms of parameters defined above, we can write

$$M = \frac{4}{3}\pi \rho_g \omega_s n_s \sigma^3 \qquad (4-53)$$

Substituting Eqs. (4-52) and (4-53) into Eq. (4-51) and solving for λ yields

$$\lambda = \frac{A}{2\sigma}\left(1+\sqrt{\frac{5}{9}+\frac{4}{A}}\right)/\left(1-\frac{A}{9}\right) \qquad (4-54)$$

where $A = 9M/(2\rho_g\omega_s)$ and is dimensionless.

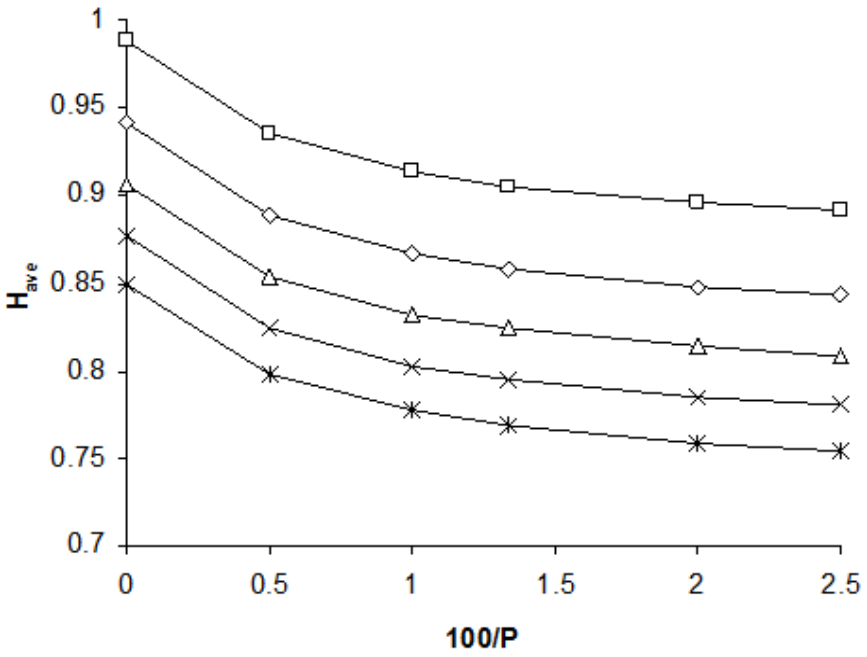

Figure 4-4) Reduced mobility versus stiffness for wormlike chains at different gel concentrations. All chains are made up of 50 beads (corresponding to 360 base pairs of duplex DNA) and the persistence length, P, is set to 50 nm. The gel concentration, M (in gm/ml) equals 0.000 (squares), 0.005 (diamonds), 0.010 (triangles), 0.015 (crosses), 0.020 (asterisks).

Shown in Figure 4-4 is H_{ave} versus 100/P (P in nm) for a 50 bead discrete wormlike chain (360 base pairs) in agarose gels of different concentration. The top to bottom curves correspond to M = 0.000, 0.005, 0.010, 0.015, and 0.020 gm/ml, respectively. Not surprisingly, the presence of a gel causes H_{ave} to decrease. As a charged particle subjected to an external electric field migrates through a gel, stationary gel segments generate hydrodynamic backflow that reduce the mobility. However, at constant gel concentration, H_{ave} decreases with decreasing P (increasing flexibility). Although counterintuitive, this behavior is consistent with Boundary Element studies of curved rods where it was observed mobility decreases as rod curvature (flexibility) increases (35). This behavior can be understood as follows. As P decreases, the largest absolute eigenvalue of the mobility tensor (corresponding to mobility in the direction of least resistance) decreases much more rapidly than the remaining two eigenvalues increase in absolute value. The net result is H_{ave} decreases with increasing flexibility. Figure 4-5 shows how flexibility and a gel influence the effect of orientational preaveraging on the same 50 bead discrete wormlike chain. At constant P, orientational preaveraging works best at low gel concentration and results in and the overestimate in H_{ave} increases gradually as M is raised from 0.000 to 0.020 gm agarose/ml. This is true regardless of P. As P is reduced from ∞ (rigid rod) to 40 nm at constant gel concentration, orientational preaveraging causes an overestimate of H_{ave} by 8 to 10 %. Thus, the error caused by orientational preaveraging is comparable for a ring and flexible wormlike chain.

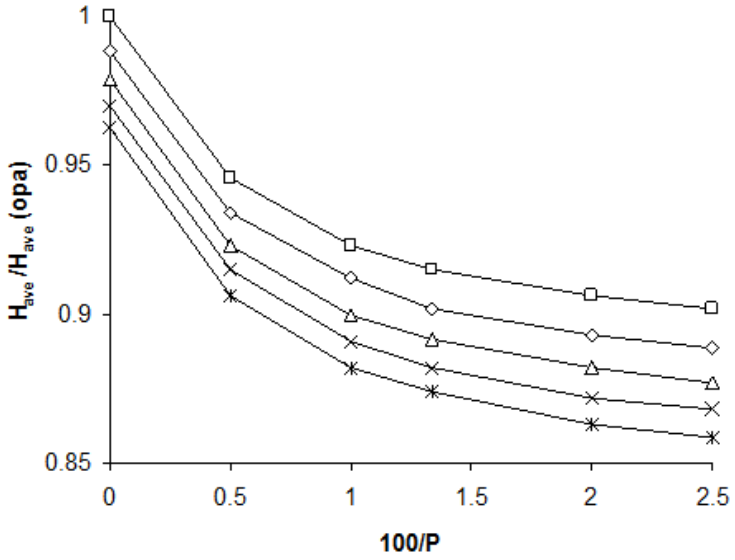

Figure 4-5) Effect of the "orientational preaveraging" approximation on the electrophoretic mobility of wormlike chains at different gel concentrations. All chains are made up of 50 beads (corresponding to 360 base pairs of duplex DNA) and the persistence length, P, is set to 50 nm. The gel concentration, M (in gm/ml) equals 0.000 (squares), 0.005 (diamonds), 0.010 (triangles), 0.015 (crosses), 0.020 (asterisks).

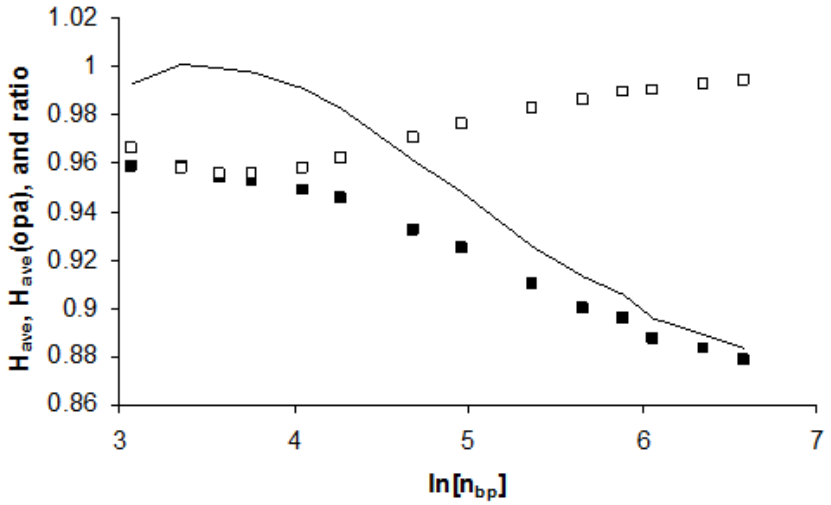

Figure 4-6) Dependence of reduced mobility (no gel) on length for wormlike chains (appropriate for DNA with P = 50 nm) and effect of orientational preaveraging. Filled squares correspond to H_{ave}, unfilled squares to H_{ave}(opa), and the solid line to the ratio, H_{ave}/H_{ave}(opa). Discrete bead models contain $n_{bp}/7.2$ touching beads of radius 1.225 nm in a salt solution of ionic strength I = 0.02 M (κa = 0.5675).

The reduced mobility of wormlike chains of variable length and P = 50 nm (appropriate for DNA (121)) in the absence of a gel are shown in Figure 4-6. Filled squares correspond to H_{ave} and open squares to H_{ave}(opa). The solid line represents H_{ave}/ H_{ave}(opa) or the effect of orientational preaveraging. Orientational preaveraging works well for short wormlike chains near the rigid rod limit, but not so well for long wormlike chains. When P = L (about 147 base pairs) orientational preaveraging overestimates H_{ave} by 5 %. Figure 4-7 is similar to Figure 4-6, except for the presence of agarose gel with M = 0.020 gm/ml. Compared to the "no gel" situation depicted in Figure 4-6, there is an overall reduction in mobility due to presence of a gel. Qualitatively, the behavior seen here is similar to that seen in Figure 4-6. Finally it should also be noted that the preaveraging effect depends on a number of factors in addition to flexibility and overall particle size. Shown in Figure 4-8 is the ratio, H_{ave}/H_{ave}(opa) for 50 bead wormlike chains (P = 50 nm, a = 1.225 nm) as a function of ionic strength. The preaveraging approximation works better low ionic strength or small κa.

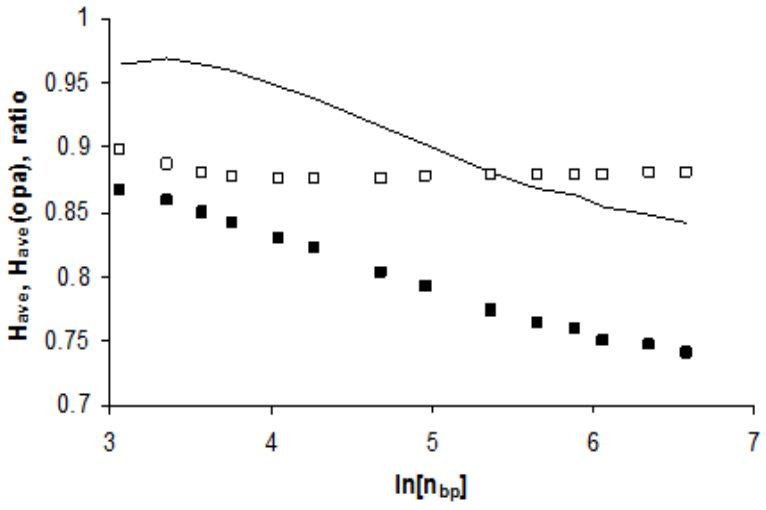

Figure 4-7) Dependence of reduced mobility (in M = 0.02 gm/ml agarose gel) on length for wormlike chains (appropriate for DNA with P = 50 nm) and effect of orientational preaveraging. Filled squares correspond to H_{ave}, unfilled squares to H_{ave}(opa), and the solid line to the ratio, H_{ave}/H_{ave}(opa). Discrete bead models contain $n_{bp}/7.2$ touching beads of radius 1.225 nm in a salt solution of ionic strength I = 0.02 M (κa = 0.5675).

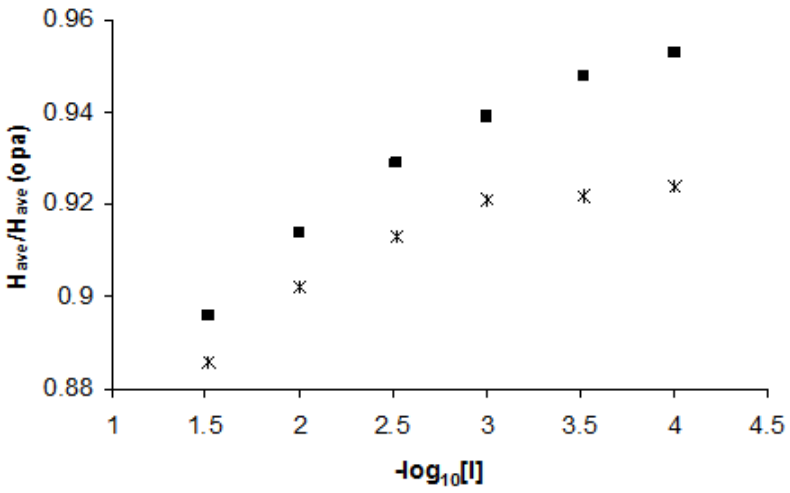

Figure 4-8) Effect of ionic strength on orientational preaveraging of 360 bp DNA wormlike chain models (P = 50 nm). Squares correspond to no gel and asterisks to M =0 .02 gm/ml agarose.

3 B) Application to Free Solution Electrophoresis of DNA

A problem of longstanding interest has been the free solution electrophoresis of DNA as a function of length. This problem has been studied theoretically by Boundary Element, BE, methods in which the DNA is modeled as a finite circular cylinder (43, 78) or in terms of a more realistic surface model (79). In free solution (no gel present), the absolute electrophoretic mobility of duplex DNA rises with increasing length and reaches a "plateau" value above several hundred base pairs, n_{bp} (128). The plateau mobility in aqueous solution depends on salt type, ionic strength, and temperature (129). BE modeling of straight rod models also exhibit plateau behavior at large n_{bp}, but the plateau value of the absolute mobility is substantially larger than observed experimentally. In addition, the rise to plateau behavior in modeling with n_{bp} is more gradual in modeling (of straight rods) than in experiment (35). By carrying out BE studies of curved DNA rod models in the 60 to 100 bp range, the discrepancy was attributed to curvature of

the DNA (35). The methodology developed in the present work gives us an opportunity to reexamine this problem and extend the analysis to longer DNA models as well as studies ensembles of wormlike chains instead of single curved species. Such studies are simply not feasible using the BE approach due to the considerable computation time involved (35). From Eq. (4-49) and (4-50), the free solution electrophoretic mobility, μ, can be written

$$\mu = \frac{2\varepsilon_w k_B T}{3C\eta q} y H X \qquad (4-55)$$

where y is the reduced zeta potential averaged over the surface of the DNA, H is the reduced Effective Medium mobility (calculated using discrete bead model wormlike chains and the procedures developed in this work), and X is the correction for the relaxation effect. The reduced zeta potential, y, can be computed by a BE procedure (35).

For globular particles such as peptides and proteins, the relaxation correction can be estimated using the relaxation correction of a sphere of hydrodynamic radius equal to that of the particle of interest (14, 52). For finite straight rods (right circular cylinders of length L and diameter d), we have determined X by a BE study of rods of different y, salt, and ξ = d/L. The relaxation correction for finite straight rods can be written

$$X = 1 - y^2(a_1 + a_2 y + a_3 y^2)/100 \qquad (4-56)$$

$$a_i = b_{0i} + b_{1i}\xi + b_{2i}\xi^2 \qquad (4-57)$$

Table 4-1 gives the b_{ji} coefficients in aqueous NaCl salt solutions at 20 °C. For other salt solutions, the relaxation correction coefficients will be different due to differences in the mobilities of mobile salt ions (14).

Table 4-1. Relaxation Coefficients for Finite Rods in NaCl Aqueous Solution at 20 °C

(NaCl) (mM)	i	b_{0i}	b_{1i}	b_{2i}
2	0	+1.436	-1.386	-1.197
"	1	-0.0015	-0.0035	-0.0079
"	2	-0.0106	+0.0106	+0.0307
20	0	+1.678	+4.098	-11.202
"	1	-0.0027	-0.0522	+0.1219
"	2	-0.0204	-0.0394	+0.1316
100	0	+2.211	+2.413	-4.921
"	1	-0.0098	-0.0670	+0.1465
"	2	-0.0387	+0.0771	-0.1316

On the basis of BE model studies, the relaxation correction for *curved* rods is greater than for straight rods under otherwise identical conditions. For curved rods or wormlike chains of persistence length P, the relaxation correction can be approximated by Eqs. (4-56) to (4-57) provided ξ is set equal to d/L_{eff} where

$$L_{eff} = P(1 - e^{-L/P}) \qquad (4-58)$$

Figure 4-9 summarizes absolute model mobilities for rigid rods (unfilled squares) and wormlike chains with P = 50 nm (filled squares) in aqueous 20 mM NaCl solution at 20 °C. The rigid rod mobilities exhibit the gradual rise to plateau behavior mentioned previously and at the longest rod studied (n_{bp} = 720), $|\mu(\text{rod})| \approx 0.43$ cm^2/kV sec. The wormlike chain model mobilities reach a plateau value of 0.375 cm^2/kV sec around 150 base pairs and then decrease,

but only slightly, for longer chains. Under these conditions, the experimental mobility, $|\mu|_{experiment}$, equals approximately 0.38 cm^2/kV sec for high molecular weight DNA (129). Thus, agreement between experiment and modeling is good provided account is made for the finite flexibility of the DNA.

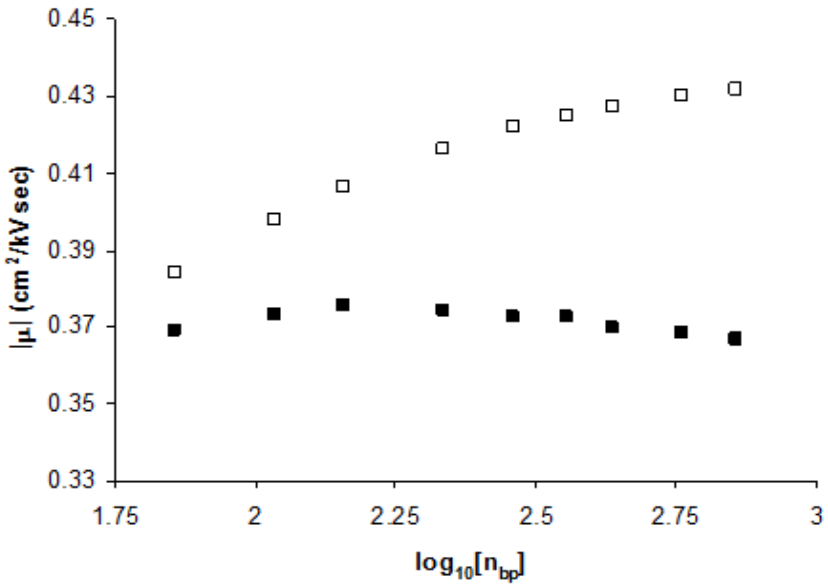

Figure 4-9) Absolute mobility versus length for model duplex DNA in 20 mM NaCl at 20 °C. Unfilled and filled squares correspond to rigid rods and flexible wormlike chains (P = 50 nm), respectively. No gel is present.

4.4 Summary

Electrophoresis remains an invaluable tool in the separation of biomolecules and nanoparticles on the basis of size and charge. It remains, however, a difficult problem to treat theoretically due to the complex interactions between the external electric field, solvent, mobile ions, and the particle/molecule on interest. The approach employed in the present study is formally grounded in continuum electro-hydrodynamic theory (41, 52, 75, 76). The

particle/molecule of interest is modeled as a flexible bead array and the fluid/gel surrounding it is modeled as an Effective Medium (105-107). The Bead Array-Effective Medium, BAEM, model developed previously (41) is generalized in the present study to remove the approximation of orientationally preaveraging, opa, hydrodynamic interaction (109-111).

In the Results section, the BAEM procedure is initially applied to rigid rods and rings made up of touching beads varying in number from 3 to 100. In order to reduce the number of variables considered, the bead size is set to 1.225 nm appropriate for duplex DNA. In addition to the components of the reduced mobilities, $H_{\parallel}$ and $H_{\perp}$, and the average reduced mobility, H_{ave}, we also studied the effects of the OPA approximation on these structures. For straight rods, the OPA approximation makes little difference, but for large rings with $\kappa a = 0.57$, it results in an overestimate of H_{ave} by about 12 %. Similar behavior is also seen for discrete wormlike chain models (P = 50 nm) of comparable bead number. It should be emphasized, however, that this preaveraging effect depends on a number of factors including the ionic strength. At low ionic strength, the error caused by the opa approximation is reduced. In addition, a smaller bead size reduces this error and that is relevant to peptide studies (41, 52, 76) where we estimate the error is closer to 5 %. In addition to free solution mobilities, the effect of a dilute gel (up to 0.02 gm dry agarose/ml) on mobility was also examined.

It should be mentioned that two model approximations have not been discussed in this chapter. The first is the neglect of the perturbation of the external electric field by the (low dielectric) interior of the bead array. As discussed in previous chapters, this approximation is expected to cause an underestimation of electrophoretic mobility by a few percent (75). A second

approximation is that the hydrodynamic force exerted by a bead on the surrounding fluid is uniform over the bead surface. In modeling studies of the translational diffusion constant of the bead arrays, this approximation causes an overestimation in the overall translational diffusion constant of the bead array by a few percent (93). Although these two approximations tend to cancel each other, the limitations of model will limit the accuracy of the predicted electrophoretic mobilities to a few percent at best.

The Results Section is ended by estimating the free solution electrophoretic mobility of duplex DNA versus length in 20 mM NaCl solution at 20 °C. Due to the high electrostatic potential of DNA, it is essential to account for the relaxation effect and this is estimated on the basis of Boundary Element modeling of finite straight and curved rods. When account is taken of the effect of flexibility on model mobility, agreement between modeling and experiment for long DNA is found to be very good.

Two future applications of the BAEM procedure include gel electrophoresis of DNA (95, 99) and bead arrays consisting of Au and Quantum Dot nanoparticles (97). More work is needed to study the steric term, S, appearing in Eq. (4-50) when the migrating particle is highly nonspherical. For spherical particles that do not interact with the gel matrix, the problem is well understood (108). Work is currently underway in our laboratory on the problem of rodlike particles migrating in a cubic gel lattice. With regard to the nanoparticle arrays, there is need for quantitative mobility data that is currently unavailable.

Chapter 5

Brownian Dynamics Simulation of the Diffusion of Rods and Wormlike Chains in a Gel Modeled as a Cubic Lattice: Application to DNA

5.1 Introduction

The present work represents a sequel to an earlier study of the translational diffusion constant of irregularly shaped particles in a gel modeled as a rigid array (45). The general problem of diffusion in a congested medium such as the cytoplasm of cells (130), concentrated suspensions (131), gels (108, 132-138) and mucus (139) is particularly relevant to the transport of drugs and biomolecules in living tissue and also in the broad field of separation science. The gel or congested medium retards the diffusion of a model particle relative to its value in free solution and this retardation is due to both long range hydrodynamic interaction and short range steric interactions. These two effects can be considered separately (108) and the translational diffusion constant, D, written

$$D = D_{EM} S \qquad (5-1)$$

where D_{EM} is the "Effective Medium" diffusion constant (which accounts for long range hydrodynamic interaction) and S represents the correction for direct interactions between the diffusing particle and the gel. Eq. (5-1) was developed initially for the diffusion of spherical particles in a gel and S is a simple function of the volume of fluid excluded to penetration by the model particle (108, 132). In previous work (45), we focused on D_{EM}, and in the present study, S for rodlike and wormlike chain model particles shall be examined. Here, we shall focus on short

range repulsive, or "steric" direct interactions. Past investigations of S have been devoted to spherical particles with steric interactions (108, 123, 132, 140, 141).

In order to model the diffusion of irregularly shaped particles through an explicit gel model, we shall use the method of Brownian dynamics simulation (103, 142, 143). Various aspects of the modeling strategy are discussed in Model Section. In Result Section, they are applied first to rodlike and then wormlike chain model particles with parameters chosen that are appropriate for duplex DNA. This methodology is then applied to the translational diffusion of duplex DNA in the size range of 100 to up to several thousand base pairs in two different "congested" media. The first is dilute (up to 2 % by weight) agarose gel and the second is cell cytoplasm. The Summary Section summarizes the principle conclusions of this work.

5.2 Model

2A) Cubic Lattice Gel Model

A gel can be characterized by its chemical composition (agarose, for example), weight density of "dry" gel material, ρ_g (which equals 1.64 gm/ml for agarose (144)), ratio of dry gel volume to hydrated gel volume, ω_s (which equals 0.625 for agarose (123)), the weight concentration of gel, M (typically in gm/ml), and possibly the concentration and composition of crosslinker if present. Once specified, however, these parameters do not lead directly to a unique gel microstructure since gel homogeneity, gel fibre thickness and shape as well as long range connectivity remain to be defined. In the present work, we shall be primarily interested in agarose gels where X-ray scattering shows evidence of a substantial population of fibres of radius 1.5 nm and a smaller population with substantially larger radius (124). Consequently, a

reasonable starting model of agarose is one in which the fibres have uniform axial radius, r_g, in the size range of 1.5 nm or higher. For sufficiently small M, previous investigation has also shown that particle migration in a gel is independent of the detailed geometry of the gel model (145). We shall model a gel as a simple cubic lattice with fibres oriented along the x, y, and z axes and separated by a near neighbor distance of A. To a good approximation, we can write (103)

$$M \cong \rho_g \omega_s \left[3\pi \left[\frac{r_g}{A} \right]^2 - 2 \left[\frac{\pi^{1/2} r_g}{A} \right]^3 \right] \qquad (5-2)$$

where the second term on the right hand side of Eq. (5-2) represents the correction for the junction (overlap of three orthogonal fibres). This correction is small unless the gel is concentrated. It is straightforward to solve for A iteratively in Eq. (5-2) once the other parameters are specified. Let $A^{(n)}$ denote the n-th estimate of A and

$$A^{(n)} = (3\pi)^{1/2} r_g \left[\frac{M}{\rho_g \omega_s} + 2 \left(\frac{\pi^{1/2} r_g}{A^{(n-1)}} \right)^3 \right]^{-1/2} \qquad (5-3)$$

Initially, one sets $A^{(0)} = \infty$ and solves Eq. (5-3) for $A^{(1)}$. This procedure is repeated until $A^{(n)}$ converges.

2B) Diffusion in a Gel: Effective Medium and Steric Interactions

Two factors act to reduce the translational diffusion constant, D, of a particle in a gel over its value in the absence of a gel, D^{ng}. One of these is long range in nature and arises from the

perturbation of the hydrodynamic flow of solvent by the rigid gel matrix. As discussed previously (45, 108, 132), the Effective Medium, EM, model can be used to treat this part of the problem. In the EM model, the "fluid" consists of solvent and also the gel matrix modeled as a continuum. This fluid is assumed to obey the Brinkman (105) and solvent incompressibility equations defined by

$$\eta\nabla^2\underline{v}(\underline{x}) - \underline{\nabla}p(\underline{x}) = \eta\lambda^2\underline{v}(\underline{x}) \qquad (5-4)$$

$$\underline{\nabla}\cdot\underline{v}(\underline{x}) = 0 \qquad (5-5)$$

where η is the solvent viscosity, $\underline{v}(\underline{x})$ is the local fluid velocity at point $\underline{x}$, p is the local pressure, and λ (units of 1/length) is the reciprocal of the gel screening length. The concentration dependence of λ can be written (45, 146)

$$\frac{1}{\lambda^2} \cong -\frac{3\rho_g\omega_s r_g^{\,2}}{20M}\left[\ln\left(\frac{M}{\rho_g\omega_s}\right) + 0.931\right] \qquad (5-6)$$

The other factor, S, is steric in nature and represents the reduction in diffusion due to short range repulsions of direct particle-gel fibre interactions. Direct interactions other than short range repulsions could also be included in general (103). This, however, shall not be done in the present study. Writing Eq. (5-1) more explicitly

$$\frac{D}{D^{ng}} = \left(\frac{D}{D^{ng}}\right)_{EM} S(M, r_g) \qquad (5-7)$$

Previous work focused on the relative diffusion within the framework of the EM model, $(D/D^{ng})_{EM}$. In the present work,we shall focus on the steric term, S. Although this term has received considerable attention for spherical particles (45, 100, 102, 123, 140, 141), it has not been investigated for nonspherical particles. For short rods, however, the form valid for spherical particles works reasonably well (103). The primary objective of the present work is to examine S for rods and wormlike chains. This is done by the technique of Brownian Dynamics simulation that shall be discussed next.

2C) Brownian Dynamics

We shall discuss two fundamentally different models used in the present work to represent linear semi-flexible chain molecules, a straight rigid rod and wormlike chain. The rigid rod (right circular cylinder) shall be discussed first. Let $\underline{r}$ denote the center of mass (center of diffusion) of the rod, L the rod length, R the axial rod radius, and $\underline{u}$ a unit vector collinear with the rod axis. Also let $\underline{v}$ and $\underline{w}$ denote unit vectors that are perpendicular to each other as well as $\underline{u}$. During Brownian dynamics, the $\underline{u}$, $\underline{v}$, and $\underline{w}$ vectors are updated after each dynamics step. Consider a Brownian dynamics step of duration δt. The change in $\underline{r}$ during the time step can be written (103)

$$\delta \underline{r} \;=\; \delta r_{\parallel}\, \underline{\mu} + \delta r_{\perp 1}\, \underline{v} + \delta r_{\perp 2}\, \underline{w} \qquad (5-8)$$

The scalar quantities $\delta r_{\parallel}$, $\delta r_{\perp 1}$, and $\delta r_{\perp 2}$ denote translational displacements along $\underline{u}$, $\underline{v}$, and $\underline{w}$, respectively. Displacements arise from free diffusion as well as external forces, $\underline{F}$, or torques, $\underline{T}$,

acting on the rod relative to its center of mass/diffusion. The scalar displacements can be written (103)

$$\delta r_{\|} = \beta D_{T\|}(\underline{F}\cdot\underline{\mu})\delta t + (2D_{T\|}\delta t)^{1/2} X_{\|} \qquad (5-9)$$

$$\delta r_{\perp 1} = \beta D_{T\perp}(\underline{F}\cdot\underline{v})\delta t + (2D_{T\perp}\delta t)^{1/2} X_{\perp 1} \qquad (5-10)$$

An expression similar to Eq. (5-10) can be written for $\delta r_{\perp 2}$. In Eqs. (5-9) to (5-10), $\beta = 1/k_B T$ (k_B is Boltzmann's constant and T is absolute temperature), $D_{T\|}$ and $D_{T\perp}$ are the free translational diffusion constants parallel and perpendicular to the rod axis (147), respectively, and $X_{\|}$, $X_{\perp 1}$, and $X_{\perp 2}$ are independent Gaussian random numbers of zero mean and variance 1.

It is also necessary to consider the rotational motion of the rod, let $\delta\theta_v$ and $\delta\theta_w$ denote angular rotations of $\underline{u}$ about directions $\underline{v}$ and $\underline{w}$, respectively. Also let $D_{R\perp}$ denote the end-over-end rotational diffusion constant of the rod (147), and X_{Rv} and X_{Rw} independent Gaussian random numbers of zero mean and variance 1. The angular displacements are given by

$$\delta\theta_v = \beta D_{R\perp}(\underline{\underline{T}}\cdot\underline{v})\delta t + (2D_{R\perp}\delta t)^{1/2} X_{Rv} \qquad (5-11)$$

with a similar expression for $\delta\theta_w$. Provided the angular displacements are small,

$$\delta\underline{\mu} \cong \underline{v}\delta\theta_w - \underline{w}\delta\theta_v \qquad (5-12)$$

To summarize, a random number generator generates the X's. These along with $\underline{u}$, $\underline{v}$, $\underline{w}$, $\underline{F}$, and $\underline{\underline{T}}$ (which are updated as the dynamics proceeds) are used in Eqs. (5-8) to (5-12) to displace the rod during a dynamics step.

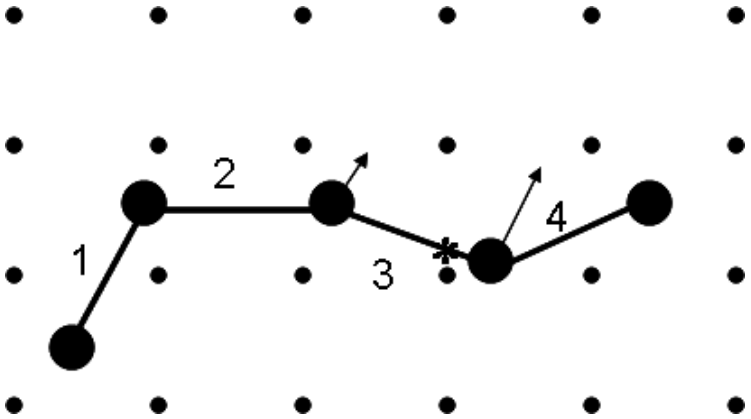

Figure 5-1) Wormlike chain in a cubic gel. The small dots represent gel fibres coming out of the plane of the figure. In this example, the wormlike chain consists of 5 beads and 4 virtual bonds,or "rodlets", and the contour length of the chain is not small compared to the fibre spacing. Also, there is a contact with a gel fibre denoted by X and this results in repulsive forces on beads 3 and 4 that are depicted by the arrows.

In the discrete wormlike chain model, the chain is modeled as N identical rigid beads of radius a connected by N-1 virtual bonds of radius R*. A schematic of a 5 bead (4 virtual bond) model chain diffusing in a cubic gel array is depicted in Figure 5-1. Let $\underline{r}_i$ denote the position of bead i and $b_i = |\underline{r}_{i+1}-\underline{r}_i|$ denote the virtual bond or "rodlet" length. Direct forces due to stretching and bending are derived from stretching, U^s, and bending, U^b, pontentials,

$$\beta U^s = \frac{h}{2b_0^2}\sum_{j=1}^{N-1}\left(b_j - b_0\right)^2 \qquad (5-13)$$

where b_0 is the separation distance at which U^s is a minimum for all virtual bond terms,

$$\beta U^b = \frac{g}{2}\sum_{j=1}^{N-2}\theta_j^2 \qquad (5-14)$$

In Eq. (5-14), θ_j is the angle between virtual bond vectors j and j+1. Explicit expressions for bending and stretching forces have been given previously (143). The Ermak-McCammon algorithm is used to displace the beads (142). In a dynamics time step of duration δt,

$$\delta \underline{r}_i = \beta \delta t \sum_{j=1}^{N} \underline{\underline{D}}_{ij} \cdot \underline{F}_j + \underline{R}_i(\delta t) \qquad (5-15)$$

where $\underline{F}_j$ is the total force on bead j (arising from stretching, bending, and direct (steric) forces due to the interaction of the bead array with the gel), $\underline{R}_i$ is a vector of Gaussian random numbers of zero mean and variance-covariance

$$< \underline{R}_i \underline{R}_j > = 2 \delta t \underline{\underline{D}}_{ij} \qquad (5-16)$$

The construction of the $\underline{R}_i$ vectors is described elsewhere (142), and $\underline{\underline{D}}_{ij}$ is the configuration dependent hydrodynamic interaction tensor between subunits i and j. In this work, the Rotne-Prager tensor (148) with stick boundary conditions is employed. The self terms are given by

$$\underline{\underline{D}}_{ii} = \frac{k_B T}{6\pi\eta a} \underline{\underline{I}} = D_0 \underline{\underline{I}} \qquad (5-17)$$

where η is the solvent viscosity, $\underline{\underline{I}}$ is the 3 by 3 identity tensor, and D_0 is the "free" diffusion constant of a spherical bead of radius a. For different and non-overlapping beads (see ref. (22, 148) for the case of overlapping beads)

$$\underline{\underline{D}}_{ij} = \frac{k_B T}{8\pi\eta r_{ij}} \left[\left(\underline{\underline{I}} + \frac{1}{r_{ij}^2} \underline{r}_{ij} \underline{r}_{ij} \right) + \frac{2a^2}{r_{ij}^2} \left(\frac{1}{3} \underline{\underline{I}} - \frac{1}{r_{ij}^2} \underline{r}_{ij} \underline{r}_{ij} \right) \right] \qquad (5-18)$$

where $\underline{r}_{ij} = \underline{r}_i - \underline{r}_j$ and $r_{ij} = |\underline{r}_i - \underline{r}_j|$. In many of the simulations carried out in this work, $\underline{\underline{D}}_{ij}$ was approximated by "preaveraging" (22, 143). In this case, $\underline{\underline{D}}_{ij}$ is replaced with

$$\underline{\underline{D}}_{ij\,opa} = \frac{1}{3}\underline{\underline{I}}\,Tr\left[<\underline{\underline{D}}_{ij}>\right] \qquad (5-19)$$

where Tr denotes the trace of the tensor and < > denotes the average over many (typically 500 to 2000) randomly generated chain conformations. The computational advantage of preaveraging is that the $\underline{\underline{D}}_{ij}$ tensors only have to be computed once at the beginning of the simulation. This results in substantially shorter simulation times.

2D) Gel-Rod and Gel-Rodlet Interaction

Direct interactions between gel and rod (or gel and rodlets in the case of a discrete wormlike chain model) are handled as simple steric repulsion interactions. For a cubic gel lattice, fibres run in three orthogonal directions. In addition, the rod (or rodlet) length is not necessarily small compared to the fibre spacing, A, for the cases of interest in this work. This is illustrated in Fig. 5-1 where the model chain extends over several fibre spacings. For this reason, it is necessary to carefully check for multiple gel-rod(let) contacts during each step of dynamics. In the following analysis, it shall be assumed we have a single rod. The more complex case of a discrete wormlike chain made up of multiple rodlets involves a straightforward extension of the simpler case of a single rod. Suppose we have a fibre oriented along k (k could be x, y, or z) and centered at $(0, x_{k1}, x_{k2})$ where the first coordinate (0) is along k and the latter two coordinates (x_{k1} and x_{k2}) are in orthogonal directions, k1 and k2, respectively. Also let the rod of length L be centered at $\underline{r} = (r_k, r_{k1}, r_{k2})$ oriented along $\underline{u} = (u_k, u_{k1}, u_{k2})$. Any point on the rod axis is given by

the coordinate ($r_k + \gamma L u_k$, $r_{k1} + \gamma L u_{k1}$, $r_{k2} + \gamma L u_{k2}$) where $-1/2 \le \gamma \le +1/2$. The square of the distance of closest approach of a point at a particular γ on the rod and the gel fibre is

$$d^2 = (r_{k1} - x_{k1})^2 + (r_{k2} - x_{k2})^2 + 2\gamma L[u_{k1}(r_{k1} - x_{k1}) + u_{k2}(r_{k2} - x_{k2})]$$

$$+ (\gamma L)^2[u_{k1}^2 + u_{k2}^2] \qquad (5-20)$$

Minimizing with respect to γ

$$\gamma = -\frac{[u_{k1}(r_{k1} - x_{k1}) + u_{k2}(r_{k2} - x_{k2})]}{L(u_{k1}^2 + u_{k2}^2)} \qquad (5-21)$$

If $\gamma < -1/2$, set $\gamma = -1/2$ and if $\gamma > +1/2$, set $\gamma = +1/2$. This value of γ is substituted into Eq. (5-20) gives the distance of closest approach of the rod and this particular gel fibre. If the distance of closest approach exceeds $R + r_g$ (rod radius plus gel fibre radius), no interaction force is included. If the distance of closest approach is less than this amount, a repulsive force, $\underline{F}'$ at point γ on the rod and directed from the gel fibre to the rodlet at the contact point is applied. When we have a discrete wormlike chain and multiple rodlets, the above procedure is repeated for each rodlet (b_i replaces L and R* replaces R) that comprises the model chain.

The repulsive displacement of a bead associated with a rodlet that "contacts" a gel fibre is approximately $|\delta\underline{r}_j^{rep}| \approx \beta\delta t_{min} D_0 |\underline{F}'|$ where D_0 is the diffusion constant of a single bead and δt_{min} is the minimum time step. As discussed later, we set $\delta t_{min} = r_g^2/200D_0$ in order to insure that the bead displacements during the shortest timesteps are small compared to the gel fibre radius, r_g. The overall displacement in one direction of a single bead with this time step will be approximately $|\delta\underline{r}_j| \approx (2D_0\ \delta t_{min})^{1/2} = r_g/10$. If a dynamics time step introduces an overlap, the

bead displacements resulting from rodlet fibre repulsions should be comparable with $r_g/10$ in order to relieve the overlap. Since r_g falls in the 1 to 3 nm size range for cases of interest in this work, $|\delta \underline{r}_j^{rep}| \approx 0.1$ to 0.3 nm. The magnitude of the repulsive force is set to $|\underline{F}'| \approx 20/\beta r_g$. The corresponding torque on the rodlet is $0.5\,\gamma\, b_j\, \underline{u} \times \underline{F}'$ (where $\times$ denotes vector cross product). This procedure is applied to all possible fibres that could possibly overlap the rod.

It is convenient to replace the rodlet force and torque with corresponding forces on the two beads that comprise a particular rodlet. Consider the situation where rodlet j overlaps a gel fibre at position γ_j and gives rise to a steric rodlet force and torque, $\underline{F}'$ and $\gamma_j\, b_j\, \underline{u}_j \times \underline{F}'$, respectively. This condition is satisfied if we write the subunit steric forces for beads j and j+1 that comprise rodlet j

$$\underline{F}'_j = (1/2 - \gamma_j)\underline{F} \qquad (5-22)$$

$$\underline{F}'_{j+1} = (1/2 + \gamma_j)\underline{F} \qquad (5-23)$$

Note that we must have $\underline{F}' = \underline{F}_j' + \underline{F}_{j+1}'$ and $\underline{T}' = b_j\, \underline{u}_j \times (\underline{F}_{j+1}' - \underline{F}_j')$. In the case of a discrete wormlike chain, it is necessary to sum over all rodlets and and all fibres that could possibly overlap each other during each dynamics step. In Fig. 5-1, the "x" on rodlet 3 denotes a contact. The arrows on beads 3 and 4 denote $\underline{F}_3'$ and $\underline{F}_4'$ determined according to Eqs. (5-22) and (5-23).

2E) Rod and Wormlike Chain Models

The particle shall be modeled either as a right circular cylinder (rod) of length L and axial radius, R, or as a wormlike chain (121) of contour length, L, axial radius, R, and persistence

length, P. Since we are primarily interested in duplex DNA in the present work, L is simply related to the number of base pairs, n_{bp} by L (in nm) =0.34 n_{bp}. Also, current consensus places R at 1.0 ± 0.1 nm (115, 116). The persistence length of DNA shows some variation with ionic strength, but a typical value is 50 nm or 147 bp (121). That value shall be used throughout the present work. For short DNA such that L << P, a rigid rod model should be a realistic one to represent the diffusion of duplex DNA in a gel or free solution. For DNAs longer than about 50 bp, however, a wormlike chain model is more appropriate.

Rather than a continuous wormlike chain model, we shall consider discrete wormlike chain models in which the chain is modeled as N beads of radius a, minimum separation of stretching potential, b_0, (Eq. (5-13)), and stretching and bending force constants, h and g, respectively (Eqs. (5-13, 5-14)). The most detailed is the "touching bead" model of Hagerman (117, 118) where b_0 = 2a and L = 2 a N. Setting the volume of a right circular cylinder, $\pi R^2 L$, equal to that of N touching beads, $4 \pi N a^3/3$, gives $a = (3/2)^{1/2} R = 1.225$ nm. For the touching bead model, n_{bp} = 7.2 N. In addition, the persistence length, P, is related to the bending force constant, g, by the relation (149) (valid for g >> 1)

$$P = \frac{<b> g}{1 - \frac{2}{3g} + \frac{14}{45g^2}} \qquad (5-24)$$

where $<b> \cong b_0(1+2/h)$ is the average rodlet or virtual bond length. The touching bead model is not suitable for Brownian dynamics simulation of the translational diffusion of long wormlike chains in a gel because of the long simulation times involved. However, it is used to calculate D_{EM} for wormliked chains in the present work (45). Also, it is useful in the present work in

defining some "free solution" parameters of wormlike chains. These include the translational diffusion constant of the wormlike chain in the absence of a gel, D^{ng}, the root mean square end-to-end distance, $\langle R^2 \rangle^{1/2}$, and the dimensionless asymmetry parameter

$$\chi = \left(\frac{\sum_{j=1}^{N} [(\underline{r}_j - \underline{r}_{CM}) - \underline{\mu}(\underline{\mu} \cdot (\underline{r}_j - \underline{r}_{CM}))]^2}{\sum_{j=1}^{N} [\underline{\mu}(\underline{\mu} \cdot (\underline{r}_j - \underline{r}_{CM}))]^2} \right)^{1/2} \qquad (5-25)$$

In Eq. (5-25), $\underline{r}_j$ is the position of bead j, $\underline{r}_{CM}$ is the position of the center of mass of the wormlike chain, and $\underline{u}$ is the end-to-end unit vector. In the limit of a straight rod, $\chi \rightarrow 0$.

As an alternative to the touching bead wormlike chain for use in Brownian dynamics simulations, we design "equivalent" wormlike chains made up of fewer subunits that have the same D^{ng}, $\langle R^2 \rangle^{1/2}$, and χ as a touching bead wormlike chain. The parameter N is chosen to give us a chain with b_0 comparable to a persistence length. Also, the stretching force constant, h, is arbitrarily set to 100. This value is small enough to allow relatively long dynamics steps and yet large enough to insure that b_j does not deviate from b_0 by more than a few percent. With N fixed, initial estimates of a and b_0 are made and then g is varied until $\chi_{equivalent} \cong \chi_{touching\ bead}$. At this point, g is uniquely determined since χ is independent of the parameters a and b_0. Now with N, h, and g fixed and using the same estimate for a, b_0 is varied until $\langle R^2 \rangle^{1/2}_{equivalent} = \langle R^2 \rangle^{1/2}_{touching\ bead}$. At this point, b_0 is uniquely determined since both χ and $\langle R^2 \rangle^{1/2}$ are independent of the remaining parameter to be determined, a. Next, a is adjusted until $D^{ng}_{equivalent} = D^{ng}_{touching\ bead}$ using well established procedures of bead hydrodynamics (22,45,150). By this procedure, it is

simple and straightforward to uniquely determine a discrete wormlike chain that captures some of the key features of a continuous wormlike chain model.

There does remain, however, one additional parameter of our equivalent wormlike chain model to specify and that is the effective rodlet axial radius, R*, which has a limiting value of 1.0 nm appropriate for DNA for a continuous wormlike chain model. This parameter is necessary in modeling the transport of a wormlike chain through a gel since we need some criteria to judge for overlap between the gel (of fibre radius r_g) and the chain (of axial radius R*). To estimate R*, an equivalent wormlike chain is randomly placed in a dilute gel with fibres running randomly in the x, y, and z directions. The average number of gel fibres intersecting the chain is

$$< N_s > \;=\; < n_{str} > (R^* + r_g)[2 < b > (N-1) + 4r_g + \pi(R^* + r_g)] \qquad (5-26)$$

where $<n_{str}> = M/(3\pi\rho_g\omega_s r_g^2)$ is the average number of gel fibres that pass through a unit area. A similar expression to Eq. (5-26) can be written down for a continuous wormlike chain of contour length L and axial radius R. Setting the two equal and solving for R* gives

$$R^* \;=\; \frac{a_1 + a_2 r_g}{a_3 + a_4 r_g + \pi R^*} \qquad (5-27)$$

where $a_1 = 2LR+\pi R^2$, $a_2 = (4+2\pi)R+2L-2<b>(N-1)$, $a_3 = 2<b>(N-1)$, and $a_4=(4+2\pi)$.

Although R* appears on both the left and right hand side of Eq. (5-27), it is straightforward to solve for R* iteratively using previous estimates on the right hand side. As an initial estimate, set R* = 1.0 nm on the right hand side of Eq. (5-27) and solve for R* to obtain an improved

estimate. Then use this improved estimate on the right hand side of Eq. (5-27) to obtain a still better estimate. This procedure is repeated until R* converges. Summarized in Table 5-1 are the equivalent chain parameters of duplex DNA of different length with P = 50 nm. A stretching force constant of h = 100 is used and r_g = 2.0 nm. (For other r_g, the parameter R* will be different but the other parameters are the same.)

2F) Timesteps, Averages, and Details of the Simulation Procedure

The general procedure used in Brownian dynamics simulation of rod and wormlike chains have been discussed previously in related applications (103,143). Briefly, the simulation is broken down into NSUB subsimulations (typically 4 to 10) and each subsimulation consists of NTRJ trajectories (typically 25 to 100). For each trajectory, a rod or wormlike chain conformation that does not overlap the gel matrix is initially generated at random from an equilibrium distribution of conformations. Brownian dynamics is carried out for each trajectory for a length of time, T, chosen long enough so that the rms diffusional displacement of the center of mass of the rod or wormlike chain is at least several times larger than the fibre spacing in the gel, A.

As discussed previously with regard to the electrophoresis of short rods in a cubic gel (103), a variable time step algorithm is much more efficient than a constant time step algorithm. A similar approach is used for the discrete wormlike chain models. As in all molecular dynamics and Brownian dynamics simulations, the dynamics time step, δt, should always be chosen sufficiently short so that the forces on the subunits do not change significantly during the duration of a time step. In the present application, this is determined either by the intersubunit

stretching forces or the gel fibre-virtual bond steric repulsive forces that are present when overlap occurs. It is straightforward to explore this problem by systematically raising the time step and seeing what effect this has on observables being measured. If the time step is too large, the observable depends on time step and if it is short enough, the observable is independent of timestep (151). For the migration of a rod or wormlike chain in a gel, too large a time step might lead to passage of the rod or wormlike chain through a gel fibre and hence a translational diffusion constant larger than it should be. In the present work, the minimum time step is taken to be $\delta t_{min} = r_g^2/(200\ D_0)$ and the maximum time step $\delta t_{max} = (<b^2>-<b>^2)/(200\ D_0)$ where D_0 is the diffusion constant of a bead of radius a. Let s denote the distance of closest approach between any point on any virtual bond and any gel fibre. Then δt is set to δt_{min} if $s \le (r_g+R^*)$ and the lesser of δt_{max} and $\delta t_{min}+(s^2-(r_g+R^*)^2)/(200\ D_0)$ if $s \ge (r_g+R^*)$. By following this procedure, relatively short timesteps are taken when overlap or near overlap occurs, but longer timesteps are allowed otherwise. A reduced sampling time is defined

$$t_{red} = \frac{100}{T} t \qquad (5-28)$$

So that $0 < t_{red} < 100$. During a trajectory, the following average is computed

$$< D(t_{red}) >_{traj} = \frac{< (\underline{r}(t'+Tt_{red}/100) - \underline{r}(t'))^2 >}{6T\, t_{red}/100} \qquad (5-29)$$

In the absence of a gel, $<D(t_{red})>_{traj} \rightarrow D^{ng}$ for all t_{red} and sufficiently long trajectories. Eq. (5-29) is further averaged over NTRJ trajectories to obtain subsimulation averages. These, in turn, are further averaged over NSUB subsimulations. From the variation in $<<D(t_{red})>_{traj}>_{NTRJ}$ over

different subsimulations, standard deviations can be estimated as well as $<D(t_{red})>$ = $<<<D(t_{red})>_{traj}>_{NTRJ}>_{NSUB}$. Finally,

$$S(M, r_g) = \lim_{T\to\infty}(\lim_{t_{red}\to 100} \frac{< D(t_{red}) >}{D^{ng}}) \qquad (5-30)$$

On physical grounds, we expect $<D(t_{red})> \rightarrow D^{ng}$ for sufficiently short t_{red} regardless of gel concentration, M. This, however, is expected to drop with increasing t_{red} and reach a plateau value at sufficiently long time or t_{red}.

5.3 Results

3A) "Steric" Effect Study for DNA

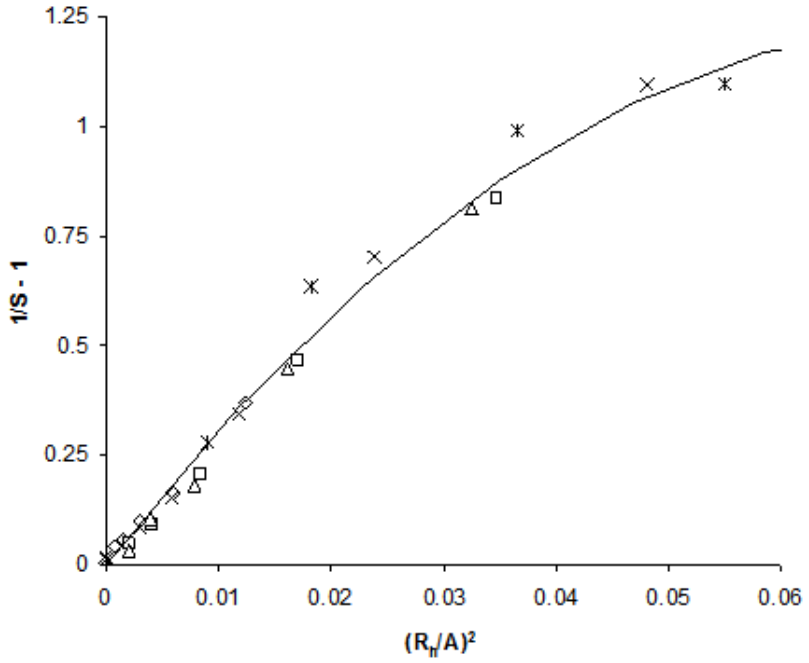

Figure 5-2) 1/S-1 versus $(R_h/A)^2$ for rigid rods, r_g = 1.3 nm. Rod axial radius = 1.0 nm and lengths (in units of base pairs of duplex DNA) are: 50 (diamonds), 100 (squares), 200 (triangles), 400 (x's), and 800 (*'s).

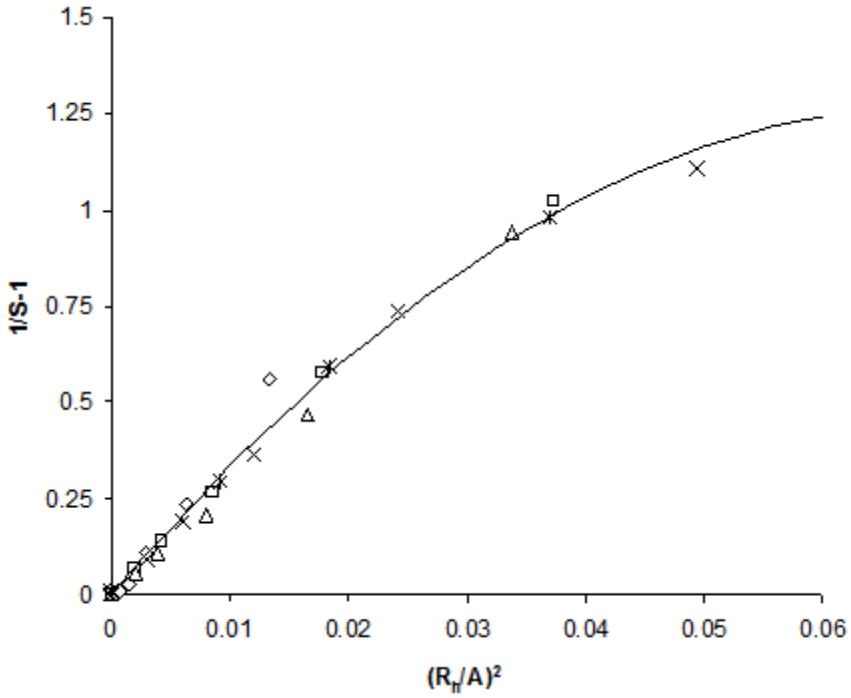

Figure 5-3) 1/S-1 versus $(R_h/A)^2$ for rigid rods, r_g = 2.6 nm. . Rod axial radius = 1.0 nm and lengths (in units of base pairs of duplex DNA) are: 50 (diamonds), 100 (squares), 200 (triangles), 400 (x's), and 800 (*'s).

As an initial application, consider duplex DNA modeled as a right circular cylinder of radius R = 1 nm and length L = 0.34 n_{bp} where n_{bp} is the number of base pairs. The diffusion constants of the rod in the absence of a gel come from reference (147). Plotted in Figures 5-2 and 5-3 is S versus $(R_h/A)^2$ for 50 to 800 bp models with r_g = 1.3 and 2.6 nm, respectively. The hydrodynamic radius, R_h, is defined

$$R_h = \frac{k_B T}{6\pi\eta D^{ng}} \quad (5-31)$$

In both cases with different r_g's, the data appears to fall on a universal curve with respect to rod length. In Figure 5-4, n_{bp} =564 bp, but r_g is varied from 1.3 to 2.6 nm. When S is plotted versus

$(R_h/A)^2$, the results appear to be independent of r_g. Thus, S for rods of variable length and r_g appear to fall on a universal curve when plotted versus $(R_h/A)^2$.

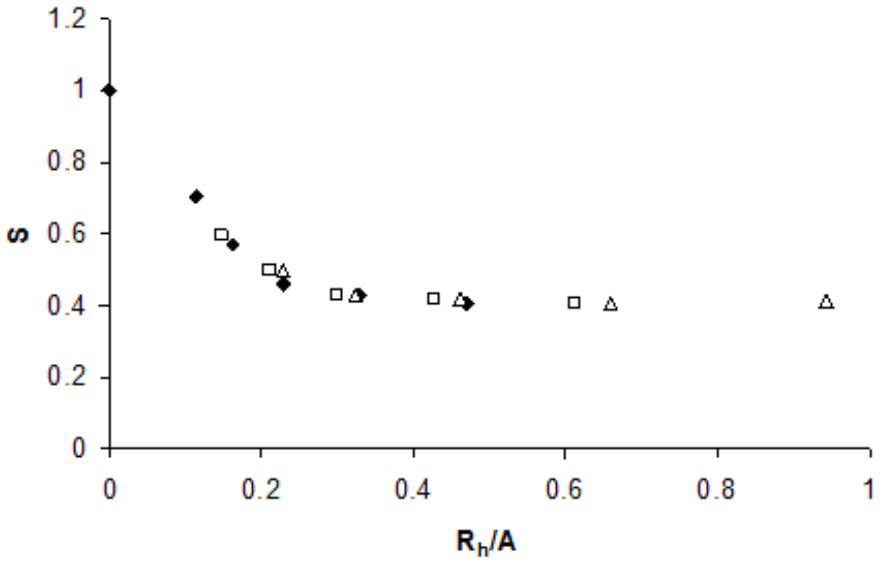

Figure 5-4) S versus (R_h/A) for rigid rod model of 564 bp DNA and variable r_g. Unfilled triangles, unfilled squares, and filled diamonds correspond to r_g = 1.3, 2.0, and 2.6 nm, respectively.

One unusual feature of Figure 5-4 is that in the limit of large R_h/A (high gel concentration, M), S appears to approach a limiting value of about 0.40 in this particular example. This can be understood as follows. For a long straight rod diffusing in a dense periodic cubic gel, diffusion will be completely eliminated in a direction perpendicular to the rod axis, but diffusion parallel to the rod will remain free provided there are no attractive gel-rod interactions. Hence, S (which equals $<D>/D^{ng}$ neglecting long range hydrodynamic interactions) should equal $D_{\|}^{ng}/(3\ D^{ng})$ in the limit of large M and this equals 0.40 in the above example. In the case of an actual duplex DNA diffusing in a real gel, curvature of the diffusing molecule and/or irregularities in the gel

structure would be expected to cause S to drop below this limiting value. This is one of the reasons for turning to wormlike chain models which is done next.

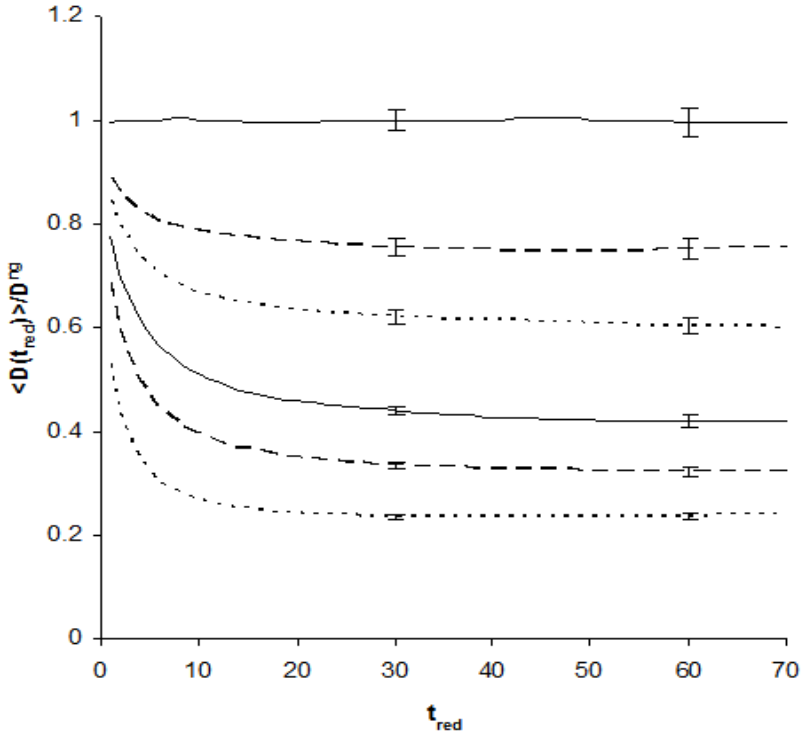

Figure 5-5) $\langle D(t_{red})\rangle/D^{ng}$ versus t_{red} for 500 bp DNA trumbell model. Top to bottom curves correspond to M = 0.000, 0.002, 0.004, 0.008, 0.016, and 0.032 gm/ml of agarose, respectively. Error bars denote variance between different subsimulations. See the text for details.

3B) Application to Duplex DNA Diffusion in Free Solution, in an Agarose Gels, and in Cell Cytoplasm

As discussed in Section 2F, diffusion of a rod or wormlike chain in a gel is expected to be time dependent, but reaching a constant value at times long compared to the time it takes for the particle to diffuse an rms distance equal to the gel spacing, A. An example of this is shown in Figure 5-5 for 500 bp DNA with P = 50 nm modeled as a trumbell (N = 3) at 6 different M. The

trumbell parameters are given in Table 5-1. The trajectory time, T, is set equal to 5 A^2/D^{ng} and this corresponds to t_{red} = 100 (see Eq. (5-29). From top to bottom in the Figure, M = 0.0, 0.002, 0.004, 0.008, 0.016, and 0.032 gm/ml, respectively. Error bars reflect the variation in $<D(t_{red})>/D^{ng}$ between different subsimulations (10 total) of 50 trajectories each. The long time limiting value of $<D(t_{red})>/D^{ng}$ gives S.

Table 5-1. Parameters for Equivalent Wormlike Chain Models

n_{bp}	N	a (nm)	b_0 (nm)	g	R* (nm)
100	3	2.23	15.0	3.50	1.215
200	3	3.51	30.1	1.40	1.263
400	3	5.00	57.2	0.61	1.443
500	3	6.90	67.1	0.50	1.656
1000	6	6.40	59.5	0.53	1.345
2027	10	7.20	71.0	0.30	1.169

For trumbell models of wormlike chains representing 100 to 500 bp duplex DNA, simulations were carried out without and with the preaveraging approximation (Eq. (5-19)). Although simulations without the preaveraging approximation required 5 times the computation time as the same simulations with the preaveraging approximation made, $<D(t_{red})>/D^{ng}$ were indistinguishable given the noise level. Shown in Figure 5-6 is a plot of –ln[S] versus x = $(R_h/A)^2$ for wormlike chains of different length with P = 50 nm. The parameters of the wormlike chains are summarized in Table 5-1 and discussed in Section 2E. To a good approximation, this data is well fit by the following empirical formula.

$$-\frac{\ln[S]}{x} = 3.0 + 16.0\,e^{-9.2x} \qquad (5-32)$$

This is true for any wormlike chain in a gel of variable r_g.

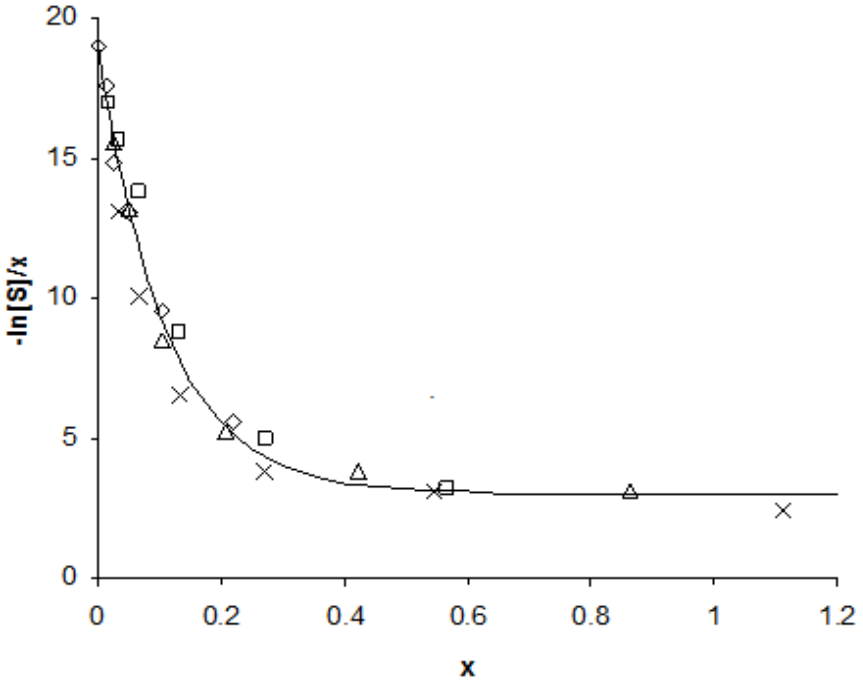

Figure 5-6) –ln[S]/x versus x for discrete wormlike chains of variable length. Persistence length, P, equals 50 nm and x = $(R_h/A)^2$. Diamonds, squares, triangles, and x's correspond to 200, 500, 1000, and 2027 bp DNA, respectively. The solid curve is an empirical fit defined by Eq. (5-32).

A number of investigations of the translational diffusion constants of duplex DNA in agarose gels have been reported (132, 133,136), but studies of short DNAs in the 100 to several thousand base pair range are very limited (132, 136). A comparison of model and experimental diffusion constants (132) in free solution (M = 0.00) and in a 2 % agarose gel (M = 0.02 gm/ml) is presented in Figure 5-7. The technique used in reference 5 was FRAP (fluorescence recovery after photobleaching (150)) and the experiments were carried out at 25 °C in a PBS buffer at an

ionic strength of 0.1 M. The open triangles represent model studies of touching bead wormlike chains (P = 50 nm) in the absence of a gel. The dashed line comes from reference 5 (M = 0.00) and the +'s from dynamic light scattering measurements of Sorlie and Pecora (152). Diffusion constants from reference 37 have been modified slightly to correct them from T = 20 to 25 °C (T/η correction). In the absence of a gel, modeling and experimental diffusion constants (from 2 independent labs employing different methodologies) are in good agreement with each other. The asterisks (with error bars) are experimental D's in 2 % agarose and the solid line represents a fit to experimental data extending out to a length of about 6000 bp (132). The corresponding model studies that include both EM (long range hydrodynamic) and steric interactions are denoted by filled squares (r_g = 2.0 nm) and filled triangles (r_g = 4.0 nm) both at M = 0.02 gm/ml. In the case of a gel, agreement is only fair. For 564 base pair DNA, a model with $r_g \cong 2.5$ nm matches experiment, but the same model substantially underestimates the diffusion constant of a longer (2000 bp) fragment. In this example, the gel model predicts a stronger dependence on length than is observed experimentally. It should be mentioned that a stronger dependence on length is also seen in experiment, but only for n_{bp} > 6000 bp (132). It is doubtful that electrostatic interactions between gel and DNA could be responsible for these differences. Agarose contains anionic pyruvate sites, buth these are effectively screened above an ionic strength of 0.02 moles/liter (138).

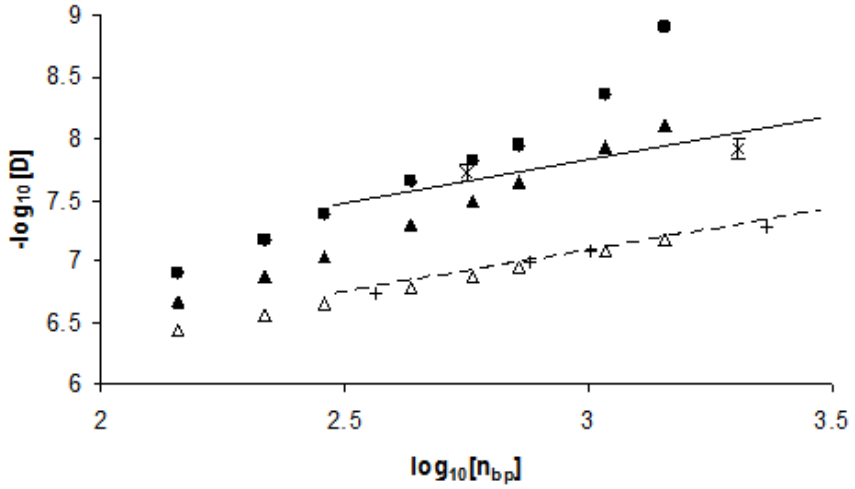

Figure 5-7) Length dependence of D for duplex DNA in free solution and in a 2 % agarose gel. Dashed and solid lines are fits to experimental data (reference (132)) in free solution and in 2 % agarose gel, respectively. Open triangles are for touching bead models in the absence of a gel (M = 0.0). +'s are from reference (151) with M = 0.0. Asterisks are from reference (132) with M = 0.02 gm/ml. Filled triangles and diamonds are touching bead model studies with M = 0.02 gm/ml and r_g = 2.0 and 4.0 nm, respectively.

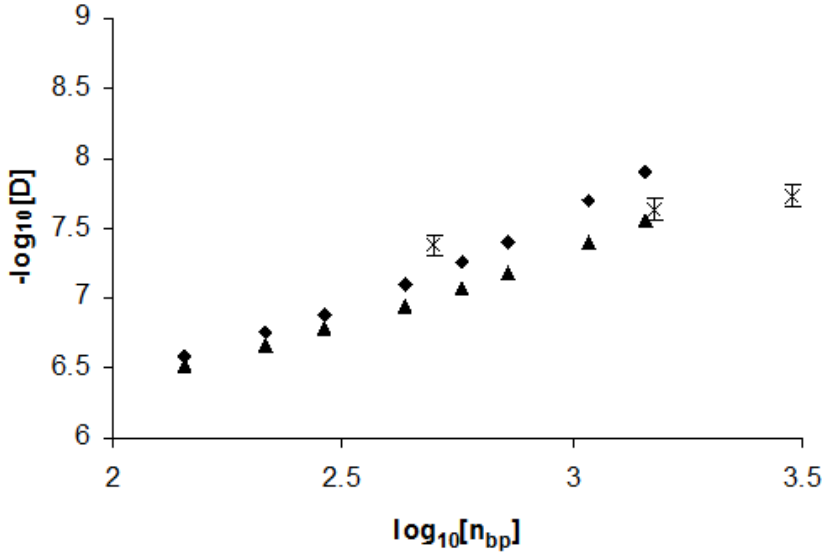

Figure 5-8) Length dependence of D for duplex DNA in 0.2 % agarose gel. Asterisks are experimental points (with error bars) from reference (136). Filled triangles and diamonds are touching bead model studies with M = 0.002 gm/ml and r_g = 2.0 and 4.0 nm, respectively.

Figure 5-8 shows a similar comparison between modeling and experiment in M = 0.002 gm/ml agarose gel and an ionic strength of about 0.01 moles/liter (136). The FRAP technique is also used in this study. In this case, modeling works better for longer fragments. As in the case of the more concentrated gel, modeling predicts stronger length dependence than is observed experimentally. It should be emphasized, however, that this observation is based on a small number of DNA lengths in the size range of interest in the present work (100 to 2000 bp).

As a final application of DNA diffusion, we shall consider the reduced diffusion of duplex DNA in cell cytoplasm (153). Cytoplasm is the jellylike material that makes up much of a living cell inside the cell membrane (130). It consists of water, salts, sugars, lipids, nucleotides, peptides and proteins. Given its complexity and heterogeneity, the present analysis must be regarded as preliminary. We shall model the cytoplasm purely as an Effective Medium (without steric interactions) and as an EM with the steric term included. Arbitrarily, we shall set $r_g = 3.0$ nm. For a 250 bp DNA fragment, Lukacs et al. report $D_{cyto}/D_w = 0.06 \pm 0.02$ where D_{cyto} is the diffusion constant of DNA in cytoplasm and D_w is the corresponding diffusion constant in water (153). For both EM and EM + steric models, M is determined which yields D_{cyto}/D_w to within the uncertainty of the experiment. These turn out to be M ≅ 0.90 gm/ml for the EM and ≅ 0.20 gm/ml for the EM + steric model. These gel concentrations are then used to model D_{cyto}/D_w for fragments of other lengths. The results are summarized in Figure 5-9 for experiment (153) (filled squares), EM model (dashed line), and EM + steric model (solid line). Although neither model fits the experimental data perfectly, it is clear that the EM + steric model is superior to the EM model alone. The EM model alone predicts a substantially weaker dependence of D_{cyto}/D_w

on length than is observed experimentally. The EM + steric model captures, to a good extent the observed length dependence.

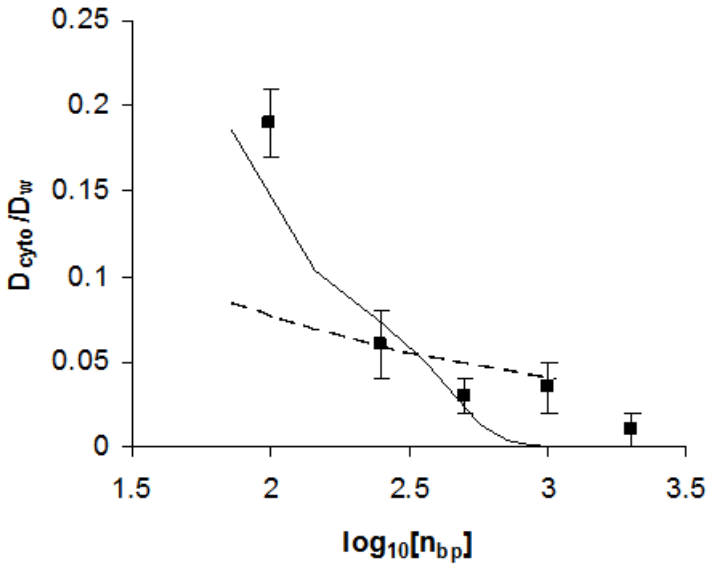

Figure 5-9) D_{cyto}/D_w versus length. Experimental ratios are denoted by filled squares with error bars and come from reference (138). EM model results (M = 0.90 gm/ml) are denoted by a dashed line and EM + steric model results (M = 0.20 gm/.ml) are denoted by a solid line.

3C) Application to Duplex DNA Mobility in an Agarose Gels

The EM model discussed in the Methodology section of this chapter is also applied to modeling the gel electrophoresis of duplex DNA in agarose gels from the experimental work of Calladine et al. (95). The relevant model parameters pertaining to agarose are given following Eq. (4-51). Since the EM model is expected to work best for dilute gels and for macromolecules that are small relative to the pore spacing in the gel, we shall concentrate on short duplex DNAs in dilute gels (9) with M in the range of 0.005 to 0.020 gm/ml. The experiments were carried out at 20 °C in a Tris borate buffer, pH = 8.3, ionic strength = 25 mM.

To model duplex DNA, the discrete wormlike chain model of Hagerman (117,118) is employed. Mobilities are obtained by averaging over 100 or main independent chain conformations. Current consensus places the hydrodynamic radius, R, (viewing duplex DNA on a local distance scale as a right circular cylinder) at 1.0 ± 0.1 nm (115, 116). Following Hagerman, one sets the contour length, L, equal to 2Na where N is the number of touching contiguous beads and a is the bead radius. Setting the volume of a model circular cylinder, $\pi R^2 L$, equal to that of N touching beads, $4\pi a^3 N/3$, gives $a = (3/2)^{1/2} R = 1.225$ nm. The number of base pairs, n_{bp}, equals 7.2N for this model. For the persistence length, P, of DNA, a value of 50 nm is assumed (121). However, μ of duplex DNA in free solution or in a dilute gel is fairly insensitive to this parameter.

In the model studies carried out in this work, we ignore the relaxation effect compute a reduced (dimensionless) mobility, μ_{red}, defined by

$$\mu_{red} = \frac{3C\eta q}{2\varepsilon_w k_B T}\left(\frac{\mu_{EM}}{y}\right) S(\phi_{ex}) \qquad (5-33)$$

where μ_{EM} is the (Effective Medium) model mobility, $y = q\zeta/k_B T$ (ζ is the electrostatic potential averaged over the surface of all beads in the model structure), and other quantities are defined in the first paragraph of Appendix A of reference 41. In the absence of a gel, μ_{red} exhibits only a very weak dependence on length as shown by the dashed line in Figure 5-10.

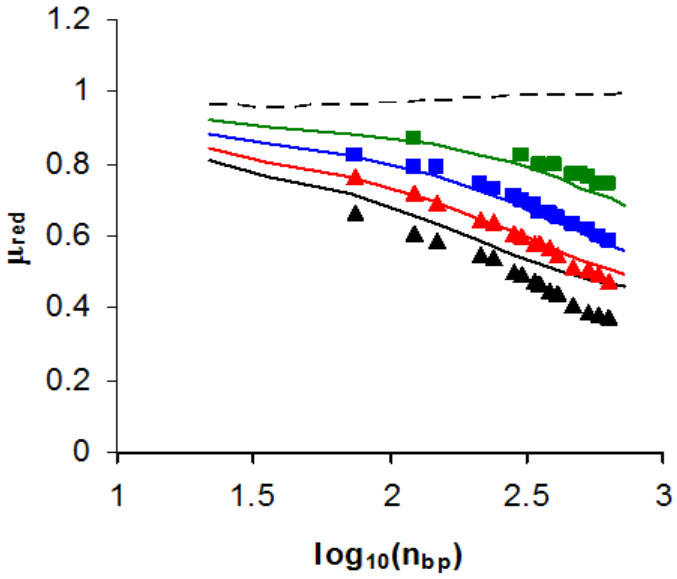

Figure 5-10) μ_{red} versus $\log_{10}(n_{bp})$ for duplex DNA in agarose gels. Experimental reduced mobilities, denoted by filled symbols (M = 0.005 gm/ml (green), 0.010 (blue), 0.015 (red), and 0.020 (black)), come from the work of Calladine et al. (95). Lines (dashed line, M = 0.0: solid lines; M = 0.005 (green), 0.010 (blue), 0.015 (red), and 0.020 (black)) are from model studies with σ = 2.0 nm.

This trend is also observed for the experimental mobility of DNA for $n_{bp} \geq 50$ (79). Since |y| is nearly independent length for long DNA (120, 154) and since the relaxation correction versus y is comparable for spheres and (long) cylinders (155), we would expect μ_{red} to equal μ_{expt} within a multiplicative constant to correct for the relaxation effect.

The ease and power of gel electrophoresis to separate DNA on the basis of length is responsible for the widespread use of the technique. Can the EM model account for the length dependence of the mobility of DNA when a gel is present? In Figure 5-10, μ_{red} is compared with experiment for DNAs shorter than 1000 bp. In order to deal with the relaxation correction discussed in the previous paragraph, experimental mobilities have been scaled to match μ_{red} for a single measurement. For this measurement, we choose a 72 bp DNA fragment with M = 0.01

gm/ml. As Figure 5-10 shows, the EM model works quite well for short DNAs and/or low gel concentrations. Given the inherent limitations of the model (9), these trends are expected.

5.4 Summary

The translational diffusion constant, D, of a particle in a gel or congested medium can be written as the product of two terms (108). In one of these, D_{EM}, long range hydrodynamic interaction between the particle and the gel is accounted for using the Effective Medium model. For an irregularly shaped object modeled as an array of non-overlapping beads, this problem has been addressed previously (45). The other term, S, accounts for direct interactions which in the present work is restricted to short range repulsive, or steric interactions. Here, S is studied for straight rods and wormlike chains with parameters chosen that are appropriate for duplex DNA in the 100 to several thousand base pair range. Brownian dynamics simulation is used to determine S for a range of DNA length, gel fibre spacing, A, and gel fibre radius, r_g. For wormlike chains with a persistence length, P, of 50 nm (appropriate for duplex DNA), a simple expression for S is deduced (Eq. (5-32)) that is valid over a broad range of DNA length as well as gel parameters.

This approach is then applied to two important systems, diffusion of DNA in dilute agarose gels and the cytoplasm of cells. For diffusion in agarose gels with M in the range of 0.002 to 0.02 gm/ml, modeling is in fair agreement with experiment for r_g = 2.0 to 4.0 nm. However, modeling tends to overestimate the length dependence of D for DNA in the size range of 500 to over 2000 base pairs. It is unlikely that direct electrosatatic interactions (138) are responsible given the relatively high ionic strengths used in the experiments (132,136). At present, we do

not have a satisfactory explanation for the difference. Given the limited amount of experimental data, particularly for short fragments (100 to 2000 base pairs), we do feel there is a great need for more measurements of D. For diffusion of DNA in cytoplasm, D_{cyto}, relative to water, D_w, it was possible to identify conditions in which the length dependence of D_{cyto}/D_w observed experimentally could be reasonably well accounted for within the framework of the EM plus steric model.

Diffusion of macromolecules in gels or congested media is an extremely important problem in molecular biology, drug delivery, and separation science. It is hoped that the methodology developed here will be of value in future studies of diffusion of irregularly shaped bodies in gels or congested media. This work is also relevant to related transport phenomena such as gel electrophoresis (103).

Chapter 6

Translational Diffusion Constants of Short Peptides: Measurement by NMR and Their Use in Structure Study of Peptides

6.1 Introduction:

The translational diffusion constant, D_T, of macromolecules is a fundamental property that widely used in biology and chemistry study. Self-diffusion constants are sensitive to particle size and conformation. This sensitivity, coupled with a wide range of available techniques that make D_T a comparatively simple quantity to measure, are responsible for its importance. For macromolecules with a molecular weight in excess of 20 kD, dynamic light scattering has long been the method of choice (156). For small molecules that do not scatter much light, methods related to boundary spreading due to a concentration gradient have long been used (157-160). In addition, pulse field NMR has become a useful method (161-165) and has the advantage of being applicable at very low concentrations. In this chapter, we are measuring the diffusion by NMR and use the result to characterize peptide conformation/aggregation in free solution.

The focus of this chapter concerns the self-diffusion constants of peptides in aqueous solution in the limit of infinite dilution. The principal objective of this work is to report diffusion constants of 5 short peptides: Gly-Gly (GG), Gly-Arg (GR), Gly-Gly-Arg (GGR), Gly-Gly-Asp-Ala (GGNA), and Gly-Gly-Arg-Ala (GGRA). The method employed is field gradient NMR and is described in detail elsewhere (161, 162).

We are also studying the effect of secondary structure to the translational diffusion constant, D_t, for peptides. Our modeling results show that there is certain kind of affect even for

small peptides contains amino acids with flexible side group. The principal objective of this work is the determination of D_T and D_T^0, where the "0" superscript represents the zero concentration limit (80), for 5 short peptides: GG, GR, GGR, GGNA, GGRA, by field gradient NMR. The diffusion constant of the amino acid glycine, G, is also reported. For G and GG, we are able to compare our D_T with earlier results measured by the concentration gradient methods (157-160). The results for G and GG are also used to adjust one parameter, the "side bead" radius of glycine, in a "bead model" that we have found particularly useful in studies of the free solution electrophoretic mobility of peptides (76). Also, when two G's condense to form GG, a single water molecule is lost and we are able to estimate the change in solvation volume due to the loss of a water molecule. We then use the peptide bead model along with the D_T's determined in this work to examine the solution conformation of the remaining peptides. Two of these, GGNA and GGRA, have been the subject of detailed study by free solution electrophoresis (62, 66).

6.2 Materials and Methods

2A) Peptide Samples. Peptide samples (GenScript) were prepared in D_2O in a buffer consisting of 80 mM sodium phosphate. Unless otherwise noted the peptide concentration was 5 mM. For peptides GG and GGRA the concentration was varied from 5 to 20 mM and the diffusion constants at zero concentration were estimated by extrapolation. The pH* (uncorrected meter reading) is adjusted to 3.05-3.09 with DCl. This corresponds to a pD of approximately 3.50 (166).

2B) NMR Spectroscopy. NMR spectra were acquired on a Bruker Avance 500 MHz spectrometer equipped with a 10 A gradient amplifier using a 5 mm TBI probe head $^{1}H\{^{13}C, X\}$ with a shielded Z-gradient coil. The gradient coil of the probe head was calibrated to 5.72 Gauss/(cm A) using a 5 mm Shigemi NMR tube (Shigemi) with a 14 mm sample window using 99.96% D_2O. All D_T measurements were recorded at 298 K using a pseudo 2D stimulated echo pulse program with 1 spoil gradient ("stegp1s") (Bruker pulse sequence "stegp1s, v.1.1.2.2") (167, 168). In the diffusion experiments, gradient delays and lengths were adjusted to cover the range of 5 to 95% of the signal intensity in 16 increments. Typically, 16-32 scans were collected for each experiment, using a relaxation delay of 8 s, and 1 to 2 Hz line broadening. The data were processed and analyzed using the T1/T2 package of XwinNMR 3.5. With the gradient calibration, a D_T of HDO (99.96% D_2O) of 2.24×10^{-9} m^2/s at 298 K is obtained. This agrees with previously reported D_T of HDO, which range from 1.90 to 2.51 X 10^{-9} m^2/s (169, 170).

Table 6-1. Important Parameters for Each Experiment.

Peptide or amino acid	p1 (us)	p30 (us)	rg
Ala	11.3	1160	128
GlyGly	11.35	1700	128
GlyArg	11.1	1520	71.8
GlyGlyArg	11.3	1525	114
GlyGlyArgAla	11.4	1900	256
GlyGlyAsnAla	11.1	1520	101.6

The gradient pulse was optimized to fit well to a SINE funtion. Parameters (Δ and δ) need to be optimized to detect the whole decay function. Typical ranges: 50 – 100 ms for (Δ, d20) amd 1ms (δ, p30). The way to optimize the gradient is to record 1D spectrum with 2% and 95% gradient (gpz6) respectively. After phasing them and baseline correction, compare their signal

intensity. The resulting spectrum should be around 5% intensity difference. Both Δ and δ can be adjusted with δ having a greater effect. In our case, we mainly change the δ value. The δ values for each case in our experiment can be seen in Table 6-1.

6.3 Results

All NMR experiments on amino acid and peptide samples were carried out in D_2O at 298 K in a buffer solution containing 80 mM sodium phosphate at pD ≅ 3.5. The translational diffusion constant in the limit of zero amino acid or peptide concentration, D_T^0, is related to the hydrodynamic radius, R_h, by the relation

$$D_T^0 = \frac{k_B T}{6\pi\eta R_h} \qquad (6-1)$$

where T is the temperature (in K), k_B is Boltzmann's constant, and η is the solvent viscosity. For a low ionic strength D_2O buffer at 298 K, η = 1.091 cp (.001091 kg/(m sec)) (171). This compares to a viscosity of a low ionic strength H_2O buffer at 298 K of 0.89 cp (8.9×10^{-4} kg/(m sec)). Assuming R_h is unaffected by the substitution of H_2O with D_2O, we can correct "raw" diffusion constants measured in D_2O to the corresponding diffusion constants in water at 298 K with

$$D_T^0(H_2O, 298K) = 1.226\, D_T^0(D_2O, 298K) \qquad (6-2)$$

In this chapter, all diffusion constants reported have been corrected to water at 298 K.

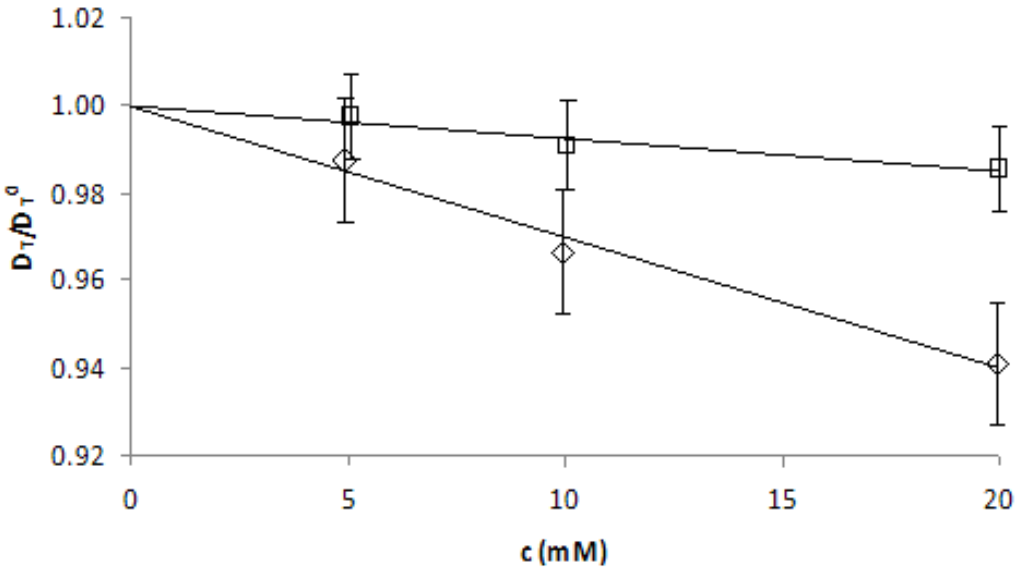

Figure 6-1) D_T/D_T^0 versus peptide concentration for GG and GGRA. The squares and diamonds correspond to experimental ratios for GG and GGRA, respectively. Measurements were carried out in D_2O at 298 K in 80 mM monosodium phosphate buffer at pD ≅ 3.50. The lines correspond to linear fits of the data and the vertical bars represent the estimated error.

NMR experiments for GG and GGRA were carried out at 5mM, 10mM, and 20mM peptide concentration, in order to examine the concentration dependence of D_T. In the limit of zero concentration, D_T extrapolates to 7.58 and 4.71 × 10^{-10} m^2/s for GG and GGRA, respectively. The ration D_T/D_T^0 is plotted in Figure 6-1 versus the peptide concentration for both GG and GGRA. The error bars reflect the estimated 1% relative uncertainty in the measured diffusion constants. The ratio D_T(0 mM)/D_T(20 mM) gives 1.015 and 1.047 for GG and GGRA respectively. For the remaining samples, D_T was only measured at 5 mM. A 4% correction for a 20 mM sample would translate into a 1% correction for a 5 mM sample, and this is comparable to the relative error in the NMR measurements themselves. The D_T^0 values are summarized in Table 6-2. For GG and GGRA, these were estimated by extrapolation. For the other samples, we simply equate D_T^0 to the measured value at 5 mM peptide concentration. Also listed in Table

6-2 are effective hydrodynamic radii using Eq. (6-1) and D_T^0's obtained from modeling. The modeling values shall be discussed in the Discusstion Section.

Table 6-2. D_T^0 (in 10^{-10} m^2/sec) and R_h for G and Peptides[(a)]

Species	D_T^0(present work)	R_h (nm)[(b)]	D_T^0(past work)	D_T^0(modeling)	Error[(c)]
G	9.88	0.248	9.6-10.7	---	---
GG	7.58	0.324	7.9-8.0	7.58	---
GR	5.62	0.437	-	5.93	+.055
GGR	5.56	0.441	-	5.31	-.045
GGRA	4.71	0.521	-	4.77	+.013
GGNA	5.19	0.473	-	5.13	-.012

(a) in dilute aqueous buffer at 298 K
(b) from Eq. (6-1)
(c) defined as D_T^0(model)/ D_T^0(experiment)-1

In comparing the present results with past work, there have been a number of previous experimental studies on both G and GG. For G, a detailed comparison of literature values for G were reported by Polson (157) and the range appearing in Table 6-3 comes from that reference corrected to 298 K. Ma and coworkers recently reported values for G (concentration range from 100 to 500 mM) and other amino acids and from their data, we estimate $D_T^0 \cong 10.56 \times 10^{-10}$ m^2/sec (160), which lies near the high end of the range reported in Table 6-3. The present NMR value (5 mM glycine) of 9.88×10^{-10} m^2/sec lies closer to the low end and is 6.7 % lower than the recent concentration gradient measurement of reference 160. In a previous analysis of D_T^0's of amino acids reported by different groups, discrepancies of up to 8 % have been reported and the discrepancy observed for glycine in the present work falls within this range. For GG, the present NMR D_T^0 lies below previously reported values (158, 159) by about 4%, which is well within the 8% range mentioned above for the amino acids.

6.4 Discussion

4A) Analysis of G and GG

In past work that has dealt primarily with the free solution electrophoretic mobility, μ, of peptides, we have developed and used a model in which each amino acid of a peptide chain is represented by two beads (52, 76). One of these beads, the "backbone bead" has a fixed radius of 0.19 nm and is chosen to reproduce the known average distance of 0.38 nm between near neighbor α-carbons (79). The remaining "side bead" is of variable radius, a_s, depending on the amino acid. Its value is determined on the basis of the translational diffusion constant of the particular amino acid (76, 80). Using well established methods of bead hydrodynamics (22) and modeling intersubunit hydrodynamic interaction at the level of the Rotne-Prager tensor (148), it is straightforward to estimate the side bead radius of an amino acid, modeled as a dimer of two touching beads of unequal radius, provided R_h is known (Eq. (6-1)).

For the R_h of G reported in Table 6-2, we obtain an a_s of 0.182 nm. However, when amino acids condense to form peptides, a single water molecule is lost for each amino acid added to a growing peptide chain. This is illustrated in Figure 6-2 for the condensation of two G's to form GG. Due to the loss of water, the side bead radius of glycine in GG will be different from the side bead radius in "free" glycine. Using the procedure described previously (38, 52, 76), several hundred peptide conformations are generated using random numbers to select the phi-psi angles between adjacent amino acids. Rotation matrices (86) are used to properly position successive bead pairs in relation to other beads lower down the chain. For each conformation, we compute D_T^0 and also other transport properties such as the electrophoretic mobility (38, 52,

76). Secondary structure can also be incorporated into this methodology (38). Final transport properties are obtained by simple averaging the single conformation transport properties over all the different conformations generated. When this procedure is applied to GG (random secondary structure) and the side bead radius of each G is left as a variable parameter, a_s equal to 0.164 nm is necessary to match model and experimental D_T^0.

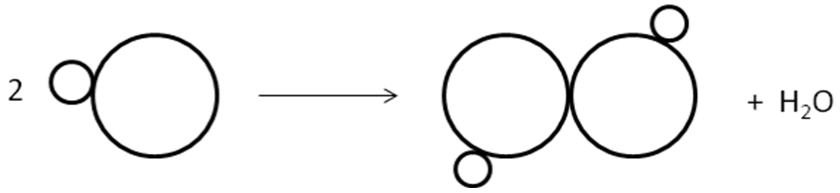

Figure 6-2. The illustration of the condensation of two G's to form GG.

We can view each G of GG as having lost one half of a water molecule each. The hydrodynamic radius, R_s, of a touching dimer of radii 0.190 and 0.164 nm is estimated to be 0.237 nm. This can be compared to R_h = 0.248 nm for "free" glycine. If a small molecule with hydrodynamic radius R_h loses volume δv, the resultant hydrodynamic radius, R_s, can be estimated to be (172)

$$R_s = R_h\left(1-\frac{3\delta v}{4\pi R_h^3}\right)^{1/3} \qquad (6-3)$$

Solving Eq. (6-2) for δv, we obtain 0.00813 nm^3 for the loss of one half of a water molecule or 0.0163 nm^3 for the loss of one full water molecule. This is slightly smaller than the value of 0.0186 nm^3 estimated previously (76). For a G entirely within a peptide chain, it will have lost one full water molecule. From Eq. (6-3), we estimate R_s = 0.225 nm (using R_h = .248 nm and δv

= 0.0163 nm^3) and a side bead radius, a_s, equal to 0.143 nm. In what follows, we shall use these adjusted side bead radii of G in modeling the other peptides. The a_s values for the remaining amino acids are the same as before and are reported elsewhere (80).

4B) Comparison of D_T^0 Between Experiment and Modeling for the Remaining Peptides.

By employing the bead model described in the previous section, we obtain model translational diffusion constants summarized in Table 6-3 along with the corresponding experimental diffusion constants and hydrodynamic radii. In modeling, the temperature was taken to be 298 K and the "random" secondary structure was assumed (38). The model diffusion constants represent the average over several hundred independently generated conformations and agreement between modeling and experiment lies within ± 5%.

In an earlier modeling study of the electrophoretic mobility, μ, of GGRA and GGNA (38) based on experiments by Messana and coworkers (62, 66), it was concluded that the mobility data of GGNA was well explained by a random model of the peptide, but this was not the case for GGRA. For GGRA, a more compact model, possibly containing an I-turn, was necessary to explain the large absolute mobility observed experimentally (38). However, such a compact model structure yields $D_T^0 = 5.50 \times 10^{-10}$ m^2/sec which is higher than the experimental value by 17%. On the basis of the present NMR measurement of D_T^0, we conclude that the solution conformation of GGRA, or more precisely, the sample examined in our NMR experiment, is a more open "random" structure rather than a compact structure.

6.5 Summary

In this chapter, field gradient NMR has been used to measure the translational diffusion constants of glycine and several short peptides. Where independent experimental data is available, the current NMR diffusion constants agree with previous values to within several percent. An advantage of NMR over concentration gradient methods is the much lower sample concentrations required. Furthermore, NMR can be used to determine translational diffusion constants of small molecules that are inaccessible to dynamic light scattering. Diffusion constants can provide valuable information about the solution conformation of peptides. When applied to short peptides such as GGNA and GGRA around a pH of 3.5 in a low salt buffer, it is concluded unequivocally that the solution conformation is random and open and not compact.

Chapter 7

Viscosity of Dilute Model Bead Arrays at Low Shear

7.1 Introduction

Modeling the intrinsic viscosity of general solutes present in dilute solution remains a challenging problem to this day. Much of this modeling is based on the "standard" model (S model for brevity) which works well when the solute is large in size relative to the solvent molecules in which it is immersed and solute/solvent interactions can be ignored, to a good approximation, beyond contact interactions at the solute-solvent interface. This model always predicts a positive intrinsic viscosity, which is at variance with experiment for certain systems such as low molecular weight alkanes in benzene (173) as well as other low molecular weight polymers in certain solvents (174). Although amino acids and short peptides in aqueous solvent have positive intrinsic viscosities (175), the S model is unable to account quantitatively for the experimental results (46). One objective of the present work is to generalize the S model in a preliminary attempt to deal with this problem.

In the S model, the solute is represented as a rigid, possibly irregularly shaped particle, or rigid bead array, immersed in a continuum incompressible Newtonian fluid (the solvent) of viscosity η_0. Solute-solvent interactions are assumed to arise strictly from short range excluded volume repulsions present at the solute-solvent interface. It is also assumed that the solvent obeys the low Reynolds Number Navier-Stokes equation (49, 50). In most applications of the S model, solute and solvent velocities are assumed to match at their interface ("stick" hydrodynamic boundary conditions). In the case of "slip" boundary conditions, only the velocity

components normal to the interface match and the hydrodynamic stress forces at the interface are also assumed to be normal (51). The applications of the S model discussed in the present work employ “stick” boundary conditions.

Using the S model, Einstein determined the intrinsic viscosity of dilute suspensions of spheres (176). Extension of the model to axially symmetric ellipsoids proved problematic. Jeffrey correctly evaluated the energy dissipation of an ellipsoid in an arbitrary shear field (177), but he did not carry out a suitable ensemble average to relate this to intrinsic viscosity. This was achieved by Simha in the limit of low shear (178) and by Scheraga under general shear conditions (179). A key feature of the Simha-Scheraga treatment involved accounting for rotational Brownian motion. Ignoring Brownian motion leads to an underestimation of the intrinsic viscosity (179). The S model (with account of Brownian motion) was extended to flexible polymers modeled as strings of beads by Kirkwood and coworkers (180, 181). This “bead method” has been refined and generalized (retaining the S model assumptions) by later investigators and applied to particles of arbitrary shape (114, 182-185). These latter applications, in which the surface of an irregularly shaped particle is modeled as a shell of closely packed beads, is similar to Boundary Element procedures, where it is modeled as a closed surface of interconnected triangular plates (187, 188). Current applications (185, 188) can handle several thousand beads or plates and the Boundary Element procedure can accommodate “stick” or “slip” hydrodynamic boundary conditions (17).

In this chapter, the BAEM approach shall be extended to the problem of the viscosity of a dilute suspension of bead arrays. By doing so, we shall show that it is possible to obtain accurate intrinsic viscosities, or viscosity shape factors, using comparatively few beads in modeling the

actual structure. Our first objective is generating a "standard" (S model for brevity) model to account more accurately for solute-solvent interactions. The approach we shall follow is very similar to that of Fixman (189). General, but *short range* solute-solvent interactions are accounted for using single bead translational friction, rotational friction, and viscosity shape factors for individual beads that may be different from those of beads that interact with the solvent under standard (S model) conditions. *Long range* hydrodynamic interactions are treated in the same way as before.

A second objective of this chapter involves taking approximate account of the variation in hydrodynamic stresses over individual beads. The present work is an extension and improvement upon our earlier treatment of this problem (46). Accounting for this variation results in a significant improvement in accuracy when the model consists of a limited number of beads. In modeling, this makes it possible to sample many conformations of large extended structures, such as wormlike chains of duplex DNA consisting of 100 to over 600 base pairs in length, at low computational cost.

The methodology is formulated in Section 2 and the S model is presented and developed for a bead array in a shear field within the BE formalism. In Section 3, the formal methodology for determining the viscosity shape factors is presented. In Section 4, the S model is applied to determine the viscosity shape factors for simple models, and then to linear strings and rings of touching beads in order to test its accuracy. Later, it is applied first to duplex DNA in aqueous media, and then to alkanes in Bezene. In Section 5. The principal results of the paper are summarized.

7.2 Viscosity Model Theory

2A) Model

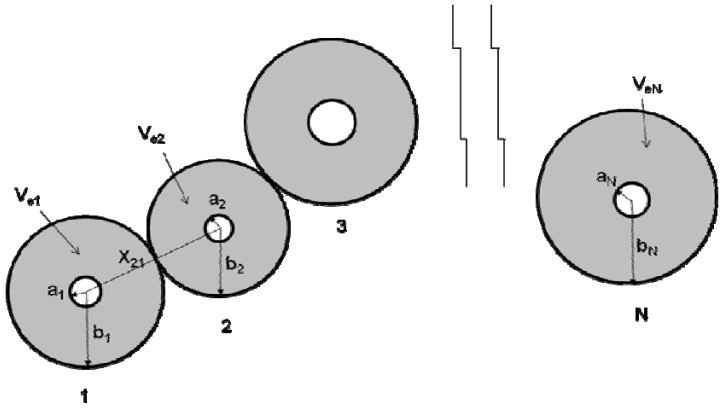

Figure 7-1) Schematic of the Bead Array Model. Inner bead radii are denoted by a_I and external forces may be present out to a distance b_I from the center of bead I. These radii may vary from bead to bead. V_{eI} denotes the fluid volume between a_I and b_I. There are a total of N beads in the array and x_{IJ} denotes the distance between the centers of beads I and J.

The solute is represented as an N bead array and is depicted in Figure 7-1. Bead J ($1 \leq J \leq N$) consists of an inner solid core of radius a_J and an outer fluid surface of radius b_J. In general, these radii can vary from bead to bead. The outer bead radii do not overlap. Stick hydrodynamic boundary conditions are assumed to prevail on the inner core bead surfaces, but an external force/volume, $\underline{s}(\underline{x})$, may be present in the fluid domain exterior to a_J, but interior to b_J, V_{eJ}. In the present work, it is useful to view $\underline{s}(\underline{x})$ as arising from the short range solute-solvent interactions that may represent "solvent breaking" or "solvent stabilizing" influences that arise when the solute is placed in the solvent. In the present work, it shall be assumed that the solute is present in dilute concentration and that solute-solute interactions (interactions between different bead arrays) can be neglected. Outside of the V_{eJ}'s, it is assumed that $\underline{s}(\underline{x})$ can be set

zero. The bead array is immersed in a simple shear field with shear gradient γ (in sec^{-1}) and it is assumed that $1/\gamma$ is long on the timescale of the array's Brownian translational and rotational motions. It is also assumed that γ is sufficiently small so that deformation of the bead array can be ignored and that its average orientation remains isotropic. Let the bead array translate with instantaneous overall velocity, $\underline{u}_0$, relative to a center of rotation, $\underline{d}$. Also let the instantaneous angular velocity of the entire bead array about $\underline{d}$ be denoted by $\underline{\omega}$, and let $\underline{x}_K$ denote the instantaneous position of the center of bead K. By "instantaneous", we mean a timescale short compared to average translational and rotational displacements of the beads, but long compared to the impulsive collision time between beads and solvent. If point $\underline{y}$ lies on the fluid/inner core surface of bead K and stick boundary conditions hold, then the rigid body particle velocity and fluid velocities match at $\underline{y}$.

$$\underline{v}_{RBM}(\underline{y}) = \underline{u}_0 + \underline{\omega} x (\underline{x}_K - \underline{d}) + \underline{\omega} x (\underline{y} - \underline{x}_K) \qquad (7-1)$$

In Eq. (7-1) above, "x" denotes the vector cross product.

Suppose our bead array is placed in a simple shear field where at $\underline{y}$, the fluid velocity in the absence of our bead array is given by

$$\underline{v}_0(\underline{y}) = \gamma \, \underline{e}_A (\underline{e}_B \cdot \underline{y}) \qquad (7-2)$$

where $\underline{e}_A$ and $\underline{e}_B$ are arbitrary, but orthogonal unit vectors ($\underline{e}_A \cdot \underline{e}_B = 0$). It is convenient to break up Eq. (7-2) into pure translational, rotational, and deformational flows,

$$\underline{v}_0(\underline{y}) = \gamma(\underline{d}\cdot\underline{e}_B)\underline{e}_A + \frac{1}{2}\gamma(\underline{y}-\underline{d})\ x\ \underline{e}_C + \frac{1}{2}\underline{\underline{E}}\cdot(\underline{y}-\underline{d}) \qquad (7-3)$$

$$\underline{e}_C = \underline{e}_A\ x\ \underline{e}_B \qquad (7-4)$$

$$\underline{\underline{E}} = \gamma(\underline{\underline{e_A e_B}} + \underline{\underline{e_B e_A}}) \qquad (7-5)$$

The second term on the right hand side of Eq. (7-3) represents rotational motion of the fluid in the absence of the bead array about position $\underline{d}$. We denote this angular velocity $\underline{\omega}_0$ and

$$\underline{\omega}_0 = -\frac{\gamma}{2}\underline{e}_C \qquad (7-6)$$

When our bead array is placed in a flow field described by Eq. (7-2), it will translate with velocity $\underline{u}_0 = \gamma(\underline{d}\cdot\underline{e}_B)\underline{e}_A$. In the limit of negligible Brownian motion, it will also rotate, but its instantaneous angular velocity, $\underline{\omega}$, may be different from $\underline{\omega}_0$. For the cases of greatest interest in this work, Brownian motion is not negligible and indeed is quite significant. For the moment, however, it shall be left unaccounted for until the methodology is developed further. Under these conditions then, the total instantaneous force and torque exerted by the bead array on the fluid vanishes. We shall return to this point later. The first two terms in Eq. (7-3) represent the local translational and rotational motions of the fluid and the final term represents the deformational motion. This last term is particularly important in determining how the bead array affects the overall viscosity of the fluid.

Exterior to the inner core of the bead surfaces, the fluid is modeled as the continuum fluid discussed in chapter 1, Eqs. (1-1) to (1-4).

2B) Viscosity of a Dilute Suspension of Irregularly Shaped Rigid Particles.

The viscosity of a Newtonian fluid in the absence of solute, η_0, subjected to a simple shear field defined by Eq, (7-2) is related to $\underline{\underline{\sigma}}_0$ (hydrodynamic stress in the absence of solute) by

$$\eta_0 \dot{\gamma} = \underline{e}_A \cdot \underline{\underline{\sigma}}_0(\underline{x}) \cdot \underline{e}_B \qquad (7-8)$$

This is readily verified by substituting Eq. (7-3) into Eq. (1-4) on the right hand side of Eq. (7-8). The presence of dilute solute of number concentration c (in particles/dm^3) alters the long range flow pattern (p, $\underline{v}$, and $\underline{\underline{\sigma}}$) in the fluid and this, in turn, alters the macroscopic viscosity, η, of the solution

$$\eta \dot{\gamma} = \underline{e}_A \cdot \underline{\underline{\sigma}}(\underline{x}) \cdot \underline{e}_B \qquad (7-9)$$

The macroscopic excess stress, $\underline{\underline{\sigma}}^e = \underline{\underline{\sigma}} - \underline{\underline{\sigma}}_0$, can be expressed in terms of single particle averages using an equation derived by Batchelor (190) (for fluids with $\underline{s}(\underline{x}) = \underline{0}$) and extended by Russell (191) to include external forces

$$\frac{\underline{\underline{\sigma}}^e}{c} = -\left\langle \int_{S_p} \{ \underline{f}(\underline{x})\,\underline{x} + \eta_0 [\underline{v}(\underline{x})\underline{n}(\underline{x}) + \underline{n}(\underline{x})\underline{v}(\underline{x})] \}\, dS_x + \int_{V_e} \underline{s}(\underline{x})\,\underline{x}\, dV_x \right\rangle \qquad (7-10)$$

In Eq. (7-10), brackets, < >, denote averaging over all possible particle positions and orientations, the surface integration over S_p is over the surface of the particle, which in the present case is the inner core surfaces of all N beads, $\underline{n}(\underline{x})$ denotes the local outward unit surface normal (into the fluid), the volume integral is over the fluid external to our particle, and

$$\underline{f}(\underline{x}) \;=\; -\underline{\underline{\sigma}}(\underline{x})\cdot\underline{n}(\underline{x}) \qquad (7-11)$$

denotes the local hydrodynamic force/area exerted by the particle on the fluid. For a particle with stick hydrodynamic boundary conditions, both terms containing $\underline{v}$ on the right hand side of Eq. (7-10) vanish. For our bead array model, the i-j component of Eq. (7-10) can be written

$$\frac{\sigma^{e}_{ij}}{c} \;=\; -\sum_{K=1}^{N}\left\langle \int_{S_K} f_i(\underline{x})\, x_j \; dS_x + \int_{V_{eK}} s_i(\underline{x})\, x_j \; dV_x \right\rangle \qquad (7-12)$$

It is useful to define a dimensionless "shape factor", ξ, by the relation

$$\xi \;=\; \lim_{c\to 0} \frac{1}{cV_p}\left(\frac{\eta}{\eta_0}-1\right) \qquad (7-13)$$

$$V_p \;=\; \sum_{K=1}^{N} V_K \;=\; \frac{4\pi}{3}\sum_{K=1}^{N} a_K^3 \qquad (7-14)$$

For the special case of a spherical particle with $\underline{s}(\underline{x}) = \underline{0}$, $\xi = 5/2$ as derived by Einstein (176). The shape factor is closely related to the viscosity "B-factor", in dm^3/mole,

$$B \;=\; \lim_{c\to 0} \frac{N_{Av}}{c}\left(\frac{\eta}{\eta_0}-1\right) \qquad (7-15)$$

and intrinsic viscosity, (η), in dm^3/gm

$$[\eta] \;=\; \lim_{c'\to 0} \frac{1}{c'}\left(\frac{\eta}{\eta_0}-1\right) \qquad (7-16)$$

where N_{Av} is Avogadro's Number and c' is the weight concentration of solute in gm/dm^3. Let M denote the solute molecular weight, in gm/mole, then ξ , B, and (η) are related to each other by

$$B = N_{Av} V_P \xi = M[\eta] \qquad (7-17)$$

Using Eqs. (7-10), (7-11), and (7-14) in Eq. (7-15)

$$\xi = -\frac{1}{\eta_0 \gamma V_P} \sum_{K=1}^{N} \underline{e}_A \cdot \left\langle \int_{S_K} \underline{f}(\underline{x})(\underline{x}-\underline{d}) dS_x + \int_{V_{eK}} \underline{s}(\underline{x})(\underline{x}-\underline{d}) dV_x \right\rangle \cdot \underline{e}_B \qquad (7-18)$$

The inclusion of $\underline{d}$ in Eq. (7-18), or any other constant vector for that matter, is allowed because the total force, $\underline{F}_{total}$, exerted by the bead array on the fluid vanishes for all conformations and/or orientations,

$$\underline{F}_{total} = \sum_{K=1}^{N} \left\{ \int_{S_K} \underline{f}(\underline{x})\, dS_x + \int_{V_{eK}} \underline{s}(\underline{x})\, dV_x \right\} = \underline{0} \qquad (7-19)$$

In order to carry out the averages indicated in Eq. (7-18) for an arbitrary conformation of our bead array, it is necessary to examine the bead array in five different elementary shear fields (187, 192), which can be written

$$\underline{\underline{E}}^{(1)} = \gamma(\underline{\underline{e_1 e_2}} + \underline{\underline{e_2 e_1}}) \qquad (7-20a)$$

$$\underline{\underline{E}}^{(2)} = \gamma(\underline{\underline{e_1 e_3}} + \underline{\underline{e_3 e_1}}) \qquad (7-20b)$$

$$\underline{\underline{E}}^{(3)} = \gamma(\underline{\underline{e_2 e_3}} + \underline{\underline{e_3 e_2}}) \qquad (7-20c)$$

$$\underline{\underline{E}}^{(4)} = \gamma(\underline{\underline{e_1 e_1}} + \underline{\underline{e_2 e_2}}) \qquad (7-20d)$$

$$\underline{\underline{E}}^{(5)} \quad = \quad \gamma(\underline{\underline{e_1 e_1}} + \underline{\underline{e_3 e_3}}) \qquad (7-20e)$$

In Eqs. (7-20), $\underline{e}_1, \underline{e}_2, and\, \underline{e}_3$ are orthogonal unit vectors in some convenient laboratory frame. Choosing $\underline{e}_A = \underline{e}_1, \underline{e}_B = \underline{e}_2$, then orientational averaging, assuming an isotropic distribution, yields (187, 192)

$$\xi = \frac{1}{5}(\xi_{12}^{(1)} + \xi_{13}^{(2)} + \xi_{23}^{(3)}) + \frac{1}{15}(\xi_{11}^{(4)} + \xi_{33}^{(4)} - 2\xi_{22}^{(4)} + \xi_{11}^{(5)} + \xi_{22}^{(5)} - 2\xi_{33}^{(5)}) \qquad (7\text{-}21)$$

where

$$\xi_{ij}^{(t)} = -\frac{1}{2\eta_0 \gamma V_p} \sum_{K=1}^{N} \left\{ \int_{S_K} \underline{p} \cdot \left(\underline{\underline{e_i e_j}} + \underline{\underline{e_j e_i}} \right) \cdot \underline{f}^{(t)}(\underline{x}) dS_x + \int_{V_{eK}} \underline{p} \cdot \left(\underline{\underline{e_i e_j}} + \underline{\underline{e_j e_i}} \right) \cdot \underline{s}^{(t)}(\underline{x})\, dV_x \right\} \quad (7-22)$$

In Eq. (7-22), p = x – d. These "elementary shape factor tensors", $\underline{\underline{\xi}}^{(t)}$, must be determined in order to evaluate ξ, B, or (η) for arbitrary rigid bead arrays. For an uncharged spherical particle with stick boundary conditions in one of the five elementary shear fields,

$$\underline{\underline{\xi}}^{(t)} \quad = \quad \frac{5}{2\gamma} \underline{\underline{E}}^{(t)} \qquad (7-23)$$

2C) Single Bead Forces and Related Quantities

Consider a single bead, K, centered at $\underline{x}_K$ and translating through the solution with velocity $\underline{u}_K$. Also let $\underline{v}_K'$ denote what the fluid velocity would be at $\underline{x}_K$ if bead K were absent. The total force exerted by bead K on the fluid can be written

$$\underline{F}_K = \int_{S_K} \underline{f}(\underline{x})\, dS_x + \int_{V_{eK}} \underline{s}(\underline{x})\, dV_x = \zeta^*_{Kt}(\underline{u}_K - \underline{v}'_K) \qquad (7-24)$$

In Eq. (7-24) ζ_{Kt}^* denotes the translational friction constant of bead K. In the absence of external forces, it is simply given by Stokes law, $6\pi\eta a_K$. It is also convenient to define

$$M_{Kji} = \int_{S_K} (x_i - x_{Ki}) f_j(\underline{x}) dS_x + \int_{V_{eK}} (x_i - x_{Ki}) s_j(\underline{x}) dV_x \qquad (7-25)$$

$$N_{Kjim} = \int_{S_K} (x_i - x_{Ki})(x_m - x_{Km}) f_j(\underline{x}) dS_x + \int_{V_{eK}} (x_i - x_{Ki})(x_m - x_{Km}) s_j(\underline{x}) dV_x \qquad (7-26)$$

Now the dyadic tensor, $\underline{\underline{M}}_K$, is related to the torque and stress on bead K. Let $\underline{T}_K$ denote the torque exerted by bead K on the fluid about its origin, $\underline{x}_K$. The angular velocity of the bead array about $\underline{d}$ is $\underline{\omega}$, and this is also the angular velocity of bead K about $\underline{x}_K$. Also let $\underline{c}_K$ denote the corresponding angular velocity of the fluid about $\underline{x}_K$ if bead K were absent. Then

$$T_{Ki} = \sum_{j,k=1}^{3} \varepsilon_{ijk} M_{Kkj} = \zeta^*_{Kr}(\omega_i - c_{Ki}) \qquad (7-27)$$

In Eq. (7-27), ε_{ijk} is the Levi-Civita symbol (which equals 1 for (ijk) = (123), (231), (312); -1 for (ijk) = (132), (321), (213); and 0 otherwise), and ζ_{Kr}^* is the rotational friction constant of bead K. In the absence of external forces, $\zeta_{Kr}^* = 8\pi\eta a_K^3$.

Now return to Eq. (7-22) and write

$$\underline{p} = (\underline{x} - \underline{x}_K) + \underline{r}_K \qquad (7-28)$$

$$\underline{r}_K = \underline{x}_K - \underline{d} \qquad (7-29)$$

Using Eqs. (7-24), (7-25), (7-28), and (7-29) in Eq. (7-22)

$$\xi_{ij}^{(t)} = -\frac{1}{2\eta_0 \gamma V_p} \sum_{K=1}^{N} \left\{ r_{Ki} F_{Kj}^{(t)} + r_{Kj} F_{Ki}^{(t)} + M_{Kji}^{(t)} + M_{Kij}^{(t)} \right\} \qquad (7-30)$$

Eq. (7-30) will be of considerable value in determining the elementary shape factor tensors of arbitrary rigid bodies. In the special case of a single bead, K, placed in elementary shear field, $\underline{\underline{E}}^{(t)}$, Eq. (7-30) reduces to

$$\underline{\underline{\xi}}_K^{(t)} = \frac{\xi_K^*}{\gamma} \underline{\underline{E}}^{(t)} = -\frac{1}{2\eta_0 \gamma V_K} \left(\underline{\underline{M}}_K^{(t)} + \underline{\underline{M}}_K^{(t)T} \right) \qquad (7-31)$$

The "T" superscript in Eq. (7-31) denotes transpose. ξ_K^* is the viscosity shape factor of a single isolated bead which equals 5/2 in the limit of an uncharged sphere. In the present work, however, it shall be left as an adjustable parameter. It could, in fact, be negative which corresponds to a negative solute intrinsic viscosity which occurs in certain systems (173, 189). The local shear gradient in the vicinity of bead K is approximated with

$$E_{Kij} = v'_{Ki,j} + v'_{Kj,i} \qquad (7-32)$$

$$v'_{Ki} = v'_i(\underline{x})\big|_{x_K} \qquad (7-33)$$

$$v'_{Ki,j} = \left. \frac{\partial v'_i(\underline{x})}{\partial x_j} \right|_{\underline{x}_K} \qquad (7-34)$$

In Eqs. (7-32) to (7-34), the fluid velocity is evaluated at the centroid of bead K, $\underline{x}_K$, with bead K removed. (In the course of this study, we also tried the more complicated procedure of averaging the fluid velocities over the surface of (removed) bead K, but actually obtained more accurate results with the simpler approach described above.) Eq. (7-31) can be written

$$M_{Kij} + M_{Kji} = -2\eta_0 V_K \xi_K^* E_{Kij} \qquad (7-35)$$

Eqs. (7-27) and (7-35) can be combined to yield

$$M_{Kij} = -\frac{\zeta_{Kr}^*}{2}\sum_{k=1}^{3}\varepsilon_{ijk}(\omega_k - c_{Kk}) - \eta_0 V_K \xi_K^* E_{Kij} \qquad (7-36)$$

Eq. (7-36) is useful since it gives the components of the tensor, $\underline{\underline{M}}_K$, in terms of single bead solute transport parameters (ζ_{Kr}^* and ξ_K^*) and the relative velocity field of the fluid in the vicinity of bead K if bead K were absent ($\underline{\omega}, \underline{c}_K, and\ \underline{\underline{E}}_K$). We can also write

$$c_{Ki} = -\frac{1}{2}\sum_{j,k=1}^{3}\varepsilon_{ijk}\, v'_{Kj,k} \qquad (7-37)$$

The components of the triadic tensor, $\underline{\underline{N}}_K$, defined by Eq. (7-26), are more difficult to deal with since they cannot, in general, be directly related to single bead transport parameters as is possible for $\underline{F}_K$ (Eq. (7-24)) and $\underline{\underline{M}}_K$ (Eq. (7-36)). However, the special case of a single bead in the absence of external forces can be solved since the hydrodynamic forces, $\underline{f}(\underline{x})$, are well known for a translating or rotating sphere, or for a sphere placed in a shear field. In this case, it can be shown

$$N_{K\,j\,i\,m} \quad = \quad \frac{a_K^2}{3}\delta_{i\,m}\,F_{K\,j} \qquad\qquad (7-38)$$

Under these conditions, translation contributes, but not rotation or shear. In the present work, we shall approximate $N_{K\,j\,i\,m}$ with Eq. (7-38). It should be noted that external forces do enter in general through $F_{K\,j}$. As we show in the next section, the components of $\underline{\underline{N}}_K$ enter as higher order correction terms in any case.

2D) Calculation of $\underline{F}_K$ and $\underline{\underline{M}}_K$

Following a Boundary element procedure developed previously (193), the fluid velocity at point $\underline{y}$ anywhere in space can be written (46)

$$\underline{v}(\underline{y})\Phi(\underline{y},V_e) = \underline{v}_0(\underline{y}) - \sum_{K=1}^{N}\underline{v}_{RBM}(\underline{y})\Phi(\underline{y},V_K) + \sum_{K=1}^{N}\{\int_{S_K}\underline{\underline{U}}(\underline{r})\cdot\underline{f}(\underline{x})dS_x + \int_{V_{eK}}\underline{\underline{U}}(\underline{r})\cdot\underline{s}(\underline{x})dV_x\} \qquad (7-39)$$

In Eq. (7-39), $\underline{v}_0(\underline{y})$ denotes the fluid velocity at $\underline{y}$ in the absence of all beads, $\underline{v}_{RBM}(\underline{y})$ denotes the rigid body motion of the bead array (Eq. (7-1)), V_K denotes the inner core volume of bead K, V_e is the fluid volume exterior to the inner core volumes, $\underline{f}(\underline{x})$ is the hydrodynamic force/area exerted by the bead on the fluid at $\underline{x}$, and $\Phi(y,V)$ equals 1 if y lies within V, it equals 0 if y lies outside of V, and it equals ½ if y lies on the boundary surface enclosing V. Also, $\underline{r} = \underline{x} - \underline{y}$ and $\underline{\underline{U}}(\underline{r})$ is the singular (Oseen) tensor defined by

$$\underline{\underline{U}}(\underline{r}) \;=\; \frac{1}{8\pi\eta_0 r}\left(\underline{\underline{I}}+\frac{1}{r^2}\underline{\underline{rr}}\right) \qquad (7-40)$$

Next, remove bead K and choose $\underline{y}=\underline{x}_K$ where $\underline{x}_K$ is the centroid of bead K. Also, expand $\underline{\underline{U}}(\underline{r})$ in Eq. (7-39) to second order about $\underline{x}_{JK}=\underline{x}_J-\underline{x}_K$ and use the definitions of Eqs. (7-24) to (7-26)

$$v'_{Ki} \cong v_{K0i}+\sum_{J\neq K}\left\{\sum_{j=1}^{3}U^{Ki}_{Jj}F_{Jj}+\sum_{j,k=1}^{3}U^{Ki}_{Jj,k}M_{Jjk}+\frac{1}{2}\sum_{j,k,m=1}^{3}U^{Ki}_{Jj,km}N_{Jjkm}\right\} \qquad (7-41)$$

where v_{Ki}' is defined by Eq. (7-33), $v_{K0i}=(\underline{v}_0(\underline{x}_K))_i$,

$$U^{Ki}_{Jj} \;=\; U_{ij}(\underline{x}_{JK}) \;=\; \underline{e}_i\cdot\underline{\underline{U}}(\underline{x}_{JK})\cdot\underline{e}_j \qquad (7-42a)$$

$$U^{Ki}_{Jj,k} \;=\; \left.\frac{\partial U_{ij}(\underline{r})}{\partial x_k}\right|_{\underline{r}=\underline{x}_{JK}} \qquad (7-42b)$$

$$U^{Ki}_{Jj,km} \;=\; \left.\frac{\partial^2 U_{ij}(\underline{r})}{\partial x_k\partial x_m}\right|_{\underline{r}=\underline{x}_{JK}} \qquad (7-42c)$$

$$\nabla^2 U^{Ki}_{Jj} \;=\; \sum_{k=1}^{3}U^{Ki}_{Jj,kk} \qquad (7-42d)$$

Truncating the expansion of U_{ij} at second order,(Eq. (7-42c)), is accurate to order x_{JK}^{-3}. In what follows, we shall be careful to retain terms to this order.

Use Eqs. (7-24) and (7-38) in Eq. (7-41)

$$F_{Ki} \cong \zeta^*_{Kt}(u_{Ki} - v_{K0i}) - \sum_{J \neq K}\left\{\sum_{j=1}^{3}\zeta^*_{Kt}\left(U^{Ki}_{Jj} + \frac{a_J^2}{6}\nabla^2 U^{Ki}_{Jj}\right)F_{Jj} + \sum_{j,k=1}^{3}\zeta^*_{Kt}U^{Ki}_{Jj,k}M_{Jjk}\right\} \quad (7-43)$$

Using Eqs. (7-1) and (7-3) in Eq. (7-43),

$$\sum_{J=1}^{N}\sum_{j=1}^{3}Q^{Ki}_{Jj}F_{Jj} + \sum_{J=1}^{N}\sum_{j,k=1}^{3}B^{Ki}_{Jjk}M_{Jjk} + \sum_{j=1}^{3}L^{Ki}_{j}\delta\omega_j = a_{Ki} \quad (7-44)$$

where we have defined

$$Q^{Ki}_{Jj} = \delta_{KJ}\delta_{ij} + (1-\delta_{KJ})\zeta^*_{Kt}\left(U^{Ki}_{Jj} + \frac{a_J^2}{6}\nabla^2 U^{Ki}_{Jj}\right) \quad (7-45)$$

$$B^{Ki}_{Jjp} = \zeta^*_{Kt}U^{Ki}_{Jj,p} \quad (7-46)$$

$$L^{Ki}_{j} = -\zeta^*_{Kt}\sum_{k=1}^{3}\varepsilon_{ijk}(x_{Kk} - d_k) \quad (7-47)$$

$$\delta\omega_j = \omega_j - \omega_j^0 \quad (7-48)$$

$$a_{Ki} = -\frac{\zeta^*_{Kt}}{2}\sum_{j=1}^{3}E_{oij}(x_{Kj} - d_j) \quad (7-49)$$

For the sake of convenience, all $U^{Ki}_{Jj}, U^{Ki}_{Jj,k}$, *and* $U^{Ki}_{Jj,km}$ terms with J = K shall included, but set to zero. This procedure shall simplify the notation in the remainder of this work.E_{0ij} in Eq. (7-49) is the shear field using $\underline{v}_0(\underline{x})$ in Eq. (7-32). Eq. (7-44) represents 3N equations in 12N+3 unknowns. The unknowns are the 3N components of $\{\underline{F}_J\}$ and the 9N components of $\{\underline{\underline{M}}_J\}$,

and the 3 components of $\underline{\delta\omega}$. Strictly speaking, the three components of the center of rotation, $\underline{d}$, are also unknown. However, for the applications of interest in this work, the center of mass and $\underline{d}$ coincide to a good approximation. For all of the applications in this work, $\underline{d}$ is approximated with the center of mass.

This is a good point to account for the effects of Brownian motion. This is a difficult problem that has been extensively addressed over many years and only some of this past work is cited here (178-180, 194, 195). Perhaps the most authoritative treatment with regards to rigid structures is given by Brenner (194). Relevant to the problem of significant Brownian motion, where $\gamma/D_r^* << 1$ (where D_r^* is the smallest eigenvalue of the rotational diffusion tensor of our bead array), and its effect on a suspension of dilute particles placed in a shear field, we need to include an additional angular velocity in the vicinity of each (removed) bead. (See Sections 7 and 8 of reference 194). Quite simply and remarkably, this added term is equivalent to setting $\delta\omega_j = 0$ in Eq. (7-48). This is also the procedure used long ago by Simha (178). In the remainder of this work, we shall follow this procedure and this reduces the number of unknowns to 12N. A closely related problem involves the effect of structural flexibility. Zimm (195) pioneered the Monte Carlo procedure of approximating the transport of flexible structures with an equilibrium ensemble of rigid conformations. Later investigators showed how this approximation provided bounds on the intrinsic viscosity (196, 197). In the applications of duplex DNA and alkanes in benzene presented in this work, the Monte Carlo procedure of Zimm (195) shall be employed.

We also need the gradient of v_{Ki}' (Eq. (7-34)). Following an analysis similar to that which led to Eq. (7-41),

$$v'_{Ki,m} \cong v_{K0i,m} - \sum_{J\neq K}\left\{\sum_{j=1}^{3} U^{Ki}_{Jj,m} F_{Jj} + \sum_{j,k=1}^{3} U^{Ki}_{Jj,km} M_{Jjk}\right\} \qquad (7-50)$$

Using Eq. (7-50) in Eqs. (7-32) and (7-37), substituting these into Eq. (7-36), we obtain an additional 9N equations,

$$\sum_{J=1}^{N}\sum_{j=1}^{3} C^{Kim}_{Jj} F_{Jj} + \sum_{J=1}^{N}\sum_{j,p=1}^{3} H^{Kim}_{Jjp} M_{Jjp} = b_{Kim} \qquad (7-51)$$

$$C^{Kim}_{Jj} = -\frac{\zeta^*_{Kr}}{4}\left(U^{Ki}_{Jj,m} - U^{Km}_{Jj,i}\right) - \eta_0 V_K \xi^*_K \left(U^{Ki}_{Jj,m} + U^{Km}_{Jj,i}\right) \qquad (7-52)$$

$$H^{Kim}_{Jjp} = \delta_{KJ}\delta_{ij}\delta_{mp} - \frac{\zeta^*_{Kr}}{4}\left(U^{Ki}_{Jj,mp} - U^{Km}_{Jj,ip}\right) - \eta_0 V_K \xi^*_K \left(U^{Ki}_{Jj,mp} + U^{Km}_{Jj,ip}\right) \qquad (7-53)$$

$$b_{Kim} = -\eta_0 V_K \xi^*_K E_{0im} \qquad (7-54)$$

Eqs. (7-45) and (7-51) can be written in compact matrix form

$$\underline{\underline{Q}} \cdot \underline{F} + \underline{\underline{B}} \cdot \underline{M} = \underline{a} \qquad (7-55)$$

$$\underline{\underline{C}} \cdot \underline{F} + \underline{\underline{H}} \cdot \underline{M} = \underline{b} \qquad (7-56)$$

In Eqs. (7-55) and (7-56), $\underline{F}$ and $\underline{a}$ are 3N by 1 column vectors formed by stacking $\underline{F}_1$, $\underline{F}_2$, … $\underline{F}_N$ and $\underline{a}_1$, $\underline{a}_2$, … $\underline{a}_N$ on top of each other. $\underline{M}$ and $\underline{b}$ are 9N by 1 column vectors formed by first writing the N dyadic (3 by 3) tensors, $\underline{\underline{M}}_J$, and $\underline{\underline{b}}_J$ as 9 by 1 column vectors. For example, we write for $\underline{M}'_J$:

$$\underline{M}_J^{'} = \begin{pmatrix} M_{J11} \\ M_{J12} \\ M_{J13} \\ M_{J21} \\ \vdots \\ M_{J33} \end{pmatrix} \qquad (7-57)$$

These N column vectors are stacked on top of each other to form $\underline{M}$. A similar procedure is used to construct $\underline{b}$. Also $\underline{\underline{Q}}$, $\underline{\underline{B}}$, $\underline{\underline{C}}$, and $\underline{\underline{H}}$ are 3N by 3N, 3N by 9N, 9N by 3N, and 9N by 9N matrices, respectively. Consider, for example, the $\underline{\underline{B}}$ matrix. $B_{J\,j\,p}^{K\,i}$ is that element of $\underline{\underline{B}}$ that occupies the 3*(K-1)+i row and 9*(J-1)+3*(j-1)+p column. Similarly, $H_{J\,j\,p}^{K\,i\,m}$ is that element of $\underline{\underline{H}}$ that occupies the 9*(K-1)+3*(i-1)+m row and 9*(J-1)+3*(j-1)+p column. Note that the superscript indices on the $\underline{\underline{Q}}$, $\underline{\underline{B}}$, $\underline{\underline{C}}$, and $\underline{\underline{H}}$ and matrices are row indices and the subscript indices are column indices.

Next, Eqs. (7-55) and (7-56) can be combined into a single "supermatrix" representation

$$\underline{\underline{G}} \cdot \underline{F}^{*} = \underline{s}^{*} \qquad (7-58)$$

$$\underline{\underline{G}} = \begin{pmatrix} \underline{\underline{Q}} & \underline{\underline{B}} \\ \underline{\underline{C}} & \underline{\underline{H}} \end{pmatrix} \qquad (7-59)$$

$$\underline{s}^{*} = \begin{pmatrix} \underline{a} \\ \underline{b} \end{pmatrix} \qquad (7-60)$$

$\underline{\underline{G}}$ is a 12N by 12N matrix; $\underline{F}^*$ and $\underline{s}^*$ are 12N by 1 column vectors. It should be emphasized that the sub-matrices $\underline{\underline{Q}}$, $\underline{\underline{B}}$, $\underline{\underline{C}}$, and $\underline{\underline{H}}$ in Eq. (7-59) are not the same size. Specifically, $\underline{\underline{Q}}$, $\underline{\underline{B}}$, $\underline{\underline{C}}$, and $\underline{\underline{H}}$ are 3N by 3N, 3N by 9N, 9N by 3N, and 9N by 9N, respectively. Once a structure is defined, all the components of $\underline{\underline{G}}$ can be determined. Once an elementary shear field is defined, the components of $\underline{s}^*$ can also be determined. Inversion of the $\underline{\underline{G}}$ matrix yields $\underline{\underline{G}}^{-1}$ and Eq. (7-58) can be written

$$\underline{F}^* = \underline{\underline{G}}^{-1} \cdot \underline{s}^* \qquad (7-61)$$

Once $\underline{F}^*$ is obtained, Eqs. (7-21) and (7-30) can be used to compute ξ. From Eq. (7-17), this can then be used to determine B and (η) for a single bead array averaged over all possible orientations in a simple shear field. The most time consuming step in this procedure is the inversion of the 12N by 12N $\underline{\underline{G}}$ matrix.

7.3 Results

3A) Dumbbell Dimer of Two Identical Beads

A dimer of two identical beads provides an excellent model system to test the equations derived in Section 2. Past studies of a touching dimer of two identical beads, ξ = 3.45 (35, 36) or 3.58 (page 263 of reference (198)). Recent "extrapolated shell" bead model calculations yield a value close to the lower value of 3.45 (186). Also, recent BE calculations using the BEST program (188) yield ξ = 3.449 which is in excellent agreement with reference (199) (Sergio

Aragon, personal correspondence). In test case of prolate and oblate ellipsoids, the BEST program yields ξs that are accurate to better than 0.01 % (188). On that basis, it is safe to say with considerable confidence that the exact value of ξ for a touching dimer of two beads is 3.45.

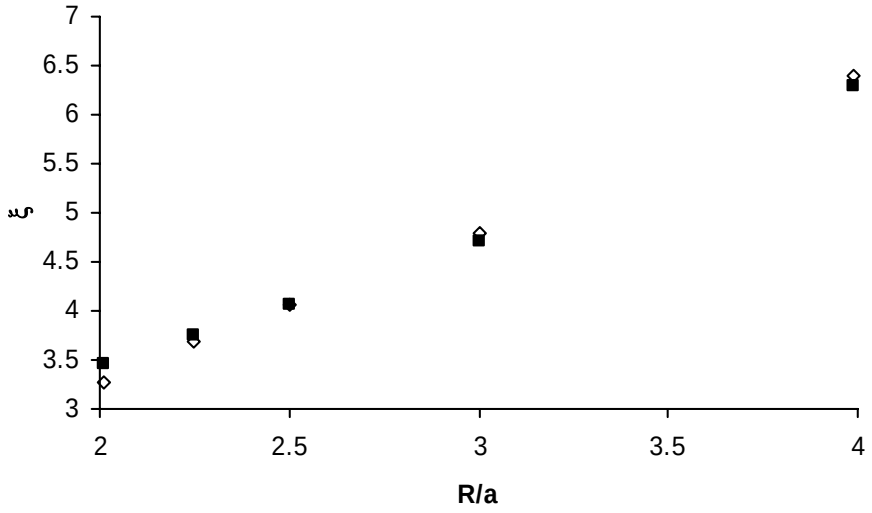

Figure 7-2) ξ versus R/a for Dimers of Two Identical Beads. R is the center-to-center distance between the two beads and a is the bead radii. Filled squares come from BE extrapolated shell calculations and unfilled diamonds come from the bead methodology developed in this work (Eqs. (39) and (41)of reference 46).

Shown in Figure 7-2 is a comparison of extrapolated shell (filled squares) and bead model results (Eqs. (39) and (41) of reference 46) for dimers composed of two identical beads or radius a and interbead separation R. The worst agreement is seen for touching beads where the bead model shape factor falls below the exact value by 5.2 %. For R/a between 3 and 4, the discrepancy is less than 2 %. For the sake of comparison, the extended Kirkwood-Riseman shape factor, ξ, for a touching bead model reportedly exceeds the extrapolated shell model value (from a bead model calculation) by 19 % (see Table 2 of reference (200) and also reference

(186)). Although Eqs. (39) and (41) of reference 46 yield approximate viscosities, they represent a significant improvement over past studies employing the same number of subunits.

3B) Rigid Rods and Simple Bead Arrays.

We shall next consider linear strings of N identical touching beads of radius a. They shall be compared to viscosity shape factors of right circular cylinders of length L and axial radius R where BE results are available (187). Structurally, bead and cylinder models are different from each other and this makes a direct comparison impossible. Nonethelss, bead and cylinder (or wormlike chain) models have been used interchangeably to describe duplex DNA with considerable success (117, 118, 143, 149). We start by setting the volumes of bead and right circular cylinder models equal

$$\pi R^2 L = \frac{4}{3}\pi a^3 N \qquad (7-62)$$

Introduce a dimensionless length variable, λ, by the definition

$$L = 2a(N-\lambda) \qquad (7-63)$$

On physical grounds, we expect $0 < \lambda < 1$. Its exact value shall be determined by finding which value gives best agreement for shape factors for bead models using Eqs. (39) and (41) of reference 46 and BE calculations on right circular cylinders. For the moment, however, λ shall be left as an adjustable parameter. Using Eq. (7-63) in (7-62)

$$a = \sqrt{\frac{3}{2}} R\left(1-\frac{\lambda}{N}\right)^{1/2} \qquad (7-64)$$

Provided $\lambda/N << 1$, $a \cong (3/2)^{1/2}R$. For R = 1.0 nm, which is appropriate for duplex DNA (115, 116), a ≅ 1.225 nm. This is the appropriate bead radius for large N. For small N, Eq. (7-64) can be used once λ is known. Also define the dimensionless variable

$$p = \frac{L}{2R} = \sqrt{\frac{3}{2}}N\left(1-\frac{\lambda}{N}\right)^{3/2} \qquad (7-65)$$

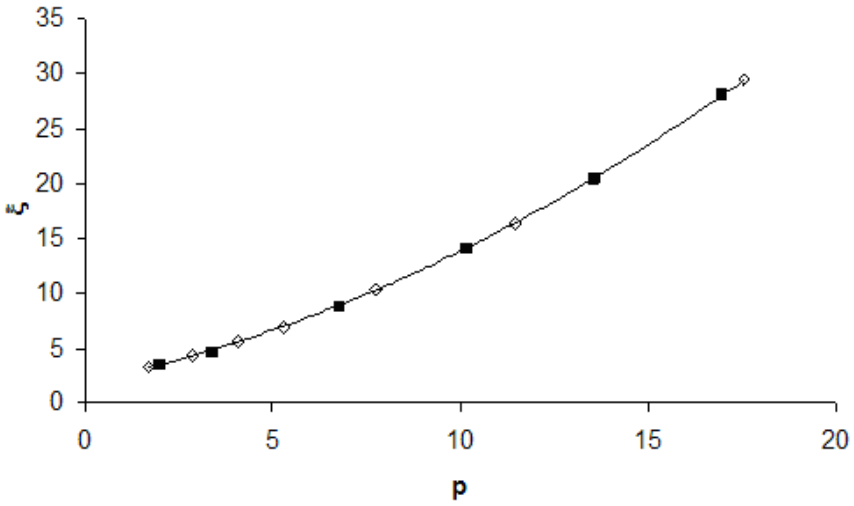

Figure 7-3) ξ versus p for Straight Rod Models. See Eq. (7-65) for a definition of p. Also, λ = 0.45 in Eq. (7-65). Filled squares correspond to BE model studies of right circular cylinders (187). Unfilled squares correspond to the bead methodology using Eqs. (39) and (41) of reference 46.

Figure 7-3 displays shape factors for right circular cylinders (filled squares) and bead models (unfilled diamonds) versus p. A value of λ = 0.45 yields best agreement between the two models. The solid line represents a quadratic fit to the data (1.5 < p < 18) which can be written

$$\xi = 1.912 + 0.702\,p + 0.0495\,p^2 \qquad (7-66)$$

The viscosity of a bead array is fairly sensitive to how the beads are arranged in space, or the conformation of the bead array. This is illustrated in Figure 7-4 for different conformations of tetramers modeled as 4 identical beads. In addition to the models, the viscosity shape factors are also given below the figures. The most compact structure, the ring of 4 beads, has the smallest ξ, and the most extended, the straight rod, has the largest. In this example, ξ_{rod}/ξ_{ring} equals 1.58.

3C) Comparison with Experiment: Amino Acids and Simple Peptides.

Systems involving few subunits where the present work would be useful include crosslinked macromolecules (201), duplex DNA (202-203), and peptides (46).

To date, there appears to be very little data available with regards to the viscosity of peptides, but there have been a number of investigations of the viscosity of dilute amino acids in aqueous solution. B-factors and also partial molar aqueous volumes in the limit of infinite dilution, V_2, of several amino acids as well as diglycine have been reported (175, 204-206). Experimental values are summarized in Table 7-1. B-factors for Gly, Ala, Leu, Val, and Gly-Gly come from reference (175) and the corresponding V_2's come from reference (206). B and V_2 for Phe come from reference (205), whereas B and V_2 for Ser, Thr, and Pro come from reference (204). The B-factors appear to be reproducible to within a relative error of about 5 %. Also shown in Table 7-1 are approximate shape factors, ξ^*, defined by

$$\xi^* = \frac{B}{V_2} \qquad (7-67)$$

By comparing Eqs. (7-67) and (7-17), it is seen that equals ξ if we set $V_2 = V_p$. The V_2 values were estimated from dilute aqueous solution density measurements (204-206). Since V_p reflects the particle volume (per mole) within the surface of hydrodynamic shear, and V_2 corresponds to the excluded volume of the solvated particle, they may not, in fact, be equal. For the moment, however, we shall simply assume that $V_2 = V_p$.

Table 7-1) B-factors, Partial Molar Volumes, V_2, and Approximate Shape Factors, ξ^*

Species	B (dm^3/mole)	V_2 (dm^3/mole)	ξ^*
Ala	.251	.0604	4.16
Gly	.143	.0432	3.31
Leu	.576	.1077	5.35
Phe	.599	.1236	4.85
Pro	..279	.0829	3.36
Ser	..225	.0607	3.71
Thr	..335	.0769	4.36
Val	.423	.0907	4.66
Gly-Gly	.352	.0763	4.61

Note that all of the ξ^* values in Table 7-1 exceed the value of 2.5 appropriate for a sphere with stick hydrodynamic boundary conditions. The most straightforward explanation for this is that the species are nonspherical and that shape is responsible for the departure of ξ^* from 2.5. On the basis of our earlier analysis of dimers and simple bead arrays, the approximate shape factors for Gly, Pro, and Ser are well explained in terms of a touching dimer model of two equivalent beads. To carry this argument further, next consider diglycine (Gly-Gly) and model it as a tetramer of 4 beads. Basically, diglycine is formed when two glycines dimerize and lose water. Figure 7-3 gives a range of possible conformations and the ξ^* value of 4.61 from Table 7-1 is compatible with structure (b) in the figure. For the remaining amino acids (Ala, Leu, Phe,

Thr, and Val) appearing in Table 7-1, model structures more complex than dimers are necessary to account for the ξ* values observed.

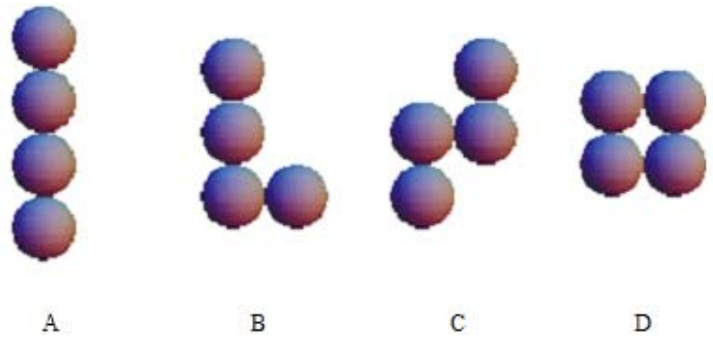

Figure 7-4) Tetramers of four identical beads. For structures A, B, C, and D; ξ = 5.57, 4.70, 4.17, and 3.53, respectively.

As Figure 7-4 demonstrates, however, even simple tetramer models are able to account for the range in ξ* values observed. For more realistic surface models that account *in detail* for the actual solvent accessible surface of the amino acid or dipeptide, bead (113,114) or BE (188) methodologies would be more appropriate than the methodology developed in the present work. What the present analysis shows is that the intrinsic viscosity of amino acids and simple peptides can be explained reasonably well by nonspherical particles of an overall size compatible with their known partial molar volumes.

We would like to carry the analysis of the viscosity of the amino acids (and Gly-Gly) further in a way that avoids setting $V_p = V_2$ as done in the previous paragraph. A more appropriate molecular volume would come from transport measurements of which viscosity is one example. Translational diffusion constants, D_T, of the amino acids have been reported by a number of investigators (81,157, 158, 160, 207). The diffusive radius, R_D, shall be defined

$$R_D = \frac{k_B T}{6\pi\eta_0 D_T} \qquad (7-68)$$

where k_B is Boltzmann's constant and T is absolute temperature. The physical significance of R_D is that it corresponds to the radius of a suspension of spheres that diffuse at the same rate as the particles in the actual suspension. It should be emphasized that we are not assuming our actual suspension is made up of spherical particles. Also introduce the "stick" diffusion constant of a sphere of volume V_p/N_{av} (N_{av} is Avogadro's Number), D_0, where V_p is the actual molar particle volume as defined following Eq. (7-14).

$$D_0 = \frac{k_B T}{6\pi\eta}\left(\frac{4\pi N_{Av}}{3V_p}\right)^{1/3} \qquad (7-69)$$

Also define the reduced translational diffusion constant, X.

$$X = \frac{D_T}{D_0} \qquad (7-70)$$

For nonspherical particles, X will deviate from 1.

In analogy to the diffusive radius, we can define the viscous radius, R_η, which corresponds to the radius of a suspension of spheres that gives the same B as the actual suspension. Setting $\xi = 2.5$ and $V_p = 4\pi N_{Av} R_\eta^3/3$ (appropriate for spheres) in Eq. (7-67),

$$R_\eta = \left(\frac{3B}{10\pi N_{Av}}\right)^{1/3} \qquad (7-71)$$

We can now use Eqs. (7-67), (7-69) to (7--71) to eliminate V_p,

$$\frac{R_\eta}{R_D} = \left(\frac{2\xi}{5}\right)^{1/3} X \qquad (7-72)$$

Eq. (7-72) is closely related to the Scheraga-Mandelkern parameter (208) and provides a way of eliminating V_p and isolating the shape dependence by combining the results from two independent transport measurements. In the present case, these are viscosity and translational diffusion and in reference (208), it was viscosity and sedimentation. An alternative, but closely related approach involves viscosity and rotational diffusion relaxation times (200, 209). An advantage of the Harding approach is its greater sensitivity to particle shape, but this approach requires rotational relaxation times that are not available to us.

Table 7-2. Viscous and Diffusive Radii

Species	R_η(nm)	R_D(nm)	R_η/R_D
Ala	.341	.267	1.28
Gly	.283	.248	1.14
Leu	.450	.339	1.33
Phe	.456	.347	1.34
Pro	.354	.268	1.32
Ser	.329	.276	1.19
Thr	.376	.304	1.24
Val	.406	.332	1.22
Gly-Gly	.382	.324	1.19

Summarized in Table 7-2 are R_η, R_D, and R_η/R_D for the same species given in Table 7-1. For the diffusive radii listed, values for Leu and Pro come from reference (157); the value for Phe comes from reference (207); values for Ala, Thr, and Val come from reference (160), and the value for Ser comes from reference (81). Values for Gly and Gly-Gly have also been available

for many years (158), but for the present work, we use results from recent field gradient NMR measurements (H. Pei, M.W. Germann, S.A. Allison, manuscript in preparation). It should be emphasized that R_η and R_D in Table 7-2 have been extracted from experiment and no assumptions beyond the operational definitions of R_η and R_D have been used. We shall next consider what modeling predicts for R_η/R_D for some simple structures. For prolate and oblate ellipsoids, right circular cylinders, and toroids, results from reference (187) are used. For the tetramer bead arrays, Eqs. (39) and (40) of reference 46 are used for ξ. For X, we employ a closely related procedure for the translation of bead arrays that accounts for the variation in hydrodynamic stresses over the bead surfaces (45). For the touching dimer, exact values are used (186, 199, 210). The results are summarized in Table 7-3.

For compact structures listed in Table 7-3, R_η/R_D lies close to 1.01 and lower. Even for needle like structures such as the a/b = 10 prolate ellipsoid and the p = 17 rod, R_η/R_D lies in the range of 1.14 to 1.21. From Table 7-2 on the other hand, R_η/R_D ranges from 1.14 (for Gly) to 1.345 (for Phe). Even for Gly, this corresponds to a highly nonspherical particle and this seems unrealistic on structural grounds. One possible explanation for the anomalously large R_η/R_D values seen in Table 7-2 is related to the validity of continuum stick hydrodynamic boundary conditions in adequately describing the solvent-particle interface for a particle/molecule as small as an amino acid in an aqueous solvent. Studies on the rotational reorientation time of small molecules such as methyl acetate in water indicate that a hydrodynamic boundary condition intermediate between stick and “slip” is more appropriate (190). In the case of slip boundary conditions, only the normal velocity component of fluid and particle match at the interface. In addition, however, there is no tangential component of normal stress at the interface (186, 51). In addition to the

mostly "stick" models considered in Table 7-3, two "slip" models have also been included for a sphere and a prolate ellipsoid with a/b = 10. In these cases, X and ξ come from reference (186). Since $(R_\eta/R_D)_{slip} > (R_\eta/R_D)_{stick}$ for both geometries, particularly for the prolate ellipsoid, this interpretation is not unreasonable.

Table 7-3. X, ξ, and R_η/R_D for some simple structures

structure	details[(a)]	X	ξ	R_η/R_D
Oblate ellipsoid	a/b = 10	.689	7.92	1.012
"	a/b = 2	.962	2.84	1.004
Sphere	(a/b = 1)	1.00	2.50	1.000
Sphere[(b)]	(a/b = 1)	1.50	1.00	1.105
Prolate ellipsoid	a/b = 2	.958	2.91	1.008
"	a/b = 5	.801	5.78	1.059
"	a/b = 10	.650	13.52	1.141
Prolate ellipsoid[(b)]	a/b = 10	5.48	7.06	7.74
Cylinder	p = 2.04	.904	3.43	1.004
"	p = 17.0	.543	28.0	1.214
Toroid	P = 2.0	.868	3.87	1.004
"	p = 10.0	.494	24.0	1.050
Dimer	Identical touching beads	.906	3.45	1.009
Tetramer	D of Fig. 4	.898	3.53	1.007
"	B of Fig. 4	.821	4.70	1.013
"	A of Fig. 4	.797	5.57	1.041

(a) for ellipsoids, a/b is the major axis/minor axis; for rods, p is given by Eq. (46) of reference 46; for toroids, p = R/r where R and r are the outer and inner toroidal radii (186).
(b) slip boundary conditions

3D) Linear Strings and Rings of Beads

As discussed in previous work (46, 185), bead models made up of a small number of beads have historically not been very accurate unless account is taken of the variation of

hydrodynamic stresses over the individual beads. The methodology employed in this chapter is simpler than that used in reference 46 in the sense that bead-bead interactions are only accounted for out to order a_J^2/r_{IJ}^3 (a_J is a bead radius and r_{IJ} is an inter-bead distance). Because of that, it is important to compare results using the methodology developed here with exact, or near exact results on certain systems. In this subsection, all model structures of interest shall consist of arrays of identical beads of radius a, and near neighbor separation, t. Define the three parameters; s_t, s_r, and s_v by the relations:

$$\zeta_t^* = s_t\,(6\pi\eta a) \qquad (7-73a)$$
$$\zeta_r^* = s_r\,(8\pi\eta a^3) \qquad (7-73b)$$
$$\xi^* = s_v\,(5/2) \qquad (7-73c)$$

In the special case of no solute-solvent interactions beyond excluded volume interactions, s_t, s_r, and s_v can all be set to 1.00. This selection is made for the model studies in this subsection and in the next.

The model system relevant to the present work where exact results are available is the touching dimer (t = 2a) of two identical beads, where $\xi_{exact} = 3.45$ (198, 199). (This value has recently been confirmed by detailed Boundary Element calculations. S. Aragon, personal correspondence, January, 2009). Recently, Garcia de la Torre and coworkers have carried out extrapolated shell calculations of bead oligomers. Each bead is modeled as a shell of many much smaller touching beads and the results extrapolated to the limit of an infinite number of smaller beads (185). In Table 7-4, we summarize viscosity shape factors, ξ, for model results employing the procedure developed in the present work with these extrapolated shell values.

The main purpose of reference 185 was not the shell model calculations themselves, but rather using them as benchmarks to test a simpler, more computationally efficient bead methodology valid in the absence of external forces. Those same shell model results are used here to test the present results. Agreement between the two lies within 5 percent of each other. It should be emphasized that results using the present methodology are not exact, but are nonetheless quite accurate for the special cases considered in Table 7-4. For additional tests/comparisons of other bead methodologies, the reader is referred to references 46, 182, and 185.

Table 7-4. Viscosity Shape Factors of Linear Strings and Rings of Touching Beads

Structure[a]	ξ_{shell}[b]	ξ[c]
L2	3.42	3.43
L3	4.58	4.68
L4	5.98	6.22
R4	3.88	3.92
L5	---	7.56
L6	9.18	9.37
R6	4.80	4.90
L7	---	11.61
L8	13.10	13.19
L9	---	15.49
L10	---	18.78

(a) Linear, Ring arrays of N beads denoted LN, RN, respectively
(b) from Shell Model results of reference (185)
(c) from the present work

3E) Duplex DNA

In this subsection, the methodology shall be applied to the intrinsic viscosity of duplex DNA fragments of specific length. The viscosity experiments were carried out at 25 ºC in a

buffer solution of ionic strength 0.1 M (or higher) and extrapolated to zero shear (211). Under these comparatively high salt conditions, electroviscous effects are expected to be small (193) and are ignored in the present work. Duplex DNA is modeled using the Hagerman discrete wormlike chain (117, 118) which is discussed in previous chapters. Following Hagerman (117, 118), we randomly generate an "ensemble" (typically 100) of independent wormlike chains, compute the intrinsic viscosity and shape factor of each one treating it as a rigid body, and then average over all conformations to obtain an ensemble average. For the chains of interest in this work, an ensemble of 100 chains is sufficient to yield intrinsic viscosities that are accurate to within about 3%. The number of beads employed ranged from 16 (115 bp) to 86 (619 bp). This example illustrates the usefulness of the method in sampling a large number of conformations of a flexible chain. A randomly generated 86 bead wormlike chain with a persistence length of 40 nm, appropriate for 619 bp duplex DNA, is illustrated in Figure 7-5.

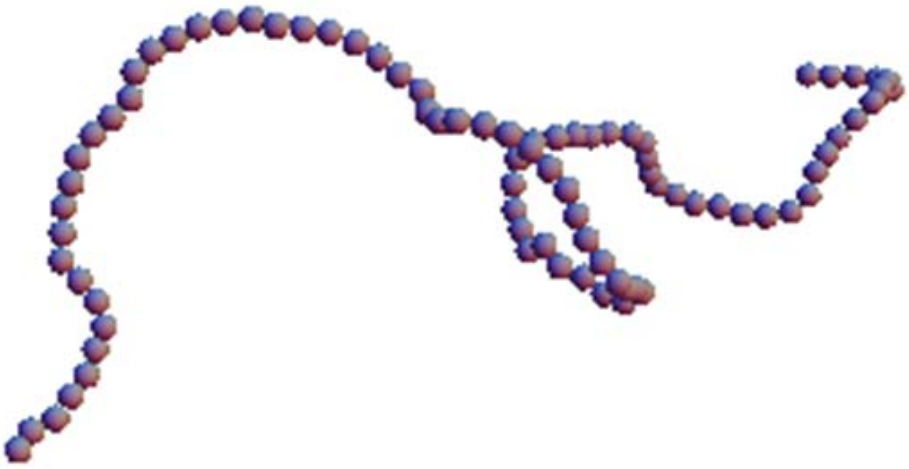

Figure 7-5) Representative wormlike chain for 619 base pair duplex DNA. The randomly generated chain consists of 86 beads with a persistence length of 40 nm. See the text for details.

Shown in Figure 7-6 are experimental (η)'s along with model viscosities for rods (dashed line) and wormlike chains with P = 50 nm (dotted line) and 40 nm (solid line). The solvent viscosity, η_0, was set to 0.89 cp, appropriate for aqueous solutions at 25 ºC. The parameters s_t, s_r, and s_v, were all set to +1.0. A wormlike chain model with P in the 40 to 50 nm range is entirely consistent with experiment.

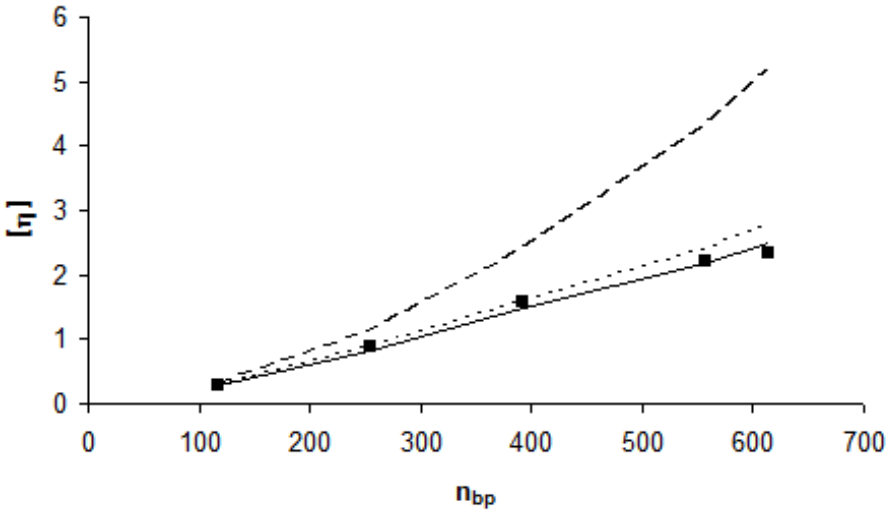

Figure 7-6) Intrinsic viscosity of DNA versus length. Experiments (filled squares) come from reference 117 were carried out at 25 ºC in aqueous media and intrinsic viscosities are in 10^2 cm^3/gm. Model mobilities are: rod (dashed line), P = 50 nm wormlike chain (dotted line), P = 40 nm wormlike chain (solid line). In the wormlike chain modeling studies, 100 conformations were averaged.

3F) Alkanes in Benzene.

A system which clearly deviates from the standard (S) model is alkanes in benzene where (η) is negative when the molecular weight of the solute (alkane) is low (173). Since the model developed in this work treats the solvent as a continuum, it should only be accurate on a distance scale comparable to or greater than the size of a solvent molecule, benzene in this case, or

approximately 0.25 nm. However, the carbon-carbon bond length is 0.154 nm (212), which means we have to choose our fundamental building block, or "monomer" to be larger than a single CH_2 group. On pragmatic grounds, we would like to choose our monomer to be small enough to capture the size dependence of (η) observed experimentally, yet large compared to a solvent molecule or atom. In the analysis presented here, we choose our monomer unit as pentane, H-C_5H_{10}-H, which has a van der Waals excluded volume of 96.4 Å^3 = 0.0964 nm^3 (81). Setting this volume equal to that of a sphere of radius a, gives a = 0.284 nm. If we view C_5H_{12}, $C_{10}H_{22}$, $C_{15}H_{32}$, etc. as effectively one, two, three, etc. linear strings of touching beads, a logical choice for the inter-bead separation, t, is simply equal to 2a or 0.568 nm.

A quantity related to the flexibility of polymers of degree of polymerization n, in a good (theta) solvent is the dimensionless characteristic ratio, which can be defined

$$C_n = \frac{< r^2 >_0}{n h^2} \qquad (7-74)$$

where $<r^2>_0$ is the mean square end-to-end distance and h is the carbon-carbon bond length (0.154 nm). For polymethylene under theta solvent conditions, C_n = 6.6 to 6.8 for large n (86). For a long wormlike chain of persistence length P made up of N = n/5 structural units of bead spacing t, $<r^2>_0 = 2PNt = 0.4nPt$ (43), Eq. (7-74) can be rearranged to give

$$P = \frac{C_n h^2}{2t}\left(\frac{n}{N}\right) \cong 0.68\, nm \qquad (7-75)$$

Since benzene at room temperature does not constitute a theta solvent for low molecular weight alkanes, the actual persistence length may be different from 0.68 nm. Nonetheless, this value

along with our choices for a and t, provide reasonable model parameters for the system of interest. Also, set T = 25 ºC and η_0 = 0.652 cp (for benzene at 25 ºC).

An estimate for s_v can now be made from the experimental value of (η) for pentane in benzene (173). From Eqs. (7-17) and (7-73),

$$s_v = \frac{2M[\eta]}{5N_{Av}V_P} \qquad (7-76)$$

In Eq. (7-76), M, (η), and V_P all refer to the monomer unit, which in this case is pentane. With M = 72 gm/mole, (η) = -2.07 cm^3/gm (1), and V_P = 96.4 $Å^3$ (42), $s_v \cong$ -1.00. Since we don't have values for s_t and s_r, these are both set to +1.00. If, for example, experimental values were available for the translational and rotational diffusion constants of pentane in benzene, s_t and s_r could be defined more precisely.

Summarized in Figure 7-6 are experimental (filled squares from reference 1) and model intrinsic viscosities of alkanes in benzene. The solid, dotted, and dashed lines come from model studies with s_v = +1.0, 0.0, and -1.0, respectively. The other parameters for the model studies have been defined previously. For N = 3 to 5 (corresponding to $C_{15}H_{32}$ to $C_{25}H_{52}$), we followed a procedure similar to that described in Section 3F. Intrinsic viscosities were calculated for 100 independent wormlike chains and the results averaged. As can be seen from Figure 7-7, the model studies with s_v = -1.0 reproduce very well the experimental (η)'s.

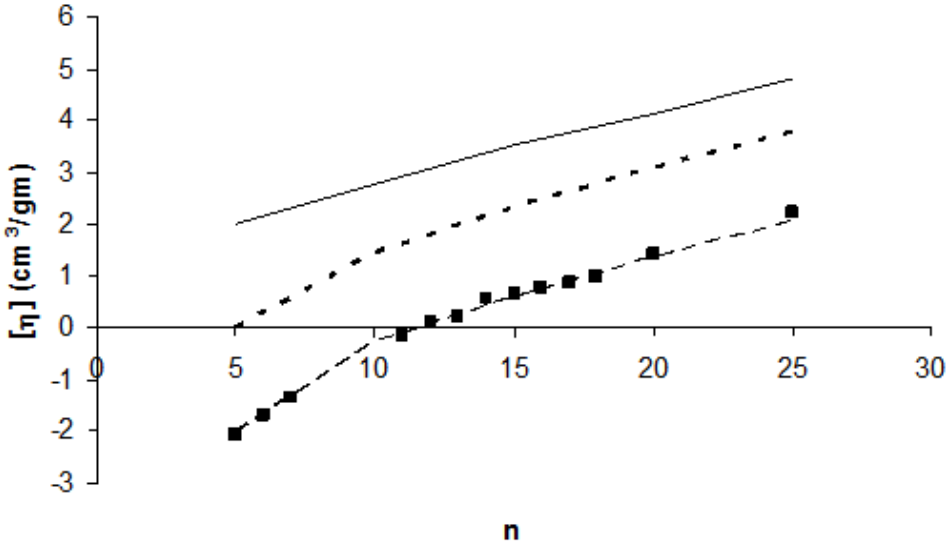

Figure 7-7) Intrinsic viscosity of alkanes in benzene versus length. Experiments (filled squares) come from reference 173 and were carried out at 25 ºC. Solid, dotted, and dashed curves come from model studies with s_v = +1.0, 0.0, and -1.0, respectively.

7.4 Summary

The principle objectives of this chapter have been to model the viscosity of a dilute bead array at low shear, to study the shape factor for arbitrary shaped bead arrays, to generalize the S model for bead arrays, test this model's accuracy, and then apply it to two very different systems: duplex DNA in aqueous media and alkanes in benzene. In modeling the viscosity of a dilute bead array at low shear, substantial error arises when account is not taken of the variation in hydrodynamic stress forces over individual beads. This problem can be addressed in two very different ways. In the first, approach, one simply uses many beads or plates to model the particle surface. Over the past 15 years, a number of thorough studies have been carried out on the viscosity of proteins. Detailed models have been constructed from known crystal structures and model intrinsic viscosities have been compared with experiment. This comparison can provide

valuable information about solution conformation and hydration. Both bead (113, 114, 199, 200) and BE (188, 213) procedures have been used with considerable success. Typically, 1000-3000 beads (10) or 2000-4000 plates (188) have been employed in these studies. In an alternative approach followed in the present work, the number of beads is kept comparatively small, but approximate account is taken of the variation in hydrodynamic stresses over the individual bead surfaces. For a dimer of two touching identical beads, the methodology developed here is off by 5.2 %. One area where the present methodology is expected to be useful is for flexible structures where many conformations have to be sampled. This includes crosslinked macromolecules (201), duplex DNA (202, 203), and peptides (38). In the present study, we have shown how a bead model in viscosity modeling can be used as a substitute for a right circular cylinder. In future work, we hope to extend this to a flexible worklike chain (117, 118, 143, 149) which is an excellent model for duplex DNA.

The model development was presented in Section 2 and the applications in Section 3. Within the framework of the S model, viscosity shape factors for dimers and linear strings and rings of touching beads are accurately reproduced with the methodology developed here. The S model is also able to explain very well the intrinsic viscosity of duplex DNA (in aqueous media) in the size range of 100 to over 600 base pairs when modeled as wormlike chains with a persistence length of between 40 and 50 nm.

Past studies of solute-solvent interactions as they relate to intrinsic viscosity have been handled differently by different investigators. A longstanding approach has been to simply add a constant term to the standard (S model) intrinsic viscosity to account for solute-solvent interactions (173, 94, 214). Although this approach appears to work well, it is difficult to explain

why it works in the context of the coarse grained methodology developed in the present work. In other words, we cannot explain how the short range solute-solvent interactions appear to "uncouple" from the long range hydrodynamic interactions. Lodge and coworkers (174, 215, 216) have advanced a model in which it is argued that solute can alter the "microviscosity" (216) of the solvent. Evidence in support of this comes from measurements of solvent rotation times and how these rotation times are altered by solute. However, this interpretation has been criticized (217). Fixman also raised specific criticisms of the concept of a "microviscosity" that varies on a molecular distance scale (189). The present work has been strongly influenced by that of Fixman (189) and draws on many of the ideas advanced in this earlier work.

The example of alkanes in benzene serves to illustrate both the strengths and shortcomings of the methodology developed in this work. On the positive side, we are able to account quite well for the length dependence of (η) observed experimentally for reasonable choices of model input parameters. It is also able to sample many conformations of a flexible structure rapidly and efficiently. On the other hand, modeling the solvent as a continuum limits one to distance scales comparable to or larger than the size of the solvent molecules themselves. Finally, we are not, at the present time, able to give a microscopic interpretation for s_v. It was chosen to reproduce the experimental (η) for pentane (our monomer) in benzene. These shortcomings aside, it is our hope that the methodology developed here will be useful to other investigators in viscosity studies of relatively low molecular weight solutes.

References

1) Vesterberg, O., Electrophoresis 1993, 14, 1243-1249.

2) Wiersema, P.H., Loeb, A.L., Overbeek, J.T.G., J. Colloid Interface Sci., 1966, 22, 78-99.

3) Henry, D.C., Proc. R. Soc. London Ser. A., 1931, 203, 106-129.

4) Hunter, R.J., "Introduction to Modern Colloid Science," Oxford University Press, Oxford, UK, 2002, Chapter 7.

5) Allison, S.A., Carbeck, J.D., Chen, C., Burkes, F., J. Phys. Chem. B, 2004, 108, 4516-4524.

6) Overbeek, J.T.G., Kolloid-Beih., 1943, 54, 287-364.

7) Booth, F., Proc. R. Soc. London Ser. A., 1950, 203, 514-533.

8) O'Brien, R.W., White, L.R., J. Chem. Soc. Faraday Trans. 2, 1978, 74, 1607-1626.

9) Allison, S.A., Xin, Y., Pei, H., Journal of Colloid Interface Science. 2007, 313(1): 328-37.

10) Stigter, D., J. Phys. Chem., 1978, 82, 1417-1423.

11) Stigter, D., J. Phys. Chem., 1978, 82, 1424-1429.

12) Yoon, B.J., Kim, S., J. Colloid Interface Sci., 1989, 128, 275-288.

13) Kim, J.Y., Ahn, S.H., Kang, S.T., Yoon, B.J., 2006, 299, 486-492.

14) Allison, S.A., J. Colloid Interface Sci., 2005, 282, 231-237.

15) Ohshima, H., J. Colloid Interface Sci., 2000, 228, 190-193.

16) Hill, R.J., Saville, D.A., Russel, W.B., J. Colloid Interface Sci., 2003, 255, 56-74.

17) Allison, S.A., J. Colloid Interface Sci., 2004, 277, 248-254.

18) McCammon, J.A., Deutch, J.M., Biopolymers, 1976, 15, 1397-1408.

19) Nakajima, H., Wada, Y., Biopolymers, 1977, 16, 875-893.

20) Garcia de la Torre, J., Bloomfield, V.A., Biopolymers, 1977, 16, 1747-1763, 1765-1778, 1779-1793.

21) Teller, D.C., Swanson, E., de Haen, C., Methods Enzymol., 1979, 61, 103-124.

22) Garcia de la Torre, J., Bloomfield, V.A., Quart. Rev. Biophys., 1981, 14, 81-139.

23) Youngren, G.K., Acrivos, A., J. Fluid Mech., 1975, 69, 377-403.

24) Fixman, M., J. Chem. Phys., 1979, 70, 4995-5005.

25) LeBret, M., Zimm, B.H., Biopolymers, 1984, 23, 270-285.

26) Murthy, C.S., Bacquet, R.J., Rossky, P.J., J. Phys. Chem., 1985, 89, 2261-2270.

27) Warwicker, J., Watson, H.C., J. Mol. Biol., 1982, 157, 671-679.

28) Zhou, H.-X., J. Chem. Phys., 1994, 100, 3152-3162.

29) Yang, A.-S., Gunner, M.R., Sampogna, R., Sharp, K., Honig, B., Proteins, 1993, 15, 252-265.

30) Antosiewicz, J., Briggs, J.M., Elcock, A.H., Gilson, M.K., McCammon, J. A., J. Comp. Chem., 1996, 17, 1633-1644.

31) Zhou, H.-X., Vijayakumar, M., J. Mol. Biol., 1997, 267, 1002-1011.

32) Allison, S.A., Macromolecules, 1996,29,7391-7401.

33) Allison, S.A., Potter, M., McCammon, J.A., Biophys. J., 1997, 73, 133-140.

34) Durant, J.A., Chen, C., Laue, T.M., Moody, T.P., Allison, S.A., Biophys. Chem., 2002, 101-102, 593-609.

35) Allison, S.A., Chen, C., Stigter, D., Biophys. J., 2001, 81, 2558-2568.

36) Allison, S.A., Wall, S., Rasmusson, M., J. Colloid Interface Sci., 2003, 263, 84-98.

37) Allison, S.A., Biophys. Chem., 2001, 93, 197-213.

38) Pei, H., Xin, Y., Allison, S.A., Journal of Separation Science. 2008, 31(3): 555-564.

39) Pei, H., Allison, S. A.; Journal of Chromatograph A. 2009, 1216(10): 1908-1916.

40) Allison, S.A., Pei, H., Baek, S., Brown, J., Lee, M.Y., Nguyen, V., Twahir, U.T., Wu, H., Electrophoresis. 2010, 31(5):920-932.

41) Allison, S.A., Pei, H., Xin, Y., Biopolymers. 2007, 87(2-3): 102-114.

42) Allison, S., Pei, H., (Editor) Progress in Nanoparticles Research. Nova Science Publishers, Inc, NY, 2008; Chapter 12.

43) Pei H, Allison S, Haynes BM, Augustin D., J Phys Chem B. 2009, 113(9):2564-2571.

44) Pei, H., Allison, S. A., Germann, M. W., Journal of Physical Chemistry B. 2009, 113(27): 9326-9329.

45) Allison, S. A., Pei, H., Haynes, M., Xin, Y., Law, L., Labrum, J., Augustin, D., Journal of Physical Chemistry B. 2008, 112(18): 5858-5866.

46) Allison, S.A., Pei, H., J Phys Chem B. 2009,113(23):8056-8065.

47) Allison, S.A., Pei, H., Baek, S., Garcia, J.N., Lee, M.Y., Nguyen, V., Twahir, U.T., J Phys Chem B. 2009,113(41):13576-13584.

49) Happel, J., Brenner, H., Low Reynolds Number Hydrodynamics, Martinus Nijhoff, The Hague, 1983.

50) Kim, S., Karilla, S.J., Microhydrodynamics, Butterworth-Heinemann, Boston, 1991.

51) Hu, C.-M., Zwanzig, R., J. Chem. Phys., 1974, 60, 4354.

52) Xin, Y., Hess, R., Ho, N., Allison, S.A., J. Phys. Chem. B., 2006, 110, 25033-25044.

53) Bashford, D.; Karplus, M., Biochemistry, 1990, 29, 10219.

54) Antosiewicz, J.; Briggs, J.M.; Elcock, A.H.; Gilson, M.K.; McCammon, J.A., J. Comput. Chem., 1996, 17, 1633.

55) Allison, S.A.; Xin, Y., J. Colloid Interface Sci., 2006, 299, 977.

56) Garcia de la Torre, J.; Navarro, S.; Lopez Martinez, M.C.; Diaz, F.G.; Lopez Casales, J.J., Biophys. J. 1994, 67, 530.

57) "Electrokinetic Phenomena. Principles and Applications in Analytical Chemistry and Microchip Technology," Rathore, A.S.; and Guttman, A., Eds., Dekker, New York 2004.

58) Grossman, P.D.; Colburn, H.H.; Lauer, H.H., Anal. Biochem. 1989, 179, 28-33.

59) Rickard, E.C.; Strohl, M.M.; Nielsen, R.G., Anal. Biochem. 1991, 197, 197-207.

60) Compton, B.J., J. Chromatogr. 1991, 559, 357.

61) Issaq, H.J.; Janini, G.M.; Atamna, I.Z.; Muschik, G.M.; Lukszo, J., J. Liq. Chromatogr. 1992, 15, 1129.

62) Castagnola, M.; Cassiano, L.; Messana, I.; Nocca, G.; Rabino, R.; Rossetti, D.V.; Giardina, B., J. Chromatogr. B 1994, 656, 87.

63) Cifuentes, A.; Poppe, H., J. Chromatogr. A 1994, 680, 321-340.

64) Basak, S.K.; Ladisch, M.R., Anal. Biochem. 1995, 226, 51.

65) Adamson, N.J.; Reynolds, E.C., J. Chromatogr. B 1997, 699, 133-147.

66) Messana, I.; Rossetti, D.V.; Cassiano, L.; Misiti, F.; Giardina, B.; Castagnola, M., J. Chromatogr. B 1997, 699, 149-171.

67) Janini, G.M.; Metral, C.J.; Issaq, H.J.; Muschik, G.M., J. Chromatogr. A 1999, 848, 417-433.

68) Sitaram, B.R., Keah, H.H., and Hearn, T.W., J. Chromatogr. A, 1999, 857, 263.

69) Janini, G.M.; Metral, C.J.; Issaq, H.J., J. Chromatogr. A 2001, 924, 291-306.

70) Kim. J.; Zand, R.; Lubman, D.M., Electrophoresis 2002, 23, 782.

71) Simo, C.; Cifuentes, A., Electrophoresis 2003, 24, 834.

72) Jalali-Heravi, M.; Shen, Y.; Hassanisadi, M.; Khaledi, M.G., J. Chromatogr. A, 2005, 1096, 58-68.

73) Offord, R.E., Nature (London) 1966, 211, 591-593.

74) Piaggio, M.V.; Peirotti, M.B.; Deiber, J.A., Electrophoresis 2005, 26, 3232-3246.

75) Allison, S.A.; Xin, Y.; Mitchell, H. in "Recent Developments in Macromolecules," Pandalai, S.G., Editor, Research Signpost, Kerali, 2005, 8, 25-46.

76) Xin, Y.; Mitchell, H.; Cameron, H.; Allison, S., J. Phys. Chem. B 2006, 110, 1038-1045.

77) Grycuk, T., J. Phys. Chem. B 2002, 106, 1434.

78) Lee, L.K.; Fitch, C.A.;, Garcia-Moreno, B.E., Protein Sci. 2002, 11, 1004.

79) Sasisekharan, V., in "Collagen," Ramanathan, N., Ed., Interscience, New York, 1962, p. 39.

80) Germann, M.W.; Turner, T.; Allison, S.A., J. Phys. Chem. B., 2007, 111, 1452.

81) Edward, J.T., J. Chem Ed. 1970, 47, 261.

82) Schultz, G.E.; Schirmer, R.H., "Principles of Protein Structure," Springer-Verlag, New York, 1979.

83) Cantor, C.R.; Schimmel, P.R., "Biophysical Chemistry, Part I", W. H. Freeman, San Francisco, 1980, Chapter 5.

84) Van Holde, K.E.; Johnson, W.C.; Ho, P.S., "Principles of Physical Biochemistry," Pearson Prentice Hall, New Jersey, 2006, Section 1.5.

85) Ramachandran, G.N.; Ramakrishnan, C.; Sasisekharan, V., J. Mol. Biol. 1963, 7, 95.

86) Flory, P.J., "Statistical Mechanics of Chain Molecules," J. Wiley, New York, 1969, Chapter 7.

87) Nozaki, Y.; Tanford, C., J. Am. Chem. Soc. 1967, 89, 742.

88) Gaggelli, E.; D'Amelio, N.; Maccotta, A.; Valensin, G., Eur. J. Biochem. 1999, 262, 268.

89) Sawyer, H.A., Ph.D. Dissertation, Texas A & M University, College Station, Texas, 2006.

90) Solinova, V., Kasicka, V., Koval, D., Hlavacek, J., Electrophoresis 2004, 25 2299.

91) Allison, S.A., Stigter, D., Biophys. J. 2000, 78 121.

92) Garcia de la Torre, J., Rodes, V., J. Chem. Phys. 1983, 79, 2454.

93) Arfken, G., Mathematical Methods for Physicists, Academic Press, New York, 1970, p. 531.

94) Garcia de la Torre, J., Jimenez, A., Freire, J.J., Macromolecules 1982, 15, 148.

95) Calladine, C.R.; Collis, C.M.; Drew, H.R.; Mott, M.R., J. Mol. Biol., 1991, 221, 981-1005.

96) Kasicka, V., Electrophoresis 2006, 27, 142-175

97) Fu, A.; Micheel, C.M.; Cha, J.; Chang, H.; Yang, H.; Alivisatos, A.P., J. Amer. Chem. Soc., 2004, 126, 10832-10833.

98) Castagnola, M.; Rossetti, D.V.; Inzitari, R.; Vitali, A.; Lupi, A.; Zuppi, C.; Cabras, T.; Fadda, M.B.; Petruzzelli, R.; Giardina, B.; Messana, I., Electrophoresis, 2003, 24, 801-807.

99) Zimm, B.H.; Levene, S.D., Quart. Rev. Biophys., 1992, 25, 171-204.

100) Ogston, A.G., Trans. Faraday Soc., 1958, 54, 1754-1757.

101) Rodbard, D.; Chrambach, A.; Proc. Natl. Acad. Sci. USA, 1970, 65, 970-977.

102) Tsai, D.S.; Strieder, W., Chem. Eng. Commun., 1986, 40, 207-218.

103) Allison, S.A.; Li, Z.; Reed, D.; Stellwagen, N.C., Electrophoresis, 2002, 23, 2678-2689.

104) Castelnovo, M.; Grauwin, S., Biophys. J., 2007, 91, 3022-3031.

105) Brinkman, H.C., Appl. Sci. Res., 1947, A1, 27-34.

106) Debye, P.; Bueche, A.M., J. Chem. Phys., 1948, 16, 573-579.

107) Felderhof, B.U.; Deutch, J.M., J. Chem. Phys., 1975, 62, 2391-2397.

108) Johnson, E.M.; Berk, D.A.; Jain, R.K.; Deen, W.M., Biophys. J., 1996, 70, 1017-1026.

109) Oppenheim, I.; Auer, P.L., Eds, in “Macromolecules: John G. Kirkwood,” Gordon and Breach, New York, 1967.

110) Zwanzig, R., J. Chem. Phys., 1966, 45, 1858-1859.

111) Garcia de la Torre, J.; Lopez Martinez, M.C.; Tirado, M.M.; Freire, J.J., Macromolecules, 1984, 17, 2715-2722.

112) Schmitz, K.S., Biopolymers, 1977, 16, 2635-2640.

113) Garcia de la Torre, J.; Huertas, M.L.; Carrasco, B., Biophys. J., 2000, 78, 719-730.

114) Garcia de la Torre, J., Biophys. Chem., 2001, 93, 159-170.

115) Eimer, W.; Williamson, J.R.; Boxer, S.G.; Pecora, R., Biochemistry, 1990, 29, 799-811.

116) Diaz, R.; Fujimoto, B.S.; Schurr, J.M., Biophys. J., 1997, 72, A322.

117) Hagerman, P.J.; Zimm, B.H., Biopolymers, 1981, 20, 1481-1502.

118) Hagerman, P.J., Biopolymers, 1981, 20, 1503-1535.

119) Stigter, D., J. Coll. Interface Sci., 1975, 53, 296-306.

120) Allison, S.A., J. Phys. Chem., 1994, 98, 12091-12096.

121) Schellman, J.A., Harvey, S.C., *Biophys. Chem.,* 1995, 55, 95-114.

122) Laurent, T.C., J. Chromatogr., 1967, 14, 317-330.

123) Johnson, E.M.; Berk, D.A.; Jain, R.K.; Deen, W.M., Biophys. J., 1995, 68, 1561-1568.

124) Djabourov, M.; Clark, A.H.; Rowlands, D.W.; Ross-Murphy, S.B., Macromol. Rev., 1989, 22, 180-188.

125) Stigter, D., Macromolecules, 2000, 33, 8878-8884.

126) Allison, S.A.; Mazur, S., Biopolymers, 1998, 46, 359-373.

127) Mazur, S.; Chen, C.; Allison, S.A., J. Phys. Chem. B, 2001, 105, 1100-1108.

128) Stellwagen, N.C.; Gelfi, C.; Righetti, P.G., Biopolymers, 1997, 42, 687-703.

129) Hoagland, D.A.; Arvanitidou, E.; Welch, C., Macromolelcules, 1999, 32, 6180-6190.

130) Zimmerman, S.B.; Minton, A., Annu. Rev. Biophys. Biomolec. Struct., 1993, 22, 27-65.

131) Dwyer, J.D.; Bloomfield, V.A., Biophys. J., 1993, 65, 1810-1816.

132) Pluen, A.; Netti, P.A.; Jain, R.K.; Deen, W.M., Biophys. J., 1999, 77, 542-552.

133) Pernodet, N.; Tinland, B.; Sturm, J.; Weil, G., Biopolymers, 1999, 50, 45-59.

134) Sass, H.-J.; Musco, G.; Stahl, S.J.; Wingfield, P.T.; Grzesiek, S., J. Biomolecular NMR, 2000, 18, 303-309.

135) Fatin-Rouge, N.; Starchev, K.; Buffle, J., Biophys. J., 2004, 86, 2710-2719.

136) Tatarkova, S.A.; Berk, D.A., Phys. Rev. E, 2005, 71, 41913-1 – 41913-5.

137) Hirota, N.; Kumaki, Y.; Narita, T.; Gong, J.P.; Osada, Y., J. Phys. Chem. B., 2000, 104, 9898-9903.

138) Fatin-Rouge, N.; Milon, A.; Buffle, J., J. Phys. Chem. B., 2003, 107, 12126-12137.

139) Shen, H.; Hu, Y.; Saltzmann, W.M., Biophys. J., 2006, 91, 639-644.

140) Johansson, L.; Lofroth, J.-E., J. Chem. Phys., 1993, 98, 7471-7479.

141) Amsden, B., Macromolecules, 1998, 31, 8382-8395.

142) Ermak, D.; McCammon, J.A., J. Chem. Phys., 1978, 69, 1352-1360.

143) Allison, S., Macromolecules, 1986, 19, 118-124.

144) Laurent, J.C., Biochim. Biophys. Acta, 1967, 136, 199-205.

145) Mercier, J.-F.; Slater, G.W., Macromolecules, 2001, 34, 3437-3445.

146) Jackson, G.W.; James, D.G., Can. J. Chem., 1986, 64, 362-374.

147) Tirado, M.M.; Martinez, C.L.; Garcia de la Torre, J., J. Chem. Phys., 1984, 81, 2047-2052.

148) Rotne, J.; Prager, S., J. Chem. Phys., 1969, 50, 4831-4837.

149) Allison, S.A.; and Schurr, J.M.; Macromolecules, 1997, 30, 7132-7142.

150) Berk, D.A.; Yuan, F.; Leunig, M.; and Jain, R.K., Biophys. J., 1993, 65, 2428-2436.

152) Sorlie, S.S.; Pecora, R., Macromolecules, 1990, 23, 487-497.

153) Lukacs, G.L.; Haggie, P.; Seksek, O.; Lechardeur, D.; Freedman, N.; and Verkman, A.S., J. Biol. Chem., 2000, 275, 1625-1629.

154) Olmstead, M.C., Bond, J.P., Anderson, C.F., Record, M.T., Biophys. J., 1995, 68, 634-647.

155) Rasmusson, M., Allison, S.A., Wall, S., J. Coll. Interface Sci., 2003, 260, 423-430.

156) Berne, B. J.; Pecora, R. Dynamic Light Scattering; J. Wiley & Sons: New York, 1976.

157) Polson, A. Biochem. J. 1937, 31, 1903.

158) Longsworth, L. G. In Electrochemistry in Biology and Medicine; Shedlovsky, T., Ed.; J. Wiley: New York, 1955; Chapter 12.

159) Ellerton, H. D.; Reinfelds, G.; Mulcahy, D. E.; Dunlop, P. J. J. Phys. Chem. 1964, 68, 403.

160) Ma, Y.; Zhu, C.; Ma, P.; Yu, K. T. J. Chem. Eng. Data 2005, 50, 1192.

161) Stejskal, E. O.; Tanner, J. E. J. Chem. Phys. 1965, 42, 288.

162) Stilbs, P. Prog. NMR Spectrosc. 1987, 19, 1.

163) Johnson, C. S. Prog. Nucl. Magn. Reson. Spectrosc. 1999, 34, 203.

164) Syvitski, R. T.; Burton, I.; Mattatall, N. R.; Douglas, S. E.; Jakeman, D. L. Biochemistry 2005, 44, 7282.

165) Inglis, S. R.; McGann, M. J.; Price, W. S.; Harding, M. M. FEBS Lett. 2006, 580, 3911.

166) Popov K, Ronkkomaki H, Lajunen LH J : Pure Appl. Chem., 2006, 78: 663-675.

167) Kotch F. W., Sidorov V., Lam Y. F., Kayser K. J., Li H., Kaucher M. S., and Davis J. T., J. AM. CHEM. SOC. 2003, 125, 15140-15150

168) Tanner, J. E., J. Chem. Phys. 1970, 52, 2523-2526.

169) Mills R, Bunsenges Ber: Phys. Chem., 1971, 75: 195-199.

170) Mills R: J. Phys. Chem., 1973, 77: 685-688,

171) Hardy RC, Cottingen RL: J. Chem. Phys., 1949, 17, 509-510.

172) Edward JT: J. Chem Ed., 1970, 47: 261-270.

173) Dewan, K.K., Bloomfield, V.A., Berget, P.G., J. Phys. Chem., 1974, 75, 3120.

174) Meerwall, E.D., Amelar, S., Smeltzly, M.A., Lodge, T.P., Macromolecules, 1989, 22, 295.

175) Banipal, T.S., Singh, G., Thermochim. Acta, 2004, 412, 63.

176) Einstein, A., Ann. Phys., 1911, 34, 591.

177) Jeffrey, G.B., Proc. R. Soc. London, 1923, A102, 161.

178) Simha, R., J. Phys. Chem., 1940, 44, 25.

179) Scheraga, H. A., J. Chem. Phys., 1955, 23, 1526.

180) Kirkwood, J.G., Macromolecules, E.P. Auer (Ed.), Gordon and Breach, New York, 1967.

181) Kirkwood, J.G., Riseman, J., J. Chem. Phys., 1948, 16, 565.

182) Garcia de la Torre, J., Bloomfield, V.A., Biopolymers, 1978, 17, 1605.

183) Garcia Bernal, J.M., Garcia de la Torre, J., Biopolymers, 1980, 19, 751.

184) Byron, O., Biophys. J., 1997, 72, 408.

185) Garcia de la Torre, J., del Rio Echenique, G., Ortega, A., J. Phys. Chem. B, 2007, 11, 955.

187) Allison, S.A., Macromolecules, 1999, 32, 5304.

188) Hahn, D.K., Aragon, S., J. Chem. Theory Comput., 2006, 2, 1416.

189) Fixman, M., J. Chem. Phys., 1990, 92, 6858.

190) Batchelor, G.K., J. Fluid Mech., 1970, 41, 545.

191) Russel, W.B., J. Colloid Interface Sci., 1976, 55, 590.

192) Allison, S.A., Macromolecules, 1998, 31, 4464.

193) Allison, S.A., Nambi, P., Macromolecules, 1992, 25, 3971.

194) Brenner, H., Chem. Eng. Sci., 1972, 27, 1069.

195) Zimm, B.H., Macromolecules, 1980, 13, 592.

196) Wilemski, G., Tanaka, G., Macromolecules, 1981, 14, 1531.

197) Fixman, M., J. Chem. Phys., 1983, 78, 1588.

198) Brenner, H., Int. J. Multiphase Flow, 1974, 1, 195.

199) Wakiya, S., J. Phys. Soc. Japan, 1971, 31, 1581; 1972, 33, 278.

200) Harding, S.E., Prog. Biophys. Mol. Biol. 1997, 68, 207.

201) Potschke, H., Barnikol, W., Kirste, R., Rosenbaum, M., Macromol. Chem. and Phys. 1996, 197, 1419.

202) Eigner, J., Doty, P., J. Mol. Biol., 1965, 12, 549.

203) Harrington, R.E., Biopolymers, 1980, 19, 449.

204) Ogawa, T., Mizutani, K., Yasuda, M., Bull. Chem. Soc. Jpn. 1984, 57, 2064.

205) Banipal, T.S., Kauer, D., Banipal, P.K., J. Chem. Thermo. 2006, 38, 1214.

206) Banipal, T.S., Singh, G., J. Solution Chem. 2003, 32, 997.

207) Cremasco, M.A., Hritzko, B.J., Xie, Y., N.H.L. Wang, Brazilian J. Chem. Eng. 2001, 18, 181.

208) Scheraga, H.A., Mandelkern, L., J. Am. Chem. Soc. 1953, 75, 179.

209) Harding, S.E., Biochem. J. 1980, 189, 359.

210) Swanson, E., de Haen, C., Teller, D.C., J. Chem. Phys. 1980, 72, 1623.

211) Tanigawa, M., Mukaiyama, N., Shimokubo, S., Wakabayashi, K., Fujita, Y., Fukudome, K., Yamaoka, K. Polymer J. (Tokyo), 1994, 26, 291.

212) McMurry, J., Organic Chemistry, 7th Edition; Thomson, Brooks, and Cole, 2008, Chapter 1.

213) Zhou, H.-X., Biophys. J., 1995, 65, 2286, 2298.

214) Abe, F., Einaga, Y., Yamakawa, H., Macromolecules, 1991, 24, 4423.

215) Lodge, T.P., J. Phys. Chem., 1993, 97, 1480.

216) Lodge, T.P, Krahn, J.R., Macromolecules, 1994, 27, 6223.

217) Yoshizaki, T., Takaeda, Y., Yamakawa, H., Macromolecules, 1993, 26, 6891.